Tracing extratidal stars of Galactic globular clusters

By

Colin Anthony Navin

A thesis submitted to Macquarie University
for the degree of Doctor of Philosophy
Department of Physics and Astronomy
January 2018

MACQUARIE
University
SYDNEY·AUSTRALIA

Typeset in LaTeX 2_ε.

Except where acknowledged in the customary manner, the material presented in this thesis is, to the best of my knowledge, original and has not been submitted in whole or part for a degree in any university.

Colin Anthony Navin

Acknowledgements

Everybody says that you should find something you love doing and make it your career. I have had the extraordinary privilege of finding, not one, but two things like that in my life. I wanted to be an airline pilot, and I did that for many years. I wanted to be an astronomer, and now I have made a start on that also. Doing a PhD has been an amazing experience. It has presented me with new challenges and the opportunity to incorporate more learning and creativity into my life. Occasionally there is also the astonishing, and gratifying, realisation that you have discovered something that nobody knew before, and have made a small contribution to scientific progress.

I would like to thank my Principal Supervisor Daniel Zucker for the enormous help and support that he has given me. It had been a (very) long time since I finished my BSc, and even with an MSc in Astronomy under my belt relatively recently, it was a big jump to starting a PhD. I appreciate his confidence that I was capable of making that step.

Sarah Martell was officially my Adjunct Supervisor for the last 2 years or so of my candidature. Unofficially she took on that role, without being asked, the day I started. She has made a huge contribution to my work in every respect and I cannot thank her enough.

I would also like to thank Mike Ireland and Richard McDermid who ably took on the role of Associate Supervisor at different periods during my time at Macquarie University.

I am so grateful to all the people at Macquarie University Department of Physics and Astronomy who have provided such wonderful friendship, encouragement and assistance to me over the last few years. In particular I thank the MQAAstro Centre directors Quentin Parker and Mark Wardle, but also all the other staff, faculty and postdocs. Of course I must mention my fellow PhD and Masters students, without you it would have been much more difficult and not nearly as much fun. And then there is my PhD buddy Danica Draskovic, who had the misfortune to be allocated the desk next to mine for most of the time we were here. Despite that she somehow became my friend - I'll miss our morning coffees and chats.

There are also many people at other institutions who helped in ways large and small. I mention in particular Jeffrey Simpson, as well as Andy Casey, Gayandhi De Silva, Pete Kuzma, Sanjib Sharma and David Yong, but there are many others and if I have missed you please accept my thanks anyway. I have also been fortunate to have become part of the Galah collaboration which has been a great experience. Thanks also to everyone at the Australian Astronomical Observatory, with whom I spent many enjoyable nights observing.

I would also like to thank my family, my brothers Kim and John and my sister Kerry for their love and support. To my mother Gwen who sacrificed everything for us, I owe a debt that can never be repaid. Although you have been gone for many years I so wish you could be here now - I suspect you would be proud of all of us.

Last, but far from least, I thank my beautiful wife Sheryl for her patience, support and love. After 34 years she keeps buying tickets on my flights even when I can't tell her the destination. I could not hope for a better best friend and partner.

List of Publications

The following original publications, which are referred to in the text by Roman numbers and listed here in reverse chronological order, were authored or co-authored during the PhD candidature. Original publications are reproduced with permission from copyright holders. Publications I, II, and VII are first-author papers which, along with introductory material, form Chapters 2, 3, and 4, respectively, of this thesis. Supplementary material for these papers is also included in Appendices A, B, and C, respectively. Paper III is included in Appendix A Section 3 for reference as it an important extension of Paper I.

VII. **C.A. Navin**; S.L. Martell; J.D. Simpson; D.B. Zucker. *Halo stars of four southern Galactic globular clusters in the AEGIS survey*. 2017, Monthly Notices of the Royal Astronomical Society, submitted.

The second and fourth authors are the candidate's supervisors. All the data analysis, figure creation and writing was carried out by the candidate, except for Section 9.3, paragraphs 3–8 which were substantially contributed by the second author. The third author is credited with technical advice in the analysis of spectra and in general editing.

VI. J.D. Simpson; G. De Silva; **C.A. Navin**; S.L. Martell. *ESO452-SC11: The lowest mass globular cluster with chemical inhomogeneity*. 2017, Monthly Notices of the Royal Astronomical Society, 472, 2856. Simpson et al. (2017b).

V. G. Traven; G. Matijevič; T. Zwitter; M. Žerjal; J. Kos; M. Asplund; J. Bland-Hawthorn; A.R. Casey; G. De Silva; K. Freeman; J. Lin; S.L. Martell; K.J. Schlesinger; S. Sharma; J.D. Simpson; D.B. Zucker; B. Anguiano; G. Da Costa; L. Duong; J. Horner; E.A. Hyde; U. Munari; D. Nataf; **C.A. Navin**; W. Reid; Y.S. Ting. *The GALAH Survey: Classification and diagnostics with T-SNE reduction of spectral data.* 2017, The Astrophysical Journal, 228, 24. Traven et al. (2017).

IV. S.L. Martell; S. Sharma; S. Buder; L. Duong; K.J. Schlesinger; J. Simpson; K. Lind; M. Ness; J.P. Marshall; M. Asplund; J. Bland-Hawthorn; A.R. Casey; G. De Silva; K.C. Freeman; J. Kos; J. Lin; D.B. Zucker; T. Zwitter; B. Anguiano; C. Bacigalupo; D. Carollo; L. Casagrande; G.S. Da Costa; J. Horner; D. Huber; E.A. Hyde; P.R. Kafle; G.F. Lewis; D. Nataf; **C.A. Navin**; D. Stello; C.G. Tinney; F.G. Watson; R. Wittenmyer. *The GALAH Survey: Observational Overview and Gaia DR1 companion.* 2017, Monthly Notices of the Royal Astronomical Society, 465, 3203. Martell et al. (2017).

III. J.D. Simpson; S.L. Martell; **C.A. Navin**. *A broad perspective on multiple abundance populations in the globular cluster NGC 1851*. 2017, Monthly Notices of the Royal Astronomical Society, 465, 1123. Simpson et al. (2017a).

This paper was substantially produced by the first author Dr Jeffrey Simpson. I contributed the bulk of Section 1 (Introduction), paragraphs seven to twelve of Section

5 (Confirmation of new members), and general assistance in editing. The second author is the candidate's adjunct supervisor.

II. **C.A. Navin**; S.L. Martell; D.B. Zucker. *New halo stars of the Galactic globular clusters M3 and M13 in the LAMOST DR1 Catalog*. 2016, The Astrophysical Journal, 829, 123. Navin et al. (2016).

The second and third authors are the candidate's supervisors. All the data analysis, figure creation and writing was carried out by the candidate.

I. **C.A. Navin**; S.L. Martell; D.B. Zucker. *New cluster members and halo stars of the Galactic globular cluster NGC 1851*. 2015, Monthly Notices of the Royal Astronomical Society, 453, 531. Navin et al. (2015).

This project was initiated by Dr Sarah Martell (the candidate's adjunct supervisor) and Dr Daniela Carollo. The second and third authors are the candidate's supervisors. All the data analysis, figure creation and writing was carried out by the candidate.

Abstract

The Milky Way Galaxy is surrounded by many satellite dwarf galaxies and globular clusters, as well as individual field stars, in a vast stellar halo extending further than 100 kpc. There is no doubt that many of the field stars in the Galactic bulge and halo formed in these satellites, which are all in the process of being disrupted and losing stars. The processes that produce this loss are thought to be well-understood and are used in simulations that predict the present-day destruction rates.

Generally, however, these models are poorly constrained by observations. This thesis looks at the identification of individual extratidal stars that have escaped from a number of globular clusters, uses these stars to estimate the actual destruction rates of the clusters, and compares them with the predicted destruction rates from the models.

Paper I identified four extratidal stars of the globular cluster NGC 1851 in an analysis of AAOmega spectra. The destruction rate that corresponds to these stars was calculated in Paper III and was found to be several orders of magnitude greater than predicted by one of the models.

Paper II identified eight extratidal stars around the globular cluster M3 and twelve around M13 in the LAMOST stellar spectroscopic survey catalog. The destruction rates corresponding to these stars were calculated and found to be several orders of magnitude greater than predicted by the models for both clusters.

The AEGIS stellar spectroscopic survey catalog was searched for globular cluster extratidal stars in Paper VII. This identified 20, 6, 1, and 6 extratidal stars around the four globular clusters ω Cen, NGC 6541, M70 and M55, respectively. The destruction rates for these clusters was calculated and, in line with previous results, found to be several orders of magnitude greater than predicted by the models.

This work has identified intriguing discrepancies between predictions of globular cluster destruction rates based on existing models of cluster destruction and observations. If future studies confirm that the discrepancies apply to a significant fraction of the globular cluster population of the Milky Way, it points to higher initial masses of globular clusters and a significant contribution to the stellar halo field star population from globular clusters.

Contents

1 Introduction

1.1 The Milky Way Galaxy

The galaxy in which we live is the Milky Way or, simply, the Galaxy. It is a vast, ancient, complex and evolving system of stars, gas, dust and dark matter. A great deal is understood about the Milky Way, but there are still many unanswered questions, both large and small, to resolve.

The Milky Way is the second largest member of the Local Group of galaxies, along with the largest member the Andromeda galaxy (M31), the Triangulum galaxy (M33), and about 70-75 dwarf galaxies. Most of the dwarf galaxies are satellites of either the Milky Way or the Andromeda galaxy. The Local Group is itself part of the enormous Virgo Supercluster of galaxies that contains about 100 galaxy groups and clusters, including the huge Virgo Cluster of around 1300 galaxies.

The Milky Way is believed to be a barred spiral galaxy and the major stellar components are the bulge and bar, the thin and thick disks and the stellar halo. The total number of stars in the Milky Way is between 100 and 400 billion, with a total stellar mass of $\sim 7 \times 10^{10}$ solar masses ($M_\odot$) (Carroll & Ostlie, 2006). The Milky Way is also orbited by satellites (dwarf galaxies and globular clusters) that themselves contain varying mixtures of stars, gas, dust and dark matter. Stellar and gaseous streams and clouds, many of which are thought to originate from these satellites, envelop the Milky Way in a complex web. A huge dark matter halo surrounds the inner components, containing perhaps 1.9×10^{12} $M_\odot$ within a radius of 230 kpc (Carroll & Ostlie, 2006). The boundaries between some of these components are not always distinct, and of course there are many varied and complex interactions between them. For this reason it is worthwhile to provide some background on all these components, even though this thesis focuses on globular clusters and the Galactic stellar halo.

The Sun is located ~8 kpc from the Galactic centre near the inner edge of a minor arm called the Orion-Cygnus Arm (sometimes the Orion Spur or the Orion arm), between the Sagittarius and Perseus Arms. It takes about 240 million years to complete an orbit of the Milky Way (Carroll & Ostlie, 2006).

1.1.1 The bulge and bar

The bulge is a concentrated region of stars at the centre of the Milky Way. Many galaxies have exponential surface brightness profiles, but for the Milky Way it is a somewhat boxy/peanut shape. This is believed to have arisen through the effects of disk instabilities, perhaps acting on a spheroidal concentration that formed from mergers. It is now believed that the bulge contains a distinct bar with a diameter of ~3.1–3.5 kpc (Gonzalez & Gadotti, 2016).

The mass of the bulge is $\sim 10^{10}$ $M_\odot$, and the stellar population consists of a mixture of three distinct age groups and metallicities. Most stars are old (7, and perhaps up to 10 Gyr) and metal-rich. Older stars are generally expected to be more metal-poor – this seemingly anomalous population is explained by an early period of intense star formation and rapid metal enrichment, with short dynamical timescales. The two smaller, younger groups, at ages of 200 Myr and from 200 Myr–7 Gyr, have a fairly uniform metallicity distribution from -2.0–0.5 dex (Carroll & Ostlie, 2006).

The origin of the bulge is still unclear. There are thought to be two types of galactic bulges. Pseudo-bulges are believed to be associated with disks and bars, and result in somewhat boxy bulges with higher-metallicity stars in orbits similar to disk stars. Classical bulges are composed of stars older than those in the disk on random orbits, similar to the spheroid of an elliptical galaxy. Some recent studies suggest the bulge of the Milky Way could include elements of both types (Gonzalez & Gadotti, 2016).

1.1.2 The thin and thick disks

The disk of the galaxy, including the stars, gas and dust, is believed to have a diameter of 40 kpc (major axis) with an ellipticity (the ratio of the minor and major axes) of ~ 0.9 (Carroll & Ostlie, 2006). There appear to be two distinct components, the thin disk and the thick disk, which have different spatial distributions, stellar populations, and kinematics. However, some lines of evidence appear able to account for observed data with a single component (e.g. Rix & Bovy, 2013, Bovy et al., 2016). The density distribution of disk stars with Galactocentric distance is commonly described by exponential laws.

The thin disk closely follows the Galactic plane. It has been proposed (Xu et al., 2015) that some outer disk structures (TriAnd1, TriAnd2, and the Monoceros Ring) are evidence that the midplane oscillates up and down and is more extended (diameter ~50 kpc). This may be the response of the disk to the passage of Milky Way satellites. The scale height (the distance from the mid plane of the disk over which the number density of stars decreases by e^{-1}) is ~350 pc in the solar neighbourhood, although this increases towards the Galactic centre where it meets the Galactic bulge.

Most of the stellar mass of $\sim 6 \times 10^{10}$ $M_\odot$ is contained in the thin disk (Carroll & Ostlie, 2006). The stellar population predominantly consists of relatively young (up to several Gyr), metal-rich (-0.5 < [Fe/H] < +0.3) stars (Population I or Pop I) (Bensby et al., 2003). However, there are also some very old (10–12 Gyr) stars in the disk that indicate that the disk is very ancient (Phelps et al., 1994), and that most of its mass was accreted early in its history. After an initial intense period, star formation, at least in the solar neighbourhood, has been relatively constant for the last 10 Gyr, with some periods of more intense activity (Rocha-Pinto et al., 2000).

The thick disk (Gilmore & Reid, 1983) is fainter and more diffuse than the thin disk. The scale height of the thick disk is ~1–1.5 kpc and the mass is $0.2\text{–}0.4 \times 10^{10}$ $M_\odot$. The thick disk has an older, more metal-poor (-2.2 < [Fe/H] < −0.5) stellar population than the thin disk

with only ~8.5 percent of its stellar density and ~10 percent of its surface brightness. There is also some good evidence that the thick disk itself has two components, a canonical thick-disk and a metal-weak-thick-disk (MWTD) (Norris et al., 1985, Morrison et al., 1990), however this issue is not settled (see e.g. Twarog & Anthony-Twarog, 1994, Beers et al., 2014). There are two major scenarios for the origin of the kinematic heating that led to the formation of the thick disk. One is that accretion events of objects such as dwarf galaxies injects energy and heats the thin disk (Di Matteo et al., 2011), the other uses internal processes such as radial migration (Loebman et al., 2011). As yet there is no clear consensus about the relationships between the thin disk, the canonical thick-disk, the MWTD and the halo.

The most conspicuous structures within the disk are, of course, the spiral arms. The spiral structure of the disk is revealed by tracing neutral or ionised hydrogen, young stars and open star clusters. Spiral structure in other galaxies is more prominent in the blue light emitted by hot, young, high-mass main-sequence stars. Massive stars are short-lived compared to the period of rotation of a galaxy, thus spiral arms are associated with ongoing star formation. However, many details remain to be settled – even the symmetry and number of spiral arms (two or four) is still being debated (e.g. Urquhart et al., 2014).

There are also major stellar substructures, see Subsection 1.3.4, in the outer disk of the Milky Way: the previously mentioned Monoceros Ring, the Anti-Center Stream, the Eastern Banded Structure and a tidal arm of the Sagittarius dwarf galaxy (the Sagittarius Stream). There are also the structures mentioned above in the area of the constellations of Triangulum and Andromeda, TriAnd1 and TriAnd2, discussed in Subsection 1.3.7.

1.1.3 The stellar halo

The stellar halo is a vast (radius >~100 kpc) sparsely populated region surrounding the bulge and disks. The field stars in the stellar halo (Subsection 1.3.1) consist of old, low-metallicity Population II (Pop II) stars. These stars are the most metal-poor and among the oldest stars in the Milky Way. They provide a picture of the early stages of the life of the Milky Way, but halo stars near the Sun are relatively rare. The total mass (~0.3×10^{10} $M_{\odot}$) is ~5 percent of the mass of the disk (Carroll & Ostlie, 2006). Detection of stellar halos in other galaxies, that might provide a comparison to the halo of the Milky Way, is very difficult due to their very low surface brightnesses. More details on the stellar halo and its origin are in Section 1.3. As well as field stars (Subsection 1.3.1), there is considerable substructure in the halo (Subsection 1.3.2), including dwarf galaxies (Subsection 1.3.3), globular clusters (Subsection 1.3.5), stellar streams (Subsection 1.3.4 and Subsection 1.3.6) and "clouds" (Subsection 1.3.7).

1.1.4 The dark matter halo

Kinematic studies have long shown that galaxies rotate faster than is consistent with the amount of visible matter (Zwicky, 1933). This led to the idea that there is a dark component of matter in galaxies (e.g. Faber & Gallagher, 1979, and others). This dark matter interacts only very weakly with electromagnetic radiation, if at all, but nevertheless drives the dynamics of galaxies through gravitational interactions. There are alternative hypotheses that modify gravity itself (e.g. Milgrom, 1983, and others) but, at the present time, the most widely-accepted explanation is that there is far more non-luminous matter in galaxies than luminous matter. The nature of the dark matter halo is still unknown, although a number of candidates such as dust have been ruled out. Others, such as massive compact halo objects (MACHOS)

– unseen brown, red or white dwarfs, neutron stars or black holes – are statistically unlikely to account for a significant fraction of the mass (Alcock et al., 2000). With these baryonic candidates eliminated, research emphasis has now shifted towards particle physics in the hope of identifying some type of non-baryonic matter with the required properties. The leading contenders at the present time are exotic fundamental particles of a class known as weakly interacting massive particles (WIMPS) (Feng, 2010). This is an exciting prospect both for particle physics, as it would move beyond the standard model, and for cosmology and astrophysics.

Although we do not yet know the nature of dark matter, it is possible to measure its mass and distribution, as its effects are clearly visible on luminous matter. The luminous, baryonic matter is only a small fraction of the total mass of the Milky Way. The bulk consists of a spheroidal dark matter halo containing containing ~95 percent of the total mass – 5.4×10^{11} $M_\odot$ within a radius of 50 kpc from the Galactic centre and, perhaps, 1.9×10^{12} $M_\odot$ within a radius of 230 kpc (Carroll & Ostlie, 2006). The density distribution varies with Galactocentric distance r out to ~100 kpc as a power law $r^{\sim -2.0}$ (Battaglia et al., 2005). The dark matter halo is not expected to be smooth, but is instead likely to have a clumpy substructure (Moore et al., 1999).

1.2 Formation and evolution of the Milky Way

Eggen et al. (1962) proposed a model for galaxy formation from a rapid collapse of gas clouds, and the final morphology of the galaxy was determined by the star formation rate. For an elliptical galaxy, the star formation rate is high and there is a brief intense burst of star formation when the galaxy is young. Most of the gas turns into stars, using up virtually all the available gas before a disk can form. The infalling motion is converted into the typical random motion of stars in an elliptical galaxy. For a spiral galaxy the star formation rate is lower, extending over billions of years, and the cloud remains gaseous. Shocks and radiative cooling dissipate the gravitational energy. Eventually angular momentum supports the shrinking cloud and a rotating disk forms. The stellar halo is populated by older, metal-poor, Pop II stars that form quickly during the initial collapse before significant enrichment occurs. Younger stars form over a longer timescale after the disk forms. Both the initial radial collapse, and the settling of gas into a rotating disk, were believed to be quite rapid. This model broadly explained the origin and structure of the Milky Way, and agreed with observations of the kinematics and metallicity distribution of field stars.

However, there were some discrepancies between observations and this model. Many stars in the outer halo are in retrograde orbits and the net rotational velocity of the outer halo seemed to be close to zero (Carollo et al., 2007, Beers et al., 2012), which is inconsistent with the collapse of a single cloud of gas. In addition, there was a ~2 Gyr spread in the age of globular clusters, which is not compatible with a relatively short collapse time. An investigation (Searle & Zinn, 1978, Zinn, 1985) revealed another discrepancy, where globular clusters were observed to be divided into two populations. The first consisted of older, metal-poor ([Fe/H] < -0.8) clusters in an extended, roughly spherical halo. The second population were younger, higher metallicity clusters ([Fe/H] > -0.8) closer to the Galactic plane and in the inner galaxy. It was also recognised that galaxy interactions and mergers were relatively common and, consequently, that galaxy evolution may have been far from homogeneous (Toomre & Toomre, 1972, Tinsley & Larson, 1979). More recent evidence for the process of galaxy formation is provided by Hubble images of galaxies in the early universe. These show

many small, irregular, galaxy-like objects in small volumes of space. Their proximity makes it very likely that they would undergo collisions and mergers to form normal-sized galaxies.

In the late 1970s another model began to emerge to explain the origin of the stellar halo, taking into account these developments. Most halo stars and clusters formed early in low-mass proto-galaxies, very similar to gas rich, irregular galaxies, and with individual chemical evolution histories. However they continued to fall in to the Milky Way long after the central regions were formed by the main collapse. There is also strong evidence that this process is continuing today. There are ~150-160 known globular clusters (Harris, 1996) (2010 edition) catalog and ~30 dwarf galaxies (McConnachie, 2012) (updated September, 2015) orbiting the Milky Way. Many show evidence of ongoing tidal disruption in the form of clumpy substructure outside the tidal radius and tidal tails. There are also stellar streams without known progenitors and amorphous overdensities or clouds of stars in the Galactic halo.

This idea was a good match with the emerging cosmological model of hierarchical structure formation, where larger and more massive structures are formed through the ongoing mergers of smaller structures. These ideas had been developed in theoretical studies in the early 1980s (White & Rees, 1978, Peebles, 1982, Bond et al., 1982, Blumenthal et al., 1982, 1984). The structures we observe in the Universe today, from the largest (sheets, voids, and filaments) through to galaxy clusters and individual galaxies, are believed to have formed in this way. The most widely-accepted paradigm since 1998 is Lambda (cosmological constant associated with dark energy) Cold (non-relativistic) Dark (non electromagnetically interacting) Matter (ΛCDM) cosmology.

The current broad picture is that galaxies (and the Milky Way in particular) initially form via a monolithic collapse but continue to build via a hierarchical aggregation of smaller elements. However there are many details to be settled and some predictions that conflict with observations. The dynamical, merger/accretion, star formation and chemical history of the Milky Way is not well characterised and observational data are needed to provide input for simulations of galaxy formation.

One of the key approaches to obtaining the required data is Galactic archaeology. The premise is that past events in the Milky Way leave traces that can be observed today, which can be used to investigate its formation and evolution. One particularly useful trace which is persistent over long time periods is stellar elemental abundances. Big bang nucleosynthesis produced only hydrogen, helium and traces of lithium. Nearly all other elements in the Universe have been been produced by stellar nucleosynthesis. The changing patterns of star-by-star chemical abundances can be used to reconstruct the original star clusters and dwarf galaxies which formed the Milky Way (Freeman & Bland-Hawthorn, 2002). In a wider context, a detailed census of the present state of ONE large spiral Galaxy provides clues for the formation and evolution history of other galaxies.

The first stars, composed only of primordial hydrogen, helium and traces of lithium produced in the big bang, were likely massive (60–300 $M_{\odot}$) (Bromm et al., 1999) and short-lived. They exploded and returned most of their matter to mix with the interstellar medium. This material included large amounts of elements other than hydrogen and helium (metals) produced in the star's core by nucleosynthesis. This polluted material formed subsequent generations of stars, in turn being recycled through stars many times and becoming more metal-rich. In general, there is a gradual increase in metallicity across subsequent generations of stars – older stars are more metal-poor and younger stars are more metal-rich. This correlation between age and chemical abundances is referred to as the age-metallicity relation.

For most stages of a star's life nuclear fusion and nucleosynthesis only occur in the core and there is no mixing between the core and the outer layers. Apart from mass transfer in

close binaries and small amounts of accretion of enriched interstellar material, its photosphere retains the same chemical composition as the gas cloud from which it formed. These persistent chemical signatures effectively measure the integrated effects of star-formation history and can be used to trace the gradual, though not necessarily steady, enrichment of stars and the interstellar matter in the Milky Way.

Spatial and kinematic coherence of Galactic substructure may be lost over quite short timespans, but the chemical coherence of groups of lower-mass stars can persist over cosmological timescales. Different groups of elements (α-elements, iron-peak elements and neutron capture elements) are associated with specific astrophysical origins such as supernovae and massive stars. With large numbers of stars chemical tagging can be carried out to identify the number and nature of the stellar structures where stars formed.

1.3 The stellar halo

1.3.1 Field stars

The density profile of the halo varies with Galactocentric distance r as a power law, $r^{\sim -3.5}$ (Morrison, 1993). Various tracers (RR Lyrae stars, BHB stars, Blue Straggler stars, and metal-poor subdwarfs in the solar neighbourhood) that are only found in old populations and are relatively bright have been used to calculate the density profile and the exponent depends to some extent on the tracer used for measurement.

There is evidence that the stellar halo may have inner (R_{gc} < 10–15 kpc) and outer (R_{gc} > 15–20 kpc) components, with differences in spatial density profiles, orbits and metallicities. The inner halo appears to have a flattened (axial ratio 0.6) spatial density profile and the stars have highly eccentric orbits with small or zero prograde rotations and a metallicity distribution function (MDF) that peaks at ~ -1.6 dex. The outer halo appears to have a more spherical spatial density profile (axial ratio 0.9) and the stars have a range of orbital eccentricities with retrograde rotations and a MDF that peaks at a low metallicity of ~ -2.2 dex (Carollo et al., 2007, 2010). These results were questioned by Schönrich et al. (2011), but Beers et al. (2012) reanalysed the original data and added new evidence that strengthened the case. Quantitative knowledge about the outermost parts of the halo is still very limited, but it is likely that the spatial distribution is probably steeper than a $r^{\sim -3}$ power law, with a median metallicity 0.3–0.5 dex lower than inner halo stars.

The origin of the stars in the halo is not completely settled. Generally, there is a reasonable agreement between the predicted stellar content of the proto-galaxies that initially formed the stellar halo and the present-day contents of the stellar halo (Bell et al., 2008). A simplistic interpretation of this would lead to the conclusion that all the stars in the Milky Way's stellar halo originated early. However, the hierarchical paradigm of galaxy formation means that all galaxies experience mergers, most commonly with dwarf galaxies as they are the most numerous type of galaxies. As discussed below, it is clear that some fraction of the stars in the halo must have formed in present-day dwarf galaxies and globular clusters.

1.3.2 Substructure

As well as individual field stars, the stellar halo of the Milky Way contains a great deal of substructure, including many satellites in the form of dwarf galaxies (Subsection 1.3.3) and globular clusters (Subsection 1.3.5).

Stellar substructures are distinguishable by characteristics shared by groups of stars. These signatures can include spatial, kinematic, and chemical coherence. These objects contain varying mixtures of stars, gas, dust and dark matter. The orbits of some of this substructure material may take it through the disk and bulge of the Milky Way. Substructure is expected to be more prominent in the outer halo, where long dynamical timescales mean structures can remain spatially and kinematically coherent for long periods (Johnston et al., 1996, Mayer et al., 2002).

Dwarf galaxies are traditionally considered to be much more massive than globular clusters, and to have multiple rather than single stellar populations. Recent discoveries of fainter, less massive, dwarf galaxies and more complex globular clusters with multiple stellar populations indicate that the distinction between the two is not so clear-cut. Figure 1.1 shows absolute magnitude versus half-light radius of Local Group dwarf galaxies and Galactic globular clusters (for reference the globular clusters studied in this thesis work are also marked). It is clear, in this plane, that there are numerous objects with characteristics that are intermediate between conventionally-defined dwarf galaxies and globular clusters (e.g. Homma et al., 2017). It is likely that a significant fraction of the Milky Way's globular clusters formed in dwarf galaxies that were accreted into the Galactic halo, most of which were subsequently destroyed. Support for this scenario is also provided by the Andromeda galaxy, where outer halo globular clusters were associated with surrounding stellar streams formed as a result of dwarf galaxy disruption (Mackey et al., 2010).

Satellite dwarf galaxies and globular clusters leave streams and clouds of stars, gas, and possibly dark matter, as they are disrupted. It is likely that the satellites we see today are the remnants of a much larger population, and that their current masses are much less than when they were formed or were accreted by the Milky way (e.g. Gnedin & Ostriker, 1997, Webb & Leigh, 2015).

These satellites are being destroyed by various internal and external processes (Section 1.4). These processes produce stellar streams from dwarf galaxies and globular clustersĊlouds may also, possibly, produce stellar streams.

Stellar streams are groups of stars, once members of dwarf galaxies or globular clusters, stretched out into linear structures along the orbit of their parent object by tidal forces. The disruption of dwarf galaxies is believed to produce wide streams with relatively high velocity dispersions (Subsection 1.3.4). Narrower, kinematically colder streams are thought to have globular clusters as their progenitor object (Subsection 1.3.6). In the last twenty years or so a number of stellar streams have been discovered around the Milky Way. Some have been discovered with deep photometric surveys while others have been found kinematically with spectroscopic stellar surveys of stars such as RR Lyrae, M giants and main-sequence turnoff (MSTO) stars. The progenitors of some streams are well-established but, for at least a dozen, a progenitor has not been found. It is very likely that some progenitors will never be discovered because they have been completely dissolved.

Clouds (Subsection 1.3.7) are amorphous stellar over-densities in the halo. They are thought to be a result of minor mergers with dwarf galaxies, but this is not a settled question.

Figure 1.2 shows some of the dwarf galaxies, stellar streams and clouds discussed in this introduction.

1.3.3 Dwarf galaxies

Dwarf galaxies are small, low-mass galaxies. They typically contain from a million to a few billion stars, although some recently discovered ultrafaint galaxies may have only a thousand

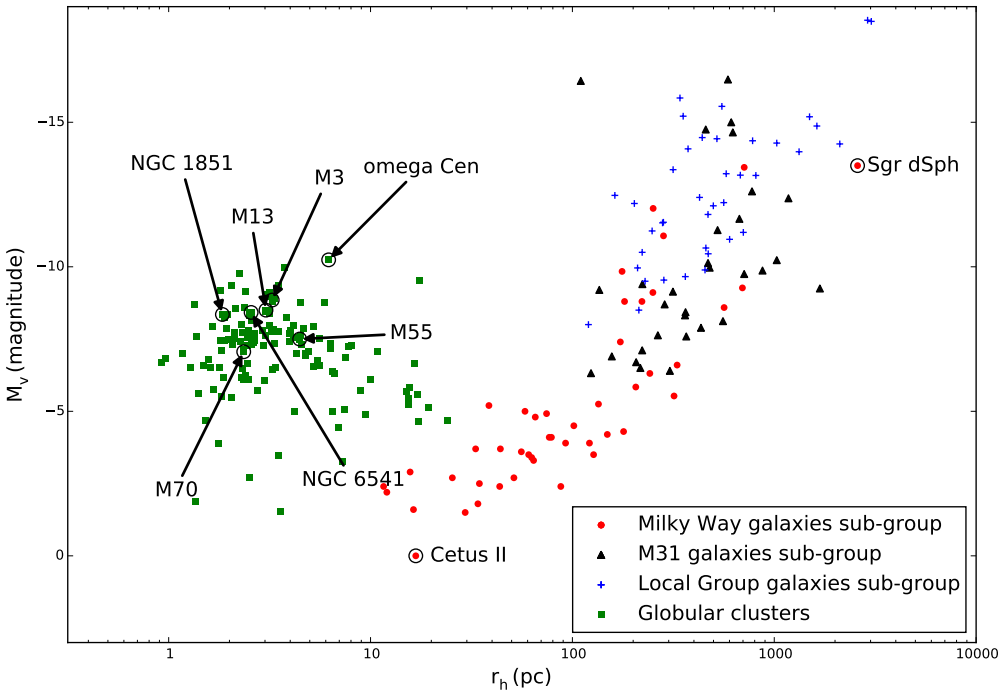

Figure 1.1: Half-light radius r_h versus absolute visual magnitude M_v of Local Group dwarf galaxies and globular clusters. Red circles denote Galactic dwarf galaxy satellites, black triangles denote M31 dwarf galaxy satellites, blue crosses denote other nearby galaxies, and green squares denote Milky Way globular clusters. Local Group galaxies data are from McConnachie (2012), Martin et al. (2015), Koposov et al. (2015), Laevens et al. (2015a,b), Bechtol et al. (2015), Drlica-Wagner et al. (2015), Homma et al. (2017), globular cluster data are from the Harris (1996) (2010 edition) catalog. The globular clusters studied in this thesis work are also labelled.

(Drlica-Wagner et al., 2015). Some contain gas and they are also usually thought to contain large amounts of dark matter. They have extended or ongoing periods of star formation and multiple stellar populations. Dwarf galaxies can be orbited by smaller dwarf galaxies and can contain globular clusters. Dwarf galaxies may have formed independently and were then accreted by the Milky Way. Tidal dwarf galaxies can also form from the debris resulting from major interactions, collisions and mergers between larger disk galaxies (e.g. Mirabel et al., 1992). In principle, some Galactic satellite dwarf galaxies could be tidal dwarfs, which could affect models of the accretion history of the Milky Way and the mass function of dwarf galaxies.

Dwarf spheroidal (dSph) galaxies are low-luminosity, low-surface-brightness dwarf galaxies. They have little or no gas and dust and show no evidence of recent star formation. They are similar to dwarf ellipticals but are spheroidal and have lower luminosity. Most satellite galaxies of the Milky Way, and the Andromeda galaxy, are dwarf spheroidals (McConnachie, 2012) (updated September, 2015).

Historically, two satellite dwarf galaxies of the Milky Way were recognised. Both the Large Magellanic Cloud (LMC) and the Small Magellanic Cloud (SMC) are large and bright enough to be visible to the naked eye. They were originally classed as dwarf irregular (dIrr)

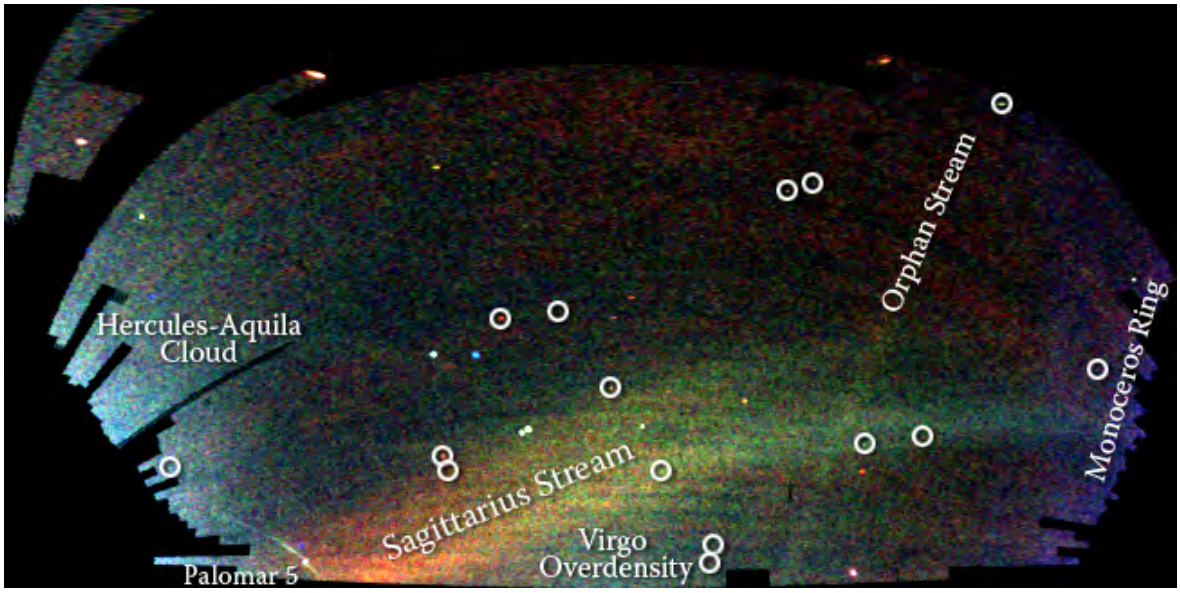

Figure 1.2: The iconic "Field of Streams" image from Belokurov et al. (2006b). This projection of SDSS images shows a number of the dwarf galaxies and faint globular clusters (circled), stellar streams and clouds discussed in this introduction. Blue denotes stars closer than ~15 kpc and red denotes stars further than ~25 kpc. Credit: V. Belokurov and the Sloan Digital Sky Survey.

galaxies but the LMC is now classified as a barred spiral of type SBm. Seven satellite dSph galaxies (Draco, Ursa Minor, Fornax, Carina, Sculptor, Leo I and Leo II) were discovered by eye on photographic plates in the period 1937 to 1977. In 1990 the Sextans dSph was discovered (Irwin et al., 1990) at a distance of 85 kpc during a search of scans of photographic plates. Ibata et al. (1994, 1995) found the Sagittarius dSph galaxy kinematically in radial velocity surveys of the Galactic bulge. This galaxy appeared to be in the process of being tidally disrupted.

The advent of the Sloan Digital Sky Survey (SDSS) (York et al., 2000), and extensions such as the SDSS Sloan Extension for Galactic Understanding and Exploration (SEGUE), revolutionised the search for dwarf galaxies and tidal streams. SDSS provided large sky area coverage, high catalogue completeness and precise CCD photometry to faint limits. Other surveys such as the 2 Micron All Sky Survey (2MASS) (Skrutskie et al., 2006), ESO VST ATLAS (Shanks et al., 2015), the Dark Energy Survey (DES) (The Dark Energy Survey Collaboration, 2005), and the Pan-STARRS 1 (PS1) 3π survey (Kaiser et al., 2010), have contributed to the tally and continue to provide new discoveries (e.g. Belokurov et al., 2006c, Laevens et al., 2015a, Homma et al., 2017).

There are more than 30 known satellite dwarf galaxies of the Milky Way (McConnachie, 2012) (updated September, 2015). Milky Way satellite dwarf galaxies are most commonly named after the constellation in which they are found, but sometimes after the discoverer or the survey in whose data they were detected.

1.3.4 Extratidal stars and tidal streams associated with dwarf galaxies

More than 15 Milky Way satellite dwarf galaxies exhibit evidence that they are being disrupted. The evidence may take the form of extended stellar halos and tidal tails around dwarf galaxies. Milky Way satellite dwarf galaxies that have observed evidence for disruption are

included in Table 1.1.

The first evidence of stellar tidal streams in the solar neighbourhood came from Helmi et al. (1999). They found that about ten percent of the metal-poor stars in the halo outside the radius of the Sun's orbit come from a single parent object. This object was likely disrupted during or soon after the Milky Way's formation and had a highly inclined orbit with a maximum distance of ~16 kpc. The progenitor was probably similar to the Fornax and Sagittarius dSph galaxies.

Table 1.1: Galactic satellite dwarf galaxies with evidence for tidal disruption or tidal tails

Dwarf galaxy	Stream	Selected references
Bootes I dSph		Belokurov et al. (2006c)
Bootes III (dSph?)	Styx stream	Grillmair (2009)
Canis Major[1]	Monoceros Ring[1]	Martin et al. (2004)
		Newberg et al. (2002)
		Lopez-Corredoira et al. (2012)
Carina dSph		Muñoz et al. (2006)
Fornax dSph		Coleman et al. (2005)
Hercules dSph		Belokurov et al. (2007a),
		Coleman et al. (2007)
Hydra I	Eastern Banded Structure	Grillmair (2011)
Large Magellanic Cloud		Saha et al. (2010),
(LMC)		Belokurov & Koposov (2015)
Leo I dSph		Harrington & Wilson (1950),
		Sohn et al. (2007)
Sagittarius dSph	Sagittarius stream	Ibata et al. (1994, 1995),
		Ibata et al. (2001)
		Majewski et al. (2003)
Small Magellanic Cloud		Saha et al. (2010),
(SMC)		Belokurov & Koposov (2015)
Ursa Major I dSph		Willman et al. (2005b),
		Okamoto et al. (2008)
Ursa Major II dSph	Orphan Stream	Zucker et al. (2006),
		Belokurov et al. (2007c),
		Fellhauer et al. (2007)
Ursa Minor dSph		Palma et al. (2003)
Willman 1 dSph		Willman et al. (2005a, 2006)

Notes: [1] This association, and even the existence of the Canis Major dwarf, is controversial.

The existence of a huge gaseous HI stream associated with the Magellanic Clouds has been known to exist for some time (Mathewson et al., 1974). Several recent studies have also found evidence of stellar streams associated with the two galaxies (Belokurov & Koposov, 2015, Belokurov et al., 2016), one of which overlaps the gaseous Magellanic Stream.

The most prominent and well-studied tidal stream in the Milky Way is the Sagittarius stream. A predicted tidal stream of stars from the Sagittarius dSph (Ibata et al., 1994,

1995) were identified (Ibata et al., 2001) in a survey of halo carbon giant stars from Palomar Sky Survey and UK Schmidt plates. Half of the stars were clustered on a great circle that intercepted the Sagittarius dSph, and they concluded that it was the source of a large proportion of the halo carbon star population. Vivas et al. (2001) observed RR Lyrae stars and confirmed that the clump of stars found by Ibata et al. (2001) was consistent with debris in this stream. Newberg et al. (2002) used photometry of 5×10^6 SDSS stars and found more probable pieces of the Sgr stream. 2MASS photometry of M-giant stars (Majewski et al., 2003) was able to provide the first all-sky map of the Sagittarius dSph and its associated stellar stream. Interestingly, the apparent mass-loss rate of the Sagittarius dSph was in contradiction to its apparent age unless it had suffered a large recent mass loss. The Sagittarius dSph also seemed likely to be the source of up to 75 percent of halo M-giants. Belokurov et al. (2006b) detected two branches/wraps (with evidence for a more distant third wrap) in SDSS data of the Sagittarius tidal stream in the halo near the north Galactic cap, see Figure 1.2.

The difficulty of teasing out the nature and relationships of dwarf galaxies and putative stellar streams is well illustrated by the Canis Major dwarf galaxy/ Monoceros Ring controversy. The Monoceros Ring was first detected by Newberg et al. (2002) and identified by Ibata et al. (2003) as a low surface brightness stellar ring circling the Milky Way at a radius of ~15 to 20 kpc. It was near the Galactic plane but possibly perturbed by the Magellanic Clouds or the Sagittarius dSph. Many studies to trace and map its extent and nature have followed its discovery. Belokurov et al. (2006b) discerned the Monoceros Ring stellar overdensity in the Galactic plane using SDSS data, see Figure 1.2. Explanations were split between a disrupting satellite and an origin as an outer Milky Way disk structure. The first scenario seemed to become more likely when Martin et al. (2004) proposed that the recently discovered Canis Major dwarf galaxy was the likely progenitor of this structure. However, this was countered by Momany et al. (2004), and others, who proposed that the warp and flare of the Galactic disk could account for the putative Canis Major dwarf galaxy. The question of the nature of the Monoceros Ring overdensities is still not settled. Conn et al. (e.g. 2012) suggests that a tidal stream model can fit the Monoceros Ring data, whereas others (Lopez-Corredoira et al., 2012, Xu et al., 2015) claim that the simplest explanation is that the Monoceros Ring is evidence for a warped and flared disk of the Milky Way.

1.3.5 Globular clusters

Globular clusters are old, roughly spherical, densely packed, gravitationally bound clusters of stars that generally do not contain gas or dark matter. There are probably about 200 globular clusters in the Milky Way globular cluster system. Some are concealed behind the Galactic disk but over 150 are catalogued (Harris, 1996, (2010 edition) catalog). About two-thirds are found in the stellar halo, with most (144) between 500 pc and 42 kpc from the Galactic centre, but six further out at distances from 69 to 123 kpc. The latter are believed by some to be captured objects (Mackey & van den Bergh, 2005).

Typically, they contain 10^5–10^6 stars within a radius less than 100 pc. In contrast to dwarf galaxies, globular clusters have lower mass; the average stellar mass is roughly solar so the total mass is 10^5–10^6 $M_\odot$. Many of their stars are post main-sequence and they contain no high mass main-sequence stars. These clusters formed when the Milky Way was very young with ages ranging from 11 to 13 Gyr (Krauss & Chaboyer, 2003, Gratton et al., 2003).

There are two general types of globular clusters. Older (~13 Gyr old) metal-poor ([Fe/H] < -0.8) clusters exist in an extended roughly spherical halo and have eccentric randomly-oriented orbits that plunge deep into the Milky Way. Younger (~11 Gyr old) higher metallicity

clusters ([Fe/H] > −0.8) are more numerous closer to the Galactic plane and in the inner Galaxy and their orbits and scale height (1 kpc) are similar to thick disk stars (Zinn, 1985).

A different classification scheme for globular clusters is that of Zinn (1993) and van den Bergh (1993) which uses cluster HB morphology and metallicity. In this scheme young halo (YH) globular clusters are thought to have formed in external satellite dwarf galaxies, while old halo (OH) and bulge/disc (BD) globular clusters are believed to have formed in the Milky Way. Mackey & Gilmore (2004) compared observational properties of these Galactic globular cluster subsytems, as well as globular clusters in the Magellanic Clouds, and the Fornax and Sagittarius dSph galaxies. They concluded that all 30 YH globular clusters and 15–17 percent of OH globular clusters were accreted, with ∼7 accretions of dSph galaxies with satellite globular clusters. They estimated that this contributed 45–50 percent of the mass of the Galactic stellar halo.

Globular clusters were conventionally characterised as having one generation of star formation and a single stellar population (SSP). All the cluster stars have the same age, helium abundance and overall [Fe/H] metallicity. However, since the first discovery of correlations between CN strength and Na and Al were found by Cottrell & Da Costa (1981), it has become increasingly clear that this is not the case. Every old globular cluster in the Milky Way shows evidence of two subpopulations (except possibly Ruprecht 106, Villanova et al. (2013)). One subpopulation consists of metal-poor stars similar to halo field stars. The second subpopulation consists of stars with the same [Fe/H] but a distinct light-element abundance pattern of enhanced N, Na and Mg, and depleted C, O and Al. These light-element abundance anticorrelations are exhibited by between 30–70 percent (Pancino et al., 2010, Carretta et al., 2009) of stars in a given globular cluster. The two main candidates for the physical site of the nucleosynthesis that produces these patterns are hot hydrogen burning in either intermediate-mass AGB stars or fast rotating massive stars, although other candidates have been proposed.

The two populations are most commonly explained by a second star-formation episode early in the history of the cluster, so the two populations are often denoted first- and second-generation. One important consequence of this explanation of the chemical anomalies in globular cluster stars is the so-called “mass budget" problem (e.g. Bastian et al., 2013). For any reasonable initial mass function (IMF) and proposed nucleosynthetic sites, there are not nearly enough first-generation stars in clusters now to generate the mass of metals required to pollute the second-generation stars. The solution proposed for this is that the first-generation was initially 10–100 times more massive, and that most of these stars have been lost from the cluster. However, there are alternative scenarios (for a review of multiple stellar populations in globular clusters see Gratton et al. (2012)).

There are also a handful of globular clusters that exhibit overall star-to-star [Fe/H] and neutron capture element variations such as ω Centauri (ω Cen) (e.g. Lee et al., 1999, Smith et al., 2000, Bedin et al., 2004, Johnson & Pilachowski, 2010). This is the largest and brightest globular cluster in the Milky Way and contains between one and ten million stars. It has a luminosity of 10^6 $L_\odot$ with a very high surface brightness. It has two main sequences and, as mentioned above, a wide metallicity range. It has been proposed that it is the core of a satellite dwarf galaxy disrupted by tidal interactions with the Milky Way (Bekki & Freeman, 2003). Other globular clusters with similar properties that are candidates as cores of dwarf galaxies are NGC 2419 (Lee et al., 2013) and NGC 6715 (M54). M54 is widely accepted as the nuclear star cluster of the Sagittarius dwarf galaxy (Law & Majewski, 2010) and it has apparent chemical similarities to ω Cen (Carretta et al., 2010b).

1.3.6 Extratidal stars and tidal streams associated with globular clusters

There is observational evidence of disruption for more than 45 Galactic globular clusters, and disruption has even been observed in some of the globular clusters of the Andromeda galaxy (Grillmair et al., 1996). The evidence for disruption may take the form of (1) extended stellar halos around a cluster, (2) tidal tails that are associated with specific clusters, (3) tidal tails that are not associated with specific clusters but are likely to have a globular cluster as a progenitor, or (4) debris with characteristics that are peculiar to globular clusters distributed widely over the sky. Globular clusters that have observed evidence for disruption, and stellar streams with unknown progenitors that are likely to be globular clusters are detailed in Table 1.2.

Table 1.2: Disrupting globular clusters and globular cluster tidal tails

Globular cluster	Stream	Selected references
Eridanus		Myeong et al. (2017)
NGC 104 (47 Tuc)		Leon et al. (2000)
NGC 288		Grillmair et al. (1995)
NGC 362		Grillmair et al. (1995)
NGC 1261		Leon et al. (2000)
NGC 1851		Leon et al. (2000)
NGC 1904 (M79)		Grillmair et al. (1995)
NGC 2298		Leon et al. (2000)
NGC 2419		Jordi & Grebel (2010)
NGC 2808		Grillmair et al. (1995)
NGC 3201		Grillmair et al. (1995)
NGC 4147		Jordi & Grebel (2010)
NGC 4590 (M68)		Grillmair et al. (1995)
NGC 5024 (M53)		Chun et al. (2010, 2014)
NGC 5053		Lauchner et al. (2006)
NGC 5139 (ω Cen)		Leon et al. (2000)
		Dinescu (2002)
		Majewski et al. (2012)
NGC 5272 (M3)		Leon et al. (2000)
NGC 5466		Lehmann & Scholz (1997)
		Belokurov et al. (2006a)
	length 45.0°	Grillmair & Johnson (2006)
NGC 5694		Leon et al. (2000)
NGC 5824		Grillmair et al. (1995)
	Cetus Polar Stream	Newberg et al. (2009)
NGC 5904 (M5)		Lehmann & Scholz (1997)
NGC 6205 (M13)		Lehmann & Scholz (1997)
NGC 6218 (M12)		Lehmann & Scholz (1997)
NGC 6254 (M10)		Leon et al. (2000)
NGC 6266 (M62)		Chun et al. (2010, 2014)
NGC 6273		Chun et al. (2010, 2014)
NGC 6341 (M92)		Testa et al. (2000)

Continued on next page

Table 1.2: Disrupting globular clusters and globular cluster tidal tails (continued)

Globular cluster	Stream	Selected references
NGC 6397		Leon et al. (2000)
NGC 6535		Leon et al. (2000)
NGC 6541		Chen & Chen (2010)
NGC 6626 (M28)		Chun et al. (2010, 2014)
NGC 6681 (M70)		Chen & Chen (2010)
NGC 6712		De Marchi et al. (1999)
NGC 6809 (M55)		Kharchenko et al. (1997)
NGC 6864 (M75)		Grillmair et al. (1995)
NGC 6934		Grillmair et al. (1995)
NGC 6981 (M72)		Grillmair et al. (1995)
NGC 7006		Jordi & Grebel (2010)
NGC 7078 (M15)		Grillmair et al. (1995)
NGC 7089 (M2)		Grillmair et al. (1995)
NGC 7099 (M30)		Chun et al. (2010, 2014)
NGC 7492		Leon et al. (2000)
Palomar 1		Niederste-Ostholt et al. (2010)
Palomar 3		Jordi & Grebel (2010)
Palomar 4		Jordi & Grebel (2010)
Palomar 5		Leon et al. (2000)
		Odenkirchen et al. (2001)
	length 18.5°	Grillmair & Dionatos (2006a)
Palomar 12		Leon et al. (2000)
Palomar 13		Côté et al. (2002)
Palomar 14		Jordi & Grebel (2010)
-	GD-1, length 63°	Grillmair & Dionatos (2006b)
-	Acheron, length 37°	Grillmair (2009)
-	Cocytos, length 80°	Grillmair (2009)
-	Lethe, length 84°	Grillmair (2009)
-	Pisces, length 12°	Bonaca et al. (2012b)
		Martin et al. (2013)
Palomar 15		Myeong et al. (2017)

Grillmair et al. (1995) produced the first evidence for the existence of globular cluster tidal tails around 12 southern halo clusters. They found that stellar surface density profiles significantly exceeded the prediction of King models in the outer parts of the clusters and extended outside the tidal radius. A halo of extratidal stars was detected around most of the clusters as well as hints of possible tidal tails from some clusters. Other studies that followed found evidence for extratidal halos around many other clusters (e.g. Olszewski et al., 2009, Carballo-Bello et al., 2012).

The first evidence for extended tidal tails was found in density enhancements surrounding Palomar 5 (Pal 5) in SDSS data (Odenkirchen et al., 2001). The tails extended a total of 2.6°, were almost symmetric, and both sides had clumps ∼0.8° from the cluster centre. Rockosi

et al. (2002) determined that 45 percent of cluster stars were in the tails. Odenkirchen et al. (2003) traced the total observed length of the tails to 10° and found that the tails were very narrow (FWHM ~120 pc) and that the number of escaped stars was ~1.2 times the number of stars still in the cluster. They concluded that the cluster was near apocentre but had suffered repeated recent disk shocks. Most of the mass-loss was in the last 2 Gyr and it was likely to be destroyed on its next disk crossing in ~100 Myr. The detected length of the trailing tail was extended to 18.5°, ~8.3 kpc, by Grillmair & Dionatos (2006a).

The other globular cluster for which very extended tidal tails have been found is NGC 5466. Lehmann & Scholz (1997) found indications of tidal tails around seven globular clusters, inlcuding NGC 5466, in the form of an increased surface density outside the tidal radius. Evidence of tidal mass loss in NGC 5466 was found by Odenkirchen & Grebel (2004) and tidal tails extending ~4° were found by Belokurov et al. (2006a). Grillmair & Johnson (2006) extended the length of the stellar stream using SDSS photometric data to 45°, equivalent to an astonishing ~20 kpc, from NGC 5466.

There have also been discoveries of stellar streams without known globular cluster progenitors. A 63° long, cold stellar stream stretching from Ursa Major to Cancer was found by Grillmair & Dionatos (2006b) using stellar density counts of SDSS photometric data. Another three stellar streams (Acheron, Cocytos, Lethe) stretching from 34 to 84° were identified in SDSS data by Grillmair (2009). The narrow widths of the streams suggested that their parent objects were probably now-disrupted globular clusters.

There have also been studies looking for widespread debris from particular globular clusters. There have been a number of models and simulations (e.g. Bekki & Freeman, 2003, Mizutani et al., 2003, Meza et al., 2005) that predict spatial, kinematic and chemical signatures of ex-member stars of ω Cen. Substructures have been observed that match some of these signatures (e.g. Dinescu, 2002, Gilmore et al., 2002, Majewski et al., 2012, Fernández Trincado et al., 2013), indicating that ω Cen is losing stars and contributing to the stellar halo.

1.3.7 Clouds

Clouds are large, non-linear, diffuse overdensities of stars in the Galactic halo. Their large size (many kiloparsecs across) and low density means that they cannot possibly be gravitationally bound. Their origins are unclear at the present time. One scenario is that they originate from accreted dwarf galaxies with highly eccentric orbits. These galaxies were tidally disrupted as they passed near, or through, the bulge of the Milky Way. The stripped stars continue in the eccentric orbit but, from our position in the disk, they would appear as diffuse clouds near the orbital apogalacticon as they spend more time near there. Carlin et al. (2012) propose that one cloud, the Virgo Overdensity (VOD), is the core of a disrupted dwarf galaxy near its perigalacticon. Another proposal, mentioned previously (Xu et al., 2015), is that some clouds (TriAnd1, TriAnd2, and the Monoceros Ring) are part of the Galactic disk.

The first hint of the presence of the VOD was in Xu et al. (2006), who utilised star-counts of SDSS data near the North Galactic pole and found that the stellar halo exhibited noticeable asymmetry, with an overdensity in the stellar halo in the direction of Virgo and an underdensity in the region of Ursa Major. Newberg et al. (2002) detected an overdensity of F-type main-sequence stars in a single stripe of SDSS data. Jurić et al. (2008) estimated the distances to ~48 million stars in SDSS data and found the same feature. The highest number density was in the direction of Virgo but it covered over 1000 deg^2 in the stellar halo, at distances from ~6–20 kpc. Bonaca et al. (2012a) expanded the coverage to ~3000

deg^2. Some studies (e.g. Vivas & Zinn, 2006, Keller et al., 2009), particularly of RR Lyrae variables, appear to show that the VOD may itself have substructures in both velocity and distance.

The Hercules-Aquila cloud was found in SDSS data by Belokurov et al. (2007b) as an overdensity of stars in the inner halo of the Milky Way. This huge structure extended 50° above and below the Galactic disk and 80° in longitude making it ~ 20×30 kpc in projection. There have been a number of subsequent studies (e.g. Sesar et al., 2010, Simion et al., 2014), especially using RR Lyrae variables, revealing a distance of 10–25 kpc and halo-like metallicity of -2.2 to -1.4. If the progenitor is a dwarf galaxy, it would be have to be quite massive.

Rocha-Pinto et al. (2004) found a clumpy tenuous structure (TriAnd1) covering ~ 50×40 deg^2 from 2MASS M giant stars in the Triangulum-Andromeda area at a distance of ~22 kpc. In a companion paper, Majewski et al. (2004) found the same structure. A second fainter structure, dubbed TriAnd2, in the same area but at a distance of ~28 kpc was revealed by Martin et al. (2007). These two structures were kinematically connected by Sheffield et al. (2014), who found similar velocities for both groups. Their metallicities were slightly different but both were much more metal-rich than typical Galactic halo stars. An N-body simulation showed that these observations are compatible with debris from consecutive orbits of a massive disrupting dwarf galaxy forming TriAnd Rings.

The Pisces overdensity was discovered by Sesar et al. (2007) and Kollmeier et al. (2009) in an analysis of RR Lyrae stars in SDSS Stripe 82. It is very distant at ~81 kpc with a metallicity of ~-1.5. Sharma et al. (2010) identified 16 halo structures using a group finding algorithm on M-giants in 2MASS photometric data, one of which was noted as a possible extension of the Pisces overdensity.

1.3.8 Satellite debris

As well as observations of extratidal structure and tails, weak chemical tagging also indicates that globular clusters are contributing to the stellar halo. Weak chemical tagging searches for globular cluster debris among the general halo field star population. Weak chemical tagging associates certain stellar abundance patterns with a class of objects, such as globular clusters, rather than with specific origins. This technique requires fewer measurements of chemical abundances than standard chemical tagging. For globular clusters, the light-element abundance anti-correlations (C-N, O-Na and Mg-Al) have only been found in the second-generation of globular cluster stars. Stars that display these patterns are very likely to have originally formed in globular clusters and then escaped into the stellar halo.

Martell & Grebel (2010) studied the SDSS-II/SEGUE spectra of ~1900 G and K-type halo giants and found that 2.5 percent showed the strong CN, weak CH abundance pattern only previously found in second-generation globular cluster stars. From models of globular cluster evolution they inferred that up to 50 percent of halo field stars initially formed within GCs. Carretta et al. (2010a) found two stars in a sample of 144 metal-poor disk, halo and bulge stars that were Na-rich and moderately Li depleted. These stars were also likely to have originated in globular clusters, and they concluded that early mass loss from globular clusters was a major contributor to the stellar halo. A further study (Martell et al., 2011) found 3 percent of 561 low-metallicity halo giant stars in SDSS-II/SEGUE 2 with the enriched CN, depleted CH pattern. This translates to a minimum of 17 percent of the present-day mass of the stellar halo originating in globular clusters, based on models at the time. Ramírez et al. (2012) found a similar fraction with two Na-rich/O-poor stars in a sample of 67 nearby

halo dwarf stars. Lind et al. (2015) found one Mg-poor, Al-rich star in a few hundred halo stars observed in the Gaia-ESO survey (Gilmore et al., 2012) which was likely to have been formed in a globular cluster.

The fraction of stars in the halo that have an origin in globular clusters depends critically on the assumed ratio of first- to second-generation stars in models of globular cluster formation. Some models require initial masses of globular clusters 10–100 times higher than at present, which would mean that most, if not all, stars in the halo originated in globular clusters (e.g. Gratton et al., 2012). A recent study, identifying N-rich globular cluster-like stars in the inner Galaxy (Schiavon et al., 2017), indicates that the contribution of globular clusters to the stellar halo may be significantly lower than suggested by previous estimates. The lower limit for the total mass of these stars is 6–8 times the mass of existing globular clusters, while they estimate that the upper limit for the fraction of globular cluster mass in stars with a first-generation abundance pattern is ~93 percent, and probably less. With reasonable assumptions regarding the ratio of first- to second-generation stars, only ~3 and ~20 percent of the stellar mass in the bulge and the inner ~2 kpc of the halo originates in globular clusters, respectively.

1.4 Satellite mass loss and dissolution

1.4.1 General

There are a number of internal and external processes that can contribute to the disruption and eventual dissolution of dwarf galaxies and globular clusters, and the mass loss rate is not constant. Different processes contribute more or less at different ages as the satellite loses mass and its member stars evolve, and even at different parts of its orbit as it moves through the varying gravitational potential of the Milky Way (e.g. Balbinot & Gieles, 2017).

Internal processes that can contribute are stellar evolution leading to gas expulsion, and two-body relaxation leading to evaporation.

Stellar evolution is driven by star formation. Massive stars that form during periods of star formation evolve quickly, have strong winds, and within a few million years they explode as supernovae and expel gas from the cluster. For globular clusters in particular this occurs early in the cluster's lifetime. Additionally, in the first few Gyr after a burst of star formation, evolved stars suffer significant mass loss due to winds with velocities that exceed the satellite's escape velocity. The loss of the mass of the gas in these situations may be so great that the cluster no longer has enough mass to hold it together and it dissolves.

Two-body relaxation is a continuous process that occurs when equipartition of energy during close encounters of the stars in satellites leads to mass segregation. Less massive stars move to the outer parts of the satellite while the more massive stars sink towards the centre. Over a period, the satellite will slowly expand and dissolve. Relaxation processes are strongly dependent on stellar density as this regulates the encounter rate. Consequently, this process is important for globular cluster evolution where stellar density is high and median relaxation times can be as low as ~1 Gyr. Dwarf galaxies have much lower stellar densities and relaxation times can be much longer than the Hubble time, so relaxation processes are not important for dwarf galaxy evolution. In globular clusters, the loss of energy from the core can lead to core-collapse, sometimes called a gravothermal instability. About 20% of Milky Way globular clusters show evidence of core-collapse (Ashman & Zepf, 2008) in the form of a power-law cusp in their surface brightness profiles.

This process, often termed evaporation, is enhanced in the presence of a tidal field, such as a that of a larger host galaxy. The two-body interactions no longer need to accelerate the star to the globular clusters escape velocity, but only push it beyond the tidal radius. If the globular cluster has an eccentric orbit, the tidal radius varies with changing Galactocentric distance. Because of mass segregation, globular clusters preferentially lose the outer low-mass stars (e.g. Baumgardt & Makino, 2003), resulting in an observed decrease in mass-function slopes and mass-to-light (M/L) ratios with age (Vesperini & Heggie, 1997, Kruijssen & Mieske, 2009).

Gravitational shock processes, which inject additional energy into the satellite, occur due to passage close to the bulge and through the Galactic disk and spiral arms. They can also occur in encounters with giant molecular clouds. The transit time through the disk or near the bulge is usually much less than the orbital period of the outer stars, so it is referred to as a shock process. On average, the satellite's stars gain energy and this enhances the escape of stars through evaporation. Tidal processes dominate during pericentre passages, particularly for satellites on elliptical orbits. Simulations by Kruijssen et al. (2011) show that tidal shocks increase dissolution events in globular clusters by up to 85 percent (depending on the galaxy model used).

Dynamical friction is also an important process in satellite evolution. The orbit of many satellites takes them near or through the Galactic bulge, disk and dark matter halo. The satellite accelerates stars and dark matter in its wake and loses momentum and energy due to this "drag". It spirals towards the centre of the Milky Way and eventually merges with it.

1.4.2 Globular cluster mass loss and dissolution models

The cluster destruction rate (the inverse of the time remaining until the complete dissolution or destruction of the cluster) is one of the key measures of globular cluster dissolution. Higher destruction rates equate to higher rates of mass loss and, observationally, a higher likelihood of finding globular cluster stars outside the tidal radius.

There have been a number of significant studies of globular cluster mass loss and destruction. Early investigations include Aguilar et al. (1988) and Hut & Djorgovski (1992).

Gnedin & Ostriker (1997) used simulations to calculate the present-day destruction rate of globular clusters, as well as the lifetime destruction rate using a scale-free power-law. Their simulations included two-body relaxation and disk and bulge gravitational shock processes. They simulated 119 clusters, a significant proportion of the ~150 known Galactic globular clusters. Figure 21 of their paper (Figure 1.3) shows the plot of cluster half-light radius r_h versus stellar mass $M/M_\odot$ of globular clusters in their study (there are several, slightly different versions of this depending on the Galactic and globular cluster system kinematic models used). The boundaries show the limits imposed by the various processes on the survival of present-day clusters. The survival boundary is defined such that the sum of the destruction rates for all the processes is equal to the inverse Hubble time t_{Hubble} (equation (31) from Gnedin & Ostriker, 1997):

$$\frac{1}{t_{Hubble}} = \frac{1}{t_{ev}} + \frac{1}{t_{sh}} + \frac{1}{t_{df}} \tag{1.1}$$

where t_{ev}, t_{sh}, and t_{df} are, respectively, the timescales over which a cluster would be destroyed by evaporation (two-body relaxation), combined disk and bulge shocks, and dynamical friction alone. The Galactocentric distance R determines the strength of the destruction processes, so the survival boundary depends on the cluster position. They concluded that

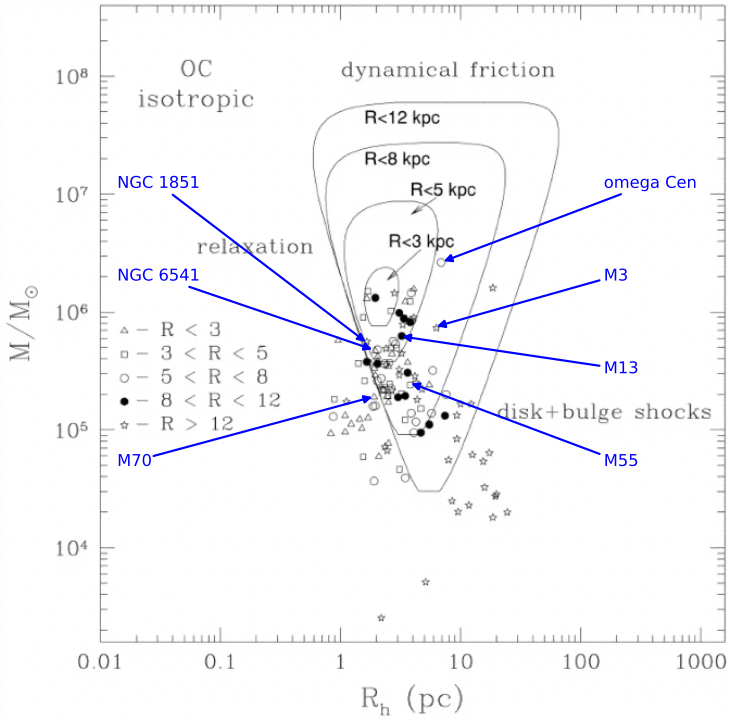

Figure 1.3: Vital diagram from Gnedin & Ostriker (1997) with the globular clusters studied in this thesis work labelled. The Galactocentric radii of the clusters are: NGC 1851 - 16.6 kpc, M3 - 12.0 kpc, M13 - 8.4 kpc, ω Cen - 6.4 kpc, NGC 6541 - 2.1 kpc, M70 - 2.2 kpc and M55 - 3.9 kpc.

most of the initial globular cluster population has not survived to the present day, and that a large fraction of the stars in the Galactic bulge and halo originate in globular clusters. They also found that the present day destruction time was similar to the typical age of a globular cluster, and that more than half of the existing globular clusters will not survive the next Hubble time.

Their study calculated destruction rates for all of the clusters (NGC 1851, M3, M13, ω Cen, NGC 6541, M70 and M55) which were included in this thesis work, and was one of the two studies selected for comparison with the mass loss rates we measured. When these clusters are located on the vital diagram (Figure 1.3), NGC 1851, M3, M13, and ω Cen are within the survival boundaries. However, NGC 6541, M70 and M55 are all likely to be destroyed within a Hubble time, favouring the likelihood of higher mass loss rates for these clusters.

A smaller sample of 38 globular clusters was simulated by Dinescu et al. (1999). They found that two-body relaxation is the principal destruction process for the majority of clusters in their sample, with a minority of globular clusters dominated by bulge and disk tidal shocks. Unlike Gnedin & Ostriker (1997), who used a statistical approach of assigning tangential velocities to the clusters, they used absolute proper motion data to calculate cluster orbits. They concluded that the destruction rates for many clusters found by Gnedin &

Ostriker (1997) may have been overestimated, as the orbits used were more destructive than are actually observed. Although the destruction rates due to two-body relaxation processes were similar, the influence of bulge and disk tidal shocks were somewhat less. They noted that, for one of our target clusters, ω Cen, the contribution to the destruction rate of tidal shocks was larger or comparable to the effect of two-body relaxation.

Allen et al. (2006, 2008) calculated the destruction rates due to Galactic disk and bulge shocks for 48 and 6 globular clusters, respectively, using a similar method to Dinescu et al. (1999). Their globular cluster orbits were based on proper motions and they compared the orbits in an axisymmetric Galactic gravitational potential and a Galaxy-like barred spiral potential. In the second paper they included the effect of three-dimensional (3D) spiral arms. They concluded that the presence of the Galactic bar only affects the orbits of globular clusters within ~4 kpc of the Galactic centre, and does not significantly change the contribution of Galactic disk and bulge shocks to the total destruction rates of globular clusters.

This study was updated in Moreno et al. (2014). This included all the elements of their previous studies, with various improvements such as using real orbits instead of linear trajectories, updated values for some input parameters, and six-dimensional positions and velocities for a total of 63 globular clusters. They found that destruction rates were not significantly affected by using linear trajectories to approximate orbits. They also determined that the contribution to total destruction rates of bulge shocks was smaller in the non-axisymmetric gravitational potential than in the axisymmetric potential for globular clusters with perigalacticons in the inner Galactic region. Their study calculated destruction rates for the clusters NGC 1851, M3, M13, ω Cen, and M55 in this thesis work, and was also used for comparison with our measured mass loss rates.

1.5 Thesis outline

Although a dwarf galaxy origin for stellar halo stars is broadly consistent with observational and theoretical evidence, it is clear from the observed mass-loss from globular clusters and debris from globular clusters in the halo that some fraction of the stars in the stellar halo originated in globular clusters. Many observations confirm the presence of extratidal substructure and tidal tails associated with specific globular cluster progenitors or, in some cases, without known parent objects, see Subsection 1.3.6. Many other studies confirm the presence of widely-scattered debris through the Milky Way from globular clusters (Subsection 1.3.8).

A number of computer simulations, discussed above in Subsection 1.4.2, of the mass-loss and dissolution of Milky Way globular clusters have been made, in particular Gnedin & Ostriker (1997) and Moreno et al. (2014). These models make predictions of destruction rates for specific globular clusters, but in general these predictions have not been constrained with direct observational evidence. The most direct method of doing this test requires identification of specific cluster escaped extratidal stars to measure the current mass-loss rate of specific globular clusters. General evidence for the existence of extratidal structure or tidal tails of globular clusters, or of the fractional contribution of the Milky Way globular cluster system to the Galactic stellar halo, do not measure this directly.

This thesis investigates the disruption of globular clusters; specifically it focuses on identifying individual stars that have escaped from globular clusters. The destruction rate corresponding to the observed mass-loss rate of escaped stars is estimated and compared with the globular cluster destruction rates calculated from the models mentioned above.

Catching stars in the act of escaping from a globular cluster is a challenge and globular

cluster extratidal stars remain a rare class of object. This study requires many stellar spectra in order to find the small fraction of globular cluster extratidal stars among the huge numbers of field stars. The enabling technology is multi-object fibre-fed spectrographs, and their use has led to wide-area observations and surveys to a sufficient depth to reach evolved and unevolved stellar sequences of globular clusters.

The broad approach to identifying globular cluster members and extratidal stars is to compare relevant measured parameters of candidate stars with the characteristics of known globular cluster member stars. Cluster members (and extratidal stars) are expected to share a number of common characteristics, i.e form a clump in parameter space, based on their common origin. These parameters can include (1) spatial proximity, (2) radial velocity (V_r), (3) colours and magnitudes, (4) effective temperature (T_{eff}) and surface gravity ($\log g$), (5) proper motions, (6) metallicity ([Fe/H]), and (7) detailed chemical abundances. The comparison is usually made with the characteristics of a globular cluster, which of course are simply various statistics of aggregates of known cluster member stars, rather than with individual stars. Field stars might exhibit some of the characteristics of stars in the cluster, but are very unlikely to share all of them. Hence, stars can be eliminated from a sample if their parameters do not match those of the globular cluster within certain limits.

Using all these parameters as a composite filter should reliably and definitively identify globular cluster members and extratidal stars. However, depending on the available data, these parameters may not be measured and data quality can be variable. In particular, detailed chemical abundances are considered the gold standard for identification, but are generally not available because the high-resolution spectroscopy required needs long integration times on large telescopes. Large samples of candidates need to be cleaned using parameters that are less costly to obtain in order to yield likely targets to maximise the chances of success with this technique. This broad approach was generally adopted throughout this thesis work, but adapted to suit the particular data that were available for the different globular clusters of interest.

Chapter 2 presents an analysis of AAOmega spectra of the member stars of one globular cluster, NGC 1851, and of stars in the surrounding area. In this study, methods of analysing spectra and identifying extratidal stars were developed. A number of new member stars were identified, as well as stars beyond the tidal radius that have escaped from the cluster. These results were published (Paper I) in the Monthly Notices of the Royal Astronomical Society journal (Navin et al., 2015), which forms this chapter. The method of calculating the destruction rate of a globular cluster from Paper II (see below) was also applied to the observed extratidal stars of NGC 1851 (Paper I). The results were similar and published in Paper III (Simpson et al., 2017a), which is included in Appendix A Section 4.

A search for extratidal stars around globular clusters was conducted in the LAMOST stellar spectroscopic survey catalog in Chapter 3. A more comprehensive filter than in Paper I, using many parameters for selecting globular cluster member and extratidal stars, was constructed. This included a method of determining membership probabilities using radial velocities. In addition, a method of calculating the destruction rates of globular clusters, based on observed mass-loss rates, was developed. The presence of member stars and extratidal stars around two globular clusters, M3 (NGC 5272) and M13 (NGC 6205) was revealed. The destruction rates calculated were several orders of magnitude greater than theoretical models predicted for both of these clusters. Paper II, published in the Astrophysical Journal (Navin et al., 2016), forms this chapter of the thesis.

Chapter 4 is similar to Paper II in exploiting an existing stellar spectroscopic survey catalogue (AEGIS) to search for extratidal stars of globular clusters. However, the original

AAOmega spectroscopic data were available from the Anglo-Australian Telescope (AAT) archive, so methods used in Paper I to analyse and reduce raw spectroscopic data could also be utilised. It incorporated new methods in the form of a PYTHON code analysis of spectra, and measurements of spectral indices. The research identified extratidal stars around four globular clusters (ω Cen, NGC 6541, M70 and M55). The observed destruction rates for all of these clusters were similar to previous results in also being much higher than predicted by the theoretical models. A third first-author Paper (VII) has been submitted to the Monthly Notices of the Royal Astronomical Society journal and is now being refereed.

Chapter 5 presents a summary and overall conclusions of the thesis work, and discusses possible future research directions.

2

New cluster members and halo stars of the Galactic globular cluster NGC 1851

This project, initiated by Dr Sarah Martell and Dr Daniela Carollo, had the aims of (1) exploring the primordial and evolutionary processes shaping the unusual chemical abundance pattern of the globular cluster NGC 1851, and (2) investigating reports of an extended halo of stars around the cluster. Good quality AAOmega spectra for 1149 stars were acquired for the project on the nights of 17th and 18th December 2012. The target sample included known cluster members with existing high-resolution spectroscopic data (Carretta et al., 2010c, 2011, Yong & Grundahl, 2008), plus others selected to search for new cluster members and extratidal stars.

This Paper I describes the observations, the initial reduction and analysis of the data, and the results obtained. Measurements of V_r were made using the near infrared Ca II triplet, from the red arm of the AAomega spectra. [Fe/H] was calculated from measurements of the equivalent widths (EWs) of the Ca II triplet. These parameters, supplemented by photometric and proper motion data, were used to search for new cluster members and extratidal stars.

In this investigation I used the following main methods in the search for extratidal globular cluster stars:

- spectroscopic data reduction and analysis using the standard 2dF data reduction pipeline 2dfdr, IRAF, and dedicated PYTHON code
- production of Galactic models and statistical comparison with the data sample, and
- identification of extratidal stars from their measured parameters

The main results from the study were the (1) recovery of 110 of 130 (~85%) previously studied stars, (2) identification of nine probable new cluster members and four escaped extratidal stars (~0.8% and (~0.3%) of targets), and (3) identification of three stars with unusually high radial velocities.

Paper I (Navin et al., 2015) which follows, resulted from this study and was published in the Monthly Notices of the Royal Astronomical Society in July 2015.

Paper III (Simpson et al., 2017a) is included in Appendix A Section 4 and was published in the Monthly Notices of the Royal Astronomical Society in February 2017. It followed on from Paper I and completed the objectives of the research proposal. It confirmed the existence of four stellar populations in the cluster as well as the identification of the four extratidal stars. The method of calculating destruction rates from Paper II was also applied to the observed extratidal stars. In this case the destruction rate was comparable to one model prediction, but several orders of magnitude greater than a second model prediction.

The measurement of V_r for the observed stars was central to the study results. Supplementary material on the calculation of the V_r uncertainties, which was not included in Paper I due to space considerations, is presented in Appendix A Section 1.

AAOmega spectra of the candidate extratidal members of NGC 1851 are presented in Appendix A Section 2.

Pages 25-34 of this thesis have been removed as they contain published material under copyright. Removed contents published as:

Colin A. Navin, Sarah L. Martell, Daniel B. Zucker, (2015) New cluster members and halo stars of the Galactic globular cluster NGC 1851, *Monthly Notices of the Royal Astronomical Society*, Vol. 453, Issue 1, pp. 531–540, https://doi.org/10.1093/mnras/stv1630

3

New halo stars of the Galactic globular clusters M3 and M13 in the LAMOST DR1 Catalog

Given the outcomes of Paper I, the next obvious step was to conduct searches for candidate globular cluster extratidal stars in other observational data. Stellar spectroscopic surveys were the clear choice as they provide (1) wide sky coverage, (2) large numbers of stellar spectra, (3) (often) catalogues of stellar parameters, such as V_r and [Fe/H]. These catalogues can be combined with others, such as photometric and proper motion catalogues, to provide a broad and comprehensive parameter space.

After consideration, the LAMOST survey (Zhao et al., 2006) was chosen as it (1) had a large publicly available catalog, Data Release 1 (DR1) (Luo et al., 2015), (2) covered the locations of a number of northern hemisphere globular clusters and, (3) was deep enough to likely include red giant member and extratidal stars of a number of clusters. In addition, a search for open and globular cluster members, but not extratidal stars, had already been undertaken by members of the LAMOST collaboration (Zhang et al., 2015). The same member stars were recovered in this study, providing a validation of the methods adopted.

The broad approach was the same as for NGC 1851 in Paper I – a comparison of relevant measured parameters of stars in the catalog with known characteristics of nearby globular clusters. Stars were eliminated if their parameters did not match those of the globular cluster within certain limits. This composite filter used as much information as possible to clean the sample of stars from DR1 and produce a list of probable extratidal halo cluster stars.

The primary parameter used was V_r. Clusters with high V_r were chosen as this made a clear distinction between field stars and possible cluster members. Indeed, in many studies, globular cluster members within the tidal radius of the cluster are identified solely by V_r. This was a successful technique for NGC 1851, which also had a high V_r. There were ten globular clusters that had high V_rs, but only two (M3 and M13) were eventually found to have candidate extratidal stars when all relevant parameters were considered. Instead of using simple estimates of V_r limits to select members as in Paper I, the probability distribution function of V_r was used in this study. This method, adopted from Frinchaboy & Majewski

(2008), enabled a more rigorous statistical determination of the limiting V_r range and also calculation of the probability of cluster membership.

The other parameters used to clean samples were photometry, T_{eff} and logg, and proper motions. In view of the large ranges and the large errors in DR1 [Fe/H] of stars in our samples, [Fe/H] was not used as a selection criterion. Detailed chemical abundances, considered the gold standard for identification of cluster members, are not available from the low-resolution LAMOST spectrographs.

In this study I introduced three new elements to the investigation of extratidal globular cluster stars:

- exploitation of the volume and complexity of data from survey catalogues,
- a rigorous statistical determination of V_r limits and cluster membership probabilities, and
- calculations of estimates of destruction rates of clusters based on the mass-loss rate corresponding to the observed extratidal stars

For M3, eight probable extratidal cluster halo stars at distances up to ~9.8 times the cluster tidal radius were identified. For M13, 12 probable extratidal cluster halo stars at distances up to ~13.8 times the tidal radius were found.

The masses of observed candidate extratidal members were used to estimate the corresponding mass-loss rates for M3 and M13. These mass-loss rates were compared to published destruction rates from simulations (Gnedin & Ostriker, 1997, Moreno et al., 2014). Interestingly, the observed destruction rates were ~1 to 3 orders of magnitude higher than those obtained from the simulations.

Paper II (Navin et al., 2016) which follows, described this study and was published in the Astrophysical Journal in October 2016.

A listing of the PYTHON code script written for the calculations of the cluster destruction rates, is included in Appendix B.

Pages 38-52 of this thesis have been removed as they contain published material under copyright. Removed contents published as:

Colin A. Navin, Sarah L. Martell, Daniel B. Zucker, (2016) New halo stars of the galactic globular clusters M3 and M13 in the LAMOST DR1 catalog, *The Astrophysical Journal*, Vol. 829, No. 2, 123, https://doi.org/10.3847/0004-637X/829/2/123.

4

Stellar halos of four southern Galactic globular clusters in the AEGIS survey catalogue

The advantages of exploiting existing stellar spectroscopic survey datasets (large numbers of uniformly reduced and analysed stellar spectra over a wide sky area) were exhibited by the successful detection of a number of probable extratidal stars around two globular clusters (M3 and M13) in Paper II. The results regarding the high observed destruction rates of these two clusters, and of NGC 1851 published in Paper III, were intriguing but far from conclusive. Only a small sample of three clusters had yet been investigated to constrain the models of globular cluster mass-loss and destruction.

Consideration of available datasets led to the AEGIS (Aaomega Evolution of GalactIc Structure) survey. This southern hemisphere survey was much sparser in sky coverage than LAMOST, but covered the area near a number of globular clusters and also had a (not yet publicly available) stellar parameters catalogue. In addition, the original AAOmega spectroscopic data were available from the AAT archive, so methods used in Paper I to analyse and reduce raw spectroscopic data could be utilised as required. The same broad approach of eliminating stars from the samples that did not match the characteristics of globular clusters was adopted. Once again, globular clusters with high V_r were targeted and V_r was used as the primary parameter as it can be accurately and reliably measured from the Ca II triplet in AAOmega red arm spectra. Other parameters used to clean the sample were photometry, T_{eff} and log g, proper motions, and (except in the case of ω Cen which is not monometallic) [Fe/H].

In this investigation I incorporated new methods to study the extratidal stars of globular clusters:

- PYTHON code analysis of spectra, and
- measurements of spectral indices

Candidate extratidal cluster stars were identified around four globular clusters: (1) twenty at distances up to ~6 times the tidal radius for ω Cen, (2) six at distances up to ~20 times the

tidal radius for NGC 6541, (3) one at a distance of ∼22 times the tidal radius for M70, and (4) six at distances up to ∼19 times the tidal radius for M55. Strikingly, the estimated observed destruction rates for all of these clusters were ∼2 orders of magnitude higher than predicted by the theoretical models, in line with the trend of the previous results for M3, M13, and NGC 1851

A third first-author Paper (VII) which follows, details the investigation and results obtained. It was submitted to the Monthly Notices of the Royal Astronomical Society journal in May 2017 and is now being refereed (Note: this is the manuscript as submitted and not the final version as published).

AAOmega spectra of candidate extratidal stars of the four target globular clusters are presented in Appendix C Section 1.

MNRAS **000**, 1–17 (2017) Preprint 30 January 2018 Compiled using MNRAS LATEX style file v3.0

Stellar halos of four southern Galactic globular clusters in the AEGIS survey catalogue

Colin A. Navin[1,4⋆], Sarah L. Martell[2]†, Jeffrey D. Simpson[1,3]‡, Daniel B. Zucker[1,3,4]§
[1]*Department of Physics and Astronomy, Macquarie University, NSW 2109, Australia*
[2]*School of Physics, University of South Wales, NSW 2052, Australia*
[3]*Australian Astronomical Observatory, 105 Delhi Rd, North Ryde, NSW 2113, Australia*
[4]*Astronomy, Astrophysics and Astrophotonics Research Centre, Macquarie University, 2109, Australia*

Accepted XXX. Received YYY; in original form ZZZ

ABSTRACT
We present the results of a search for extratidal halo stars of Galactic globular clusters in the AEGIS Survey catalogue. ω Centauri (NGC 5139), NGC 6541, M70 (NGC 6681), and M55 (NGC 6809) all had previous reports of surrounding stellar halos. We identify 20 candidate extratidal cluster halo stars at distances up to ∼6 times the tidal radius for ω Cen, six candidates at distances up to ∼20 times the tidal radius for NGC 6541, one candidate at a distance of ∼22 times the tidal radius for M70, and six candidates at distances up to ∼19 times the tidal radius for M55. These results support previous indications that these globular clusters are surrounded by extended stellar halos. We find that, similar to our previous results for NGC 1851, M3 and M13, the cluster destruction rates corresponding to the observed stellar mass loss are considerably higher than theoretical studies predict.

Key words: techniques: spectroscopic - globular clusters: general - globular clusters: individual: ω Cen (NGC 5139) - globular clusters: individual: NGC 6541) - globular clusters: individual: M70 (NGC 6681) - globular clusters: individual: M55 (NGC 6809)

1 INTRODUCTION

It is widely accepted that the current masses of globular clusters are much less than when they were formed and that the population of Galactic globular clusters has significantly decreased since their formation, as many have been completely destroyed (e.g. Gnedin & Ostriker 1997; Mackey & Gilmore 2004; Webb & Leigh 2015). Interactions with the Galaxy and internal processes both play a part in the loss of stars by globular clusters. Gravitational shocks due to passages close to the bulge and through the disk of the Galaxy, tidal disruption, and dynamical friction, all contribute to stripping stars from globular clusters. Internally, dynamical processes such as two-body relaxation and stellar evolution may cause a globular cluster to eject stars. The mass loss rate is not constant during the life of a cluster as the cluster loses mass and its member stars evolve, and the rate can even change substantially during individual orbits as the cluster moves through the gravitational potential of the Galaxy (e.g. Balbinot & Gieles 2017).

Stars lost by globular clusters are important markers of both the history and evolution of the clusters themselves, as well as their host galaxies. The original properties of globular clusters, and of the Galactic globular cluster system, can only be fully determined if we understand these mass loss processes. In a wider context, the mass loss from globular clusters also informs us about aspects of the history and evolution of the Galaxy. Tidal tails can be used as tracers of the Galactic gravitational potential and stars lost from globular clusters contribute to the mix of the Galaxy's stellar population. Some globular clusters are believed to be satellites of dwarf galaxies that were accreted e.g. Whiting 1, NGC 5634, Terzan 8 and Arp 2 from the Sagittarius dwarf spheroidal galaxy (Law & Majewski 2010). Some are believed to be the nuclei of dwarf galaxies e.g. M54 in the Sagittarius dwarf (Ibata et al. 1995) or ω Cen (Lee et al. 1999) where the original dwarf galaxy is now dissolved, so they also provide pointers to the history of the Galaxy.

The first discovery of Galactic globular cluster tidal tails was made by Grillmair et al. (1995) in the form of tidal structures visible in two-dimensional surface density maps around 12 southern Galactic halo clusters. The development of techniques such as matched filtering (Odenkirchen et al. 2001), and the advent of wide-field photometric surveys such as 2MASS (Skrutskie et al. 2006) and SDSS (York et al. 2000) made it possible to trace these tails across large areas of sky.

⋆ E-mail: colin.navin@mq.edu.au
† E-mail: s.martell@unsw.edu.au
‡ E-mail: jeffrey.simpson@aao.gov.au
§ E-mail: daniel.zucker@mq.edu.au

There is now evidence of surrounding stellar halos and/or tidal tails for many other globular clusters (e.g. Leon et al. 2000; Odenkirchen et al. 2001; Olszewski et al. 2009; Navin et al. 2015; Navin et al. 2016; Anguiano et al. 2016). Some of these tidal tails extend for considerable distances on the sky (e.g. Grillmair & Johnson 2006; Kuzma et al. 2015). There are also stellar streams, such as the 63° long GD-1 (Grillmair & Dionatos 2006b) and the Aquarius Stream (Williams et al. 2011), that may originate from tidally disrupted star clusters. These kinematically cold structures point to a globular cluster as a parent but have no association with known clusters.

There is evidence that globular clusters are the origin of a significant fraction of stars in the bulge and halo of the Galaxy. Martell & Grebel (2010) found that 2.5 percent of ~1900 G- and K-type halo giants showed unusual light element abundance enhancements, which they interpreted as evidence that those stars had originally formed within globular clusters and then escaped from the cluster into the Galactic halo field. This abundance pattern had previously only been found in globular cluster stars. The generally accepted explanation for the light-element abundance variations in globular clusters is that they result from a second star-formation episode early in the history of the cluster, but there are alternate scenarios – for a review see Gratton et al. (2012). A further study, (Martell et al. 2011), showed that a minimum of 17 percent of the present-day mass of the stellar halo originally formed in globular clusters.

Globular cluster stellar streams have been used to trace the orbit of their progenitors and hence map the gravitational potential of the Galaxy. The stellar stream associated with Pal 5 was used to constrain the Galactic mass within its apogalactic radius (Küpper et al. 2015). Koposov et al. (2010) constrained the circular velocity at the Sun's radius, and the flattening of the Galactic total potential using the GD-1 stellar stream. Asymmetry, width variations and bumps and dips in the spatial density of tidal tails of globular clusters have been used to investigate the possible masses of dark matter subhaloes (Erkal et al. 2016), although other explanations such as the Galactic bar or giant molecular clouds were not definitively ruled out.

In this study, we conduct a search for extratidal halo stars around southern hemisphere globular clusters in the AEGIS (Aaomega Evolution of GalactIc Structure) spectroscopic survey catalogue. In Section 2 we describe the survey and the method we used to select target clusters. We provide some basic information on our target globular clusters in Section 3. From initial samples of candidate stars selected by V_r and position in Subsection 4.1, we utilise photometry in Subsection 4.2, $\log g$ and T_{eff} in Subsection 4.3, proper motions in Subsection 4.4 and metallicities in Subsection 4.5 to clean our samples. We also reduce and analyse the original AAOmega spectra of the observed fields within 5° of our target clusters to independently determine V_r and [Fe/H], and to measure spectral indices in Section 5. We look at the spatial distribution of the candidate member samples with respect to the adopted tidal radii in Section 6. We estimate the destruction rates of the clusters and compare them with the destruction rates from simulations in Section 7. Finally, we present and discuss the final list of candidate cluster halo stars in Section 8.

2 DATA AND INITIAL SELECTION PROCESS

AEGIS was a spectroscopic survey of 71,173 stars over ~630 deg^2 of the Southern sky (Figure 1). The general aim of the survey was to determine the density, chemistry and kinematics of thick disk and halo stars in order to constrain the chemodynamical evolution of the Galaxy.

The specific objectives were to (1) quantitatively determine the fraction of halo and thick disk stars accreted in mergers and find how this varied as a function of Galactocentric radius, (2) find the masses and star formation histories of accreted systems, and (3) understand dynamical heating from accretion, as well as how the processes of secular evolution, radial migration and in situ star formation affect metallicity and [α/Fe] gradients in the thick disk using abundance information. Part of the survey strategy was to allocate targets to specifically search for globular cluster tidal features. The observed fields covered areas in the vicinity of a number of southern hemisphere globular clusters, so the dataset potentially also included serendipitously observed extratidal stars of clusters.

Observations were obtained using the AAOmega spectrograph on the 3.9 m Anglo-Australian Telescope (AAT) at Siding Spring Observatory in Two-degree Field (2dF) fibre positioner multi-object spectrograph (MOS) mode[1]. AAOmega allows for the simultaneous acquisition of red and blue spectra with independent arms. For these observations, the red arm used the 1700D grating centred on 8540 Å to derive radial velocities (V_r) and overall metallicities ([Fe/H]) from the near-infrared Ca II triplet absorption lines (8498, 8542, and 8662 Å). The blue arm used the 580V grating to obtain overall [Fe/H] as well as [α/Fe] and [C/H]. The data were reduced using the standard 2dF data reduction pipeline (2dfdr) software and a modified SEGUE Stellar Parameter Pipeline (Lee et al. 2011) called the AEGIS Stellar Parameter Pipeline (ASPP). Depending on the target, parameters available from the ASPP include distance, V_r, T_{eff}, $\log g$, luminosity class, [Fe/H], [α/Fe], [Sr/Fe], [Ba/Fe] and [C/Fe].

The diversity of target types necessary to realise the AEGIS project goals required a complex target selection strategy. As described in the observing proposal for AAT time dated 14 Sep 2011:

> Targets are to be selected from... KM giants from combined SkyMapper and VISTA photometry, BHBs from $(u-v)$ SkyMapper colours, red clump from SkyMapper $(u-v)$ (to isolate low surface gravity) and VISTA IR colours, the thick disk from SkyMapper $(g-i)$ colour.

An important part of the overall strategy preferentially selected low-metallicity stars using photometric pre-imaging from the SkyMapper (Keller et al. 2007) survey, which observed the AEGIS fields in its commissioning phase. SkyMapper is an Australian photometric survey project of the Southern sky. It utilises an SDSS-like filter system, modified to include a Strömgren u filter that spans the Balmer jump and a v filter similar to DDO38 that spans the Ca II H and K lines. The u and v filters can be used to construct colour indices correlated with metallicity or surface gravity.

[1] Manuals and technical details at `http://www.aao.gov.au/science/instruments/current/AAOmega`

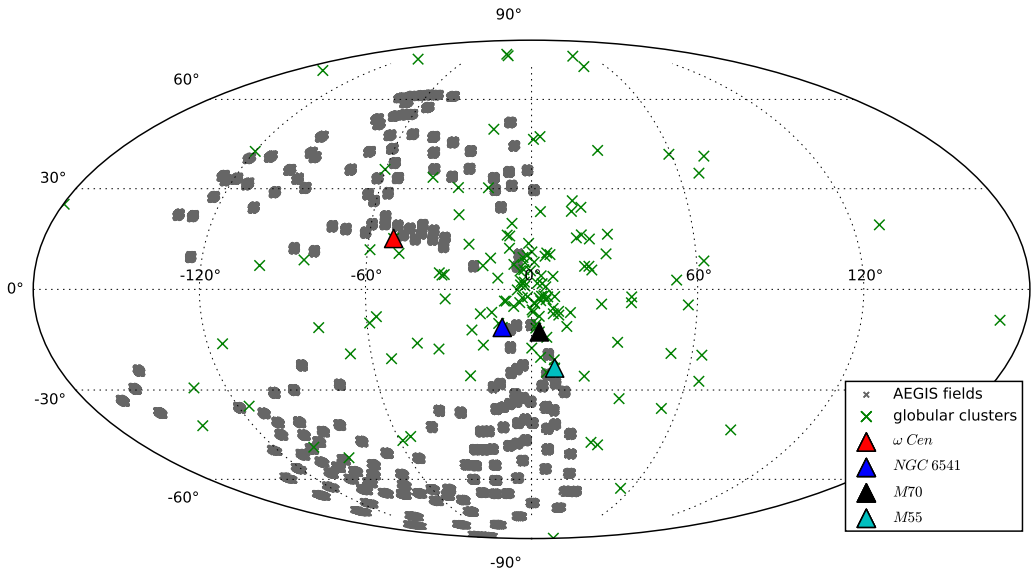

Figure 1. AEGIS AAOmega fields in Galactic coordinates centred at (l=0°, b=0°). All observed AEGIS stars are gray, green crosses show the positions of globular clusters, triangles show the position of our four target clusters.

The success of the selection for low [Fe/H] can be clearly seen in Casey et al. (2012, their fig 1) and in the top panels of Figure 8 where the [Fe/H] of observed stars around our target globular clusters is contrasted with that from a Galactic model of the same sky area produced by the Galaxia code (Sharma et al. 2011). In addition, targets were allocated to search for sparsely distributed objects, such as extremely metal-poor stars and QSOs, for which acquisition is normally costly in resources.

We used the Galaxia code to generate synthetic catalogues of stars to compare with the observations. We used the Besançon Milky Way model of Robin et al. (2003) for the disk and the simulated N-body models of Bullock & Johnston (2005) for the stellar halo. We generated 10 complete synthetic catalogues covering a 5° radius around each of our four target cluster's central position, giving radial velocities, space motions, metallicities and other properties of a stellar sample in those sky areas. To construct a model sample to match survey data it is necessary to select stars from the models with the same method used in the target input catalogue selection strategy. If the underlying selection function is simple and based on photometric colours and magnitudes, and the observational campaign is not substantially affected by weather and other practical constraints, the distribution of targets in a colour-magnitude plane enables a straightforward recovery of the selection strategy.

As described above, however, AEGIS used a complex selection function. This became obvious when we plotted various colour-magnitude diagrams (CMDs) of the catalogue members, e.g. V versus V-K$_s$ (see Figure 2). We reverse-engineered a reasonable envelope based on this V versus V-K$_s$ CMD and used it to construct distributions of the model stars, summed and normalised to have the same number of stars as the number of observed stars. This envelope was used to (1) construct the $V_{\rm r}$ and [Fe/H] distributions of model stars generated by Galaxia in Subsection 4.1 and Subsection 4.5, and (2) estimate AEGIS sample completeness for the calculation of cluster destruction rates in Section 7. We found significant differences between the distributions of $V_{\rm r}$ and [Fe/H] of the model and observed stars. The observed $V_{\rm r}$ distribution functions have offset peaks and show distinct extended high $V_{\rm r}$ tails compared to the model distributions (see the top panels of Figure 4). For the [Fe/H] distributions, the model distribution functions are narrower and much more metal-rich than those observed (see the top panels of Figure 8).

For this study the AEGIS data are supplemented with photometric data from the APASS (Henden et al. 2009) and 2MASS (Skrutskie et al. 2006) catalogs, and proper motions from the UCAC4 catalog (Zacharias et al. 2013).

In this search for extratidal stars of clusters, our first step was to identify target globular clusters that might have easily identifiable members or extratidal stars in the AEGIS catalog. We identified Southern Hemisphere globular clusters that had relatively high heliocentric radial velocities ($|V_{\rm r}| > 100$ km s^{-1}) to simplify differentiation of candidate stars from field stars in the same area of sky (typically field stars will have $|V_{\rm r}| < 50$ km s^{-1}). For each of these

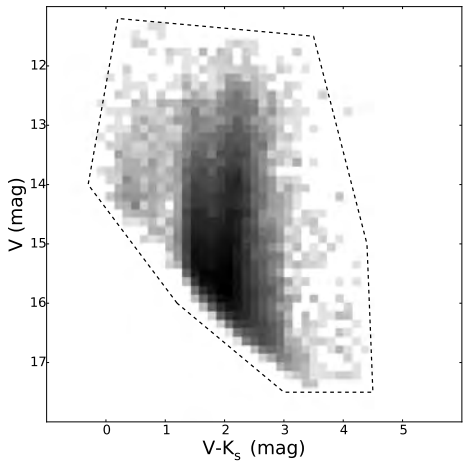

Figure 2. Hess diagram of the V versus V-K$_s$ CMD of 30339 stars with tabulated V and K$_s$ photometry observed by the AEGIS survey. The dashed black lines show the reverse-engineered envelope used to reconstruct the survey target selection strategy. There are 30290 stars inside the selection region.

clusters, we searched the AEGIS catalog to find 2dF fields with stars that had a $V_{\rm r}$ within ± 20 km s^{-1} of the cluster $V_{\rm r}$ and were within an angular distance of 5° of the cluster central position. We found candidate stars in the catalogue around six globular clusters that satisfied these criteria: ωCen (NGC 5139), M19 (NGC 6273), NGC 6541, M70 (NGC 6681), M55 (NGC 6809), and Terzan 8.

Terzan 8 and M19 are considerably fainter than the other clusters. Terzan 8 had only three candidate stars, and M19 had no candidate stars with photometry consistent with cluster red giant branch (RGB) stars. None of the Terzan 8 stars had all parameters consistent with cluster membership, so our analysis did not detect any candidate extratidal stars around either cluster. We investigate the stars around the remaining four clusters in this study.

3 BACKGROUND

Basic data on the target globular clusters is included in Table 1.

3.1 ω Cen (NGC 5139)

ω Cen is the most massive Galactic globular cluster and has been extensively studied and modelled. It is a complex system and there are multiple strands of evidence that it is the stripped core of a now-destroyed dwarf galaxy (Bekki & Freeman 2003). It has a wide metallicity range and two main sequences (e.g. Lee et al. 1999; Smith et al. 2000; Bedin et al. 2004; Johnson & Pilachowski 2010). It has a very low-inclination retrograde orbit (Dinescu et al. 1999), is currently crossing the plane of the Galactic disk, and has an overall rapid rotation (Merritt et al. 1997). It also has a high central velocity dispersion, which may be an indication that it hosts an intermediate mass black hole (Noyola et al. 2008). Another clue to its origin are the parallels with M54 (NGC 6715), another massive Galactic globular cluster. M54 is widely accepted as the nuclear star cluster of the Sagittarius dwarf galaxy and it has apparent chemical similarities to ω Cen (Carretta et al. 2010b).

Searches for the remains of the now destroyed progenitor of ω Cen in the surrounding area have yielded mixed results. Leon et al. (2000) found evidence of two large tidal tails perpendicular to the Galactic plane, which they estimated corresponded to ~0.6 percent of the total cluster mass. A study of stars in 2MASS data by Law et al. (2003) found apparent tidal tails around the cluster, but they disappeared when differential reddening was taken into account. They proposed that the tidal tails of Leon et al. (2000) could also have been artefacts of differential reddening as they were spatially very similar. Chen & Chen (2010) used the spatial distribution of 2MASS point sources to determine the morphological distortion of 116 globular clusters. ω Cen was listed as exhibiting possible filamentary structures or clumpiness, perhaps as a result of stripped cluster members, but the authors acknowledged that these density enhancements could be a result of random statistical fluctuations.

Da Costa & Coleman (2008) conducted an extensive spectroscopic survey of RGB stars in a 2.4° × 3.9° area around ω Cen. They identified only six likely extratidal stars among 4105 photometrically selected candidates, corresponding to ~0.7 percent of the total cluster mass. This was consistent with models that predict that most of the tidal stripping occurred a long time ago and that most ex-cluster members would now be widely distributed around the Galaxy. However, Anguiano et al. (2015) identified 52 potential stellar members of ω Cen in the RAVE catalogue (Steinmetz et al. 2006), and 21 of those stars were outside the tidal radius.

Studies finding evidence of even more widely distributed debris from ω Cen have been somewhat more successful. Numerical simulations (e.g. Bekki & Freeman 2003) show that stellar debris from ω Cen (NGC 5139) is likely to be found moving in retrograde orbits near the solar circle. Dinescu (2002) identified stars in a large low metallicity sample (Beers et al. 2000) with a retrograde signature resembling that of the orbit of ω Cen. Mizutani et al. (2003) modelled a tidally disrupted dwarf with an ω Cen-like central cluster and found that the model predicts a kinematic substructure similar to a large radial velocity stream observed by Gilmore et al. (2002). Meza et al. (2005) also used simulations that predicted a distinct kinematic substructure in nearby metal-poor stars. They found nearby stars in compilations (Gratton et al. 2003) that not only exhibited this signature, but also had distinct chemical abundance signatures similar to those of ω Cen. Majewski et al. (2012) found a number of kinematically coherent groups of giant stars in the solar neighbourhood. One group, covering 60° in Galactic longitude, had distances and velocities consistent with models of ω Cen debris. High-resolution spectra of a sample of these stars showed most had a [Ba/Fe] versus [Fe/H] chemical signature thought to be specific to ω Cen mem-

Table 1. Basic data on the target globular clusters

	E($B-V$) (mag)	V_{HB} (mag)	$(m-M)_V$ (mag)	V_t (mag)	$R_\odot$ (kpc)	R_{gc} (kpc)	[Fe/H] (dex)	V_r (km s^{-1})	$\mu_\alpha cos(\delta)$ (mas yr^{-1})	μ_δ (mas yr^{-1})	r_t (arcmin)
ω Cen (NGC 5139)	0.12	14.51	13.94	3.68	5.2	6.4	−1.53	232.1	−6.01	−5.02	48.4
NGC 6541	0.14	15.35	14.82	6.30	7.5	2.1	−1.81	−158.7	−3.24	−1.74	13.0
M70 (NGC 6681)	0.07	15.55	14.99	7.87	9.0	2.2	−1.62	220.3	3.84	−5.78	9.5
M55 (NGC 6809)	0.08	14.40	13.89	6.32	5.4	3.9	−1.94	174.7	0.49	−8.49	15.3

Notes. Data from Harris (1996) (2010 edition) catalog. V_{HB} is the V magnitude of the horizontal branch (HB), $(m-M)_V$ is the apparent visual distance modulus, V_t is the integrated V magnitude of the cluster. Proper motions $\mu_\alpha cos(\delta)$ and μ_δ are from Kharchenko et al. (2013). Central concentration (c) and core radius (r_c) from McLaughlin & van der Marel (2005), tidal radius (r_t) calculated from $c = log\,\frac{r_t}{r_c}$

bers. Fernández Trincado et al. (2013) found an overdensity of 13 extratidal RR Lyrae stars at distances similar to ω Cen (5.2 kpc) up to 9° from the centre of the cluster.

3.2 NGC 6541

NGC 6541 is a relatively unstudied metal-poor globular cluster located in the inner halo or bulge. Its location near the Galactic bulge (R_{gc} = 2.1 kpc and z = -1.5 kpc) suggests an increased likelihood of tidal tail formation. Bica et al. (2016) classed NGC 6541 as a probable halo intruder, however O'Malley et al. (2017) characterised it as a bulge globular cluster as its orbit did not extend further than 4 kpc from the Galactic centre. The previously cited Chen & Chen (2010) study included NGC 6541 and listed it as exhibiting clumpy features. It lies outside the survival boundaries on the globular cluster vital diagrams shown as figures 21–24 of Gnedin & Ostriker (1997), favouring the possibility of a higher mass loss rate. The only existing spectroscopic study (Lee & Carney 2001) consists of just two RGB stars, yielding an overall [Fe/H] = -1.76 dex and abundances for 15 other elements.

3.3 M70 (NGC 6681)

M70 is metal-poor, characterised as a disk globular cluster by O'Malley et al. (2017) as its orbit extended to 8 kpc from the Galactic centre but no further than 5 kpc from the Galactic plane. Chen & Chen (2010) also listed M70 as clumpy. There is an increased likelihood of tidal tail formation due to its current location near the Galactic bulge (R_{gc}= 2.2 kpc). An increased rate of mass loss is probable as, like NGC 6541, it is also outside the survival boundaries of the globular cluster vital diagrams (figures 21–24 of Gnedin & Ostriker (1997)).

3.4 M55 (NGC 6809)

M55 is relatively nearby, luminous, and metal-poor. It is only 3.9 kpc from the Galactic centre, but has been classed as a halo intruder to the Galactic bulge by Bica et al. (2016). O'Malley et al. (2017) characterise it as a disk globular cluster. Its Galactic latitude (b = -23°) means that interstellar reddening and contamination are low. It is another cluster that lies outside the survival boundaries on the vital diagrams. Leon et al. (2000) found evidence of overdensities aligned with the tidal field gradient that could result from tidal shocking, but conceded that dust absorption made the interpretation difficult for this cluster. Chen & Chen (2010) also listed M55 as exhibiting clumpy structure. However, Kiss et al. (2007) found little evidence of the presence of extratidal stars in a 2° radius around M55 in a study of 3571 photometrically selected RGB stars.

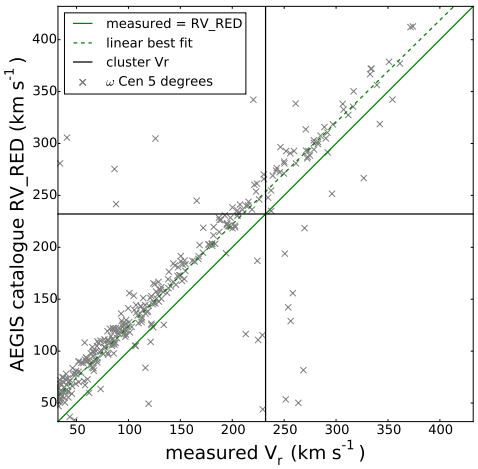

Figure 3. Offset between our measurements of V_r using the original AAOmega spectra and the V_r in the AEGIS catalogue measured from the red spectra (RV_RED) for stars within 5° of the centre of ω Cen. The solid green line shows the one-to-one relationship, the dashed green line shows the linear best fit to the data. The horizontal and vertical black lines show the ω Cen V_r.

4 CANDIDATE SELECTION

4.1 Heliocentric radial velocities

We chose to use our own V_r measurements for candidate selection rather than the AEGIS catalogue V_r. There are several V_r measurements in the AEGIS catalogue, the most

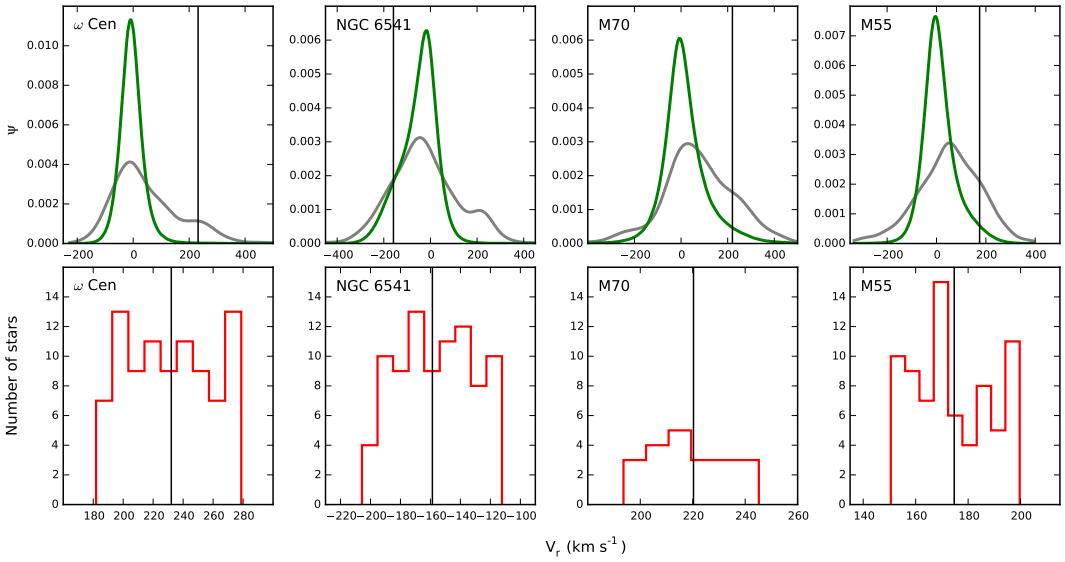

Figure 4. Top panels: Gray: Kernel density estimations of the V_r distributions of all the observed stars within a radius of 5° of the central position of the target globular clusters. Green: Kernel density estimations of the predicted V_r distributions of the Milky Way model generated by the Galaxia code. Bottom panels: Histograms of the V_r distributions of the candidate halo stars for the target clusters. The vertical black lines show the cluster V_r (Harris 1996) (2010 edition) catalog.

relevant of which is RV_RED – the "radial velocity from red spectral region (6000-9000 Å)" in the AEGIS catalogue description. As part of our analysis we re-measured the V_r for all the stars in the observed fields within 5° of our target clusters. For this we used the Ca II triplet lines in the red arm spectra from the original AAOmega spectra obtained from the AAT archive (see Section 5), as described in Subsection 5.1. We found a significant systematic offset (see Figure 3; the plots for the other clusters are similar) of ~20-25 $\mathrm{km\,s^{-1}}$ between our measurements and RV_RED. To try to find the source of this offset, we cross-checked the AEGIS catalogue against the RAVE DR5 catalog (Kunder et al. 2016) and found 56 stars in common. The V_r values of the stars in the RAVE catalog also showed an offset of similar size and in the same sense. Inspection of plots of the original spectra with spectra from AEGIS data files shows that the AEGIS data spectra appear to be redshifted by ~1 Å. We suspect that this offset was introduced by an "off-by-one-pixel" error in the wavelength solution used by the ASPP. Consequently, we used our own V_r measurements for candidate selection.

None of the target cluster centres were covered by an observed AAOmega field as a result of the sparse sampling of sightlines in the AEGIS survey (see Figure 1 and Figure 12). This meant that the technique of Frinchaboy & Majewski (2008), which we applied in Navin et al. (2015), could not be used to select candidate members using V_r. The method assumes that stars between two and three (or some reasonable multiples) times the tidal radius of the cluster central position constitute a sample of field stars with minimal contamination by cluster stars, and stars inside the tidal radius constitute a sample of cluster stars with minimal contamination by field stars. The product of the process is a probability distribution function based on the radial velocities of the cluster members. This can be used to determine a reasonable limit of V_r around the systemic cluster V_r for selection of candidates, and to calculate the cluster membership probabilities P_c of those candidates on the basis of V_r.

We had no other parameters available where (1) cluster stars have an area in the parameter space that is only occupied by them with minimal contamination by field stars, and (2) field stars have an area in parameter space that is only occupied by them with minimal contamination by cluster stars. We considered all the parameters that we used for selection (photometry, log g and T_{eff}, proper motions and [Fe/H]) but there was likely to be considerable contamination of candidate samples by field stars in all these parameters. As it was not possible to use this method with this dataset, we used a simple V_r cut to select candidate stars. We adopted the limits for each cluster as the quadrature addition of the mean V_r errors of the AEGIS stars within 5° of each cluster centre plus the central velocity dispersion of the cluster from the Harris (1996) (2010 edition) catalog.

Figure 4 shows kernel density estimations and histograms of the measured V_r for stars around our target clusters. All the V_r distributions of the observed stars in the top panels show a prominent peak that we identify as predominantly Galactic disk or halo field stars (not members of the cluster), plus (possibly) an unknown number of cluster extratidal stars. The top panels also show the model V_r distribution of stars in the same area of sky generated by the Galaxia code as described in Section 2. The clear differences between the model and observed V_r distributions (offset peaks and extended high V_r tails) reflect the AEGIS target selection strategy. The bottom panels are expanded histograms centred on the V_r of the cluster, showing only the candidate stars.

The numbers of stars selected by V_r plus the adopted V_r limit for each of our target clusters is shown in Table 2, and the V_r for each of our final list of candidates is shown in Table 3.

4.2 Photometry

Figure 5 shows the V versus V-K$_s$ CMD of candidate stars around our target clusters.

The plots also show the PARSEC isochrones (Bressan et al. 2012) generated for each cluster that we used to determine the selection limits. We adopted [α/Fe] = 0.30 dex for all target clusters as they all had [Fe/H] < -1.0 dex (Marin-Franch et al. 2009), and age = 12.6 Gyr from the Milky Way Star Clusters (MWSC) catalog (Kharchenko et al. 2013), as input parameters for calculation of the isochrones for all the clusters. The parameters ([Fe/H], $(m-M)_V$ and V_{HB}) for producing the isochrones are in Table 1. Other inputs to the isochrone calculations are as follows: ω Cen - Z = 0.00073, total extinction A_v = 0.384 mag; NGC 6541 - Z = 0.00038, A_v = 0.448 mag; M70 - Z = 0.00060, A_v = 0.224 mag; M55 - Z = 0.00029, A_v = 0.256 mag.

We based our V versus V-K$_s$ limits on selecting stars close to the cluster PARSEC isochrone RGB. The magnitudes of the observed stars with respect to the isochrones mean that any dwarfs observed must be foreground stars and potential cluster members must be giants. The dashed black lines show the V versus V-K$_s$ boundaries we adopted for candidate selection. We chose the boundaries as ±0.5 mag in V-K$_s$ and the V magnitude range to incorporate the range of the RGB.

The numbers of stars selected by photometry for each of our target clusters are shown in Table 2, and the V and K$_s$ magnitudes for each of our final list of candidates is shown in Table 3.

4.3 Stellar parameters (surface gravity and effective temperature)

Figure 6 shows the log g versus T$_{\rm eff}$ diagram of candidate stars around our target clusters. The plots show the same PARSEC isochrones for each cluster in log g versus T$_{\rm eff}$ space, produced with the same input parameters as the V versus V-K$_s$ isochrones.

As with the photometry (Subsection 4.2), we based the log g versus T$_{\rm eff}$ limits on selecting stars close to the cluster PARSEC isochrone RGB. The dashed black lines show the log g versus T$_{\rm eff}$ boundaries that we adopted. This incorporates a cut at log g = 3.5 to separate dwarfs from giants and the width of the box is ±0.05 in log(T$_{\rm eff}$).

The numbers of stars selected by log g and T$_{\rm eff}$ for each of our target clusters are shown in Table 2, and the log g and T$_{\rm eff}$ for each of our final list of candidates is shown in Table 3.

4.4 Proper motions

We also used proper motions to identify and remove field star contamination from our data set. We obtained the absolute proper motions of all remaining candidate stars of the target clusters from the UCAC4 catalog (Zacharias et al. 2013). We obtained the cluster proper motions (listed in Table 1) from Kharchenko et al. (2013). Figure 7 shows plots of the absolute proper motions of the candidate stars. We accepted stars with proper motions that are within 10 mas yr^{-1} of the cluster proper motion (black dashed circles on Figure 7).

The numbers of stars selected by proper motions for each of our target clusters are shown in Table 2, and the proper motions for each of our final list of candidates is shown in Table 3.

4.5 Metallicities

Extratidal halo stars of a globular cluster are expected to have a similar [Fe/H] to that of stars in the cluster. ω Cen is known to have a wide [Fe/H] range of ~ -2.2– -0.5 dex with a metallicity distribution function (MDF) peak at ~-1.7 dex (Smith et al. 2000; Johnson & Pilachowski 2010). No studies have shown star-to-star [Fe/H] metallicity variations for NGC 6541 (Chen & Chen 2010), M70 (Carretta et al. 2009c) or M55 (Carretta et al. 2009c,b,a).

Kernel density estimations and histograms of the AEGIS catalogue [Fe/H] for stars around our target globular clusters are shown in Figure 8. We identify the prominent peak in all the [Fe/H] distributions of the observed stars in the top panels as predominantly Galactic disk or halo field stars (non-cluster members), plus potentially an unknown number of cluster extratidal stars. The model [Fe/H] distribution of stars in the same area of sky Section 2 are also shown in the top panels. The differences between the model and observed [Fe/H] distributions (the data are generally wider and much more metal-poor) reflect the AEGIS target selection strategy. The bottom panels are expanded versions showing only the candidate stars centred on the [Fe/H] of the cluster.

In view of the large [Fe/H] range of ω Cen, we did not eliminate any of the candidates on the basis of [Fe/H]. For the other clusters, we adopted a limit of ±0.2 dex of the cluster mean.

The numbers of stars selected by [Fe/H] for each of our target clusters are shown in Table 2, and the [Fe/H] for each of our final list of candidates is shown in Table 3.

5 ANALYSIS OF ORIGINAL AAOMEGA SPECTRA

We obtained the original spectra of the fields surrounding our target clusters (see Figure 1 and Figure 12) from the

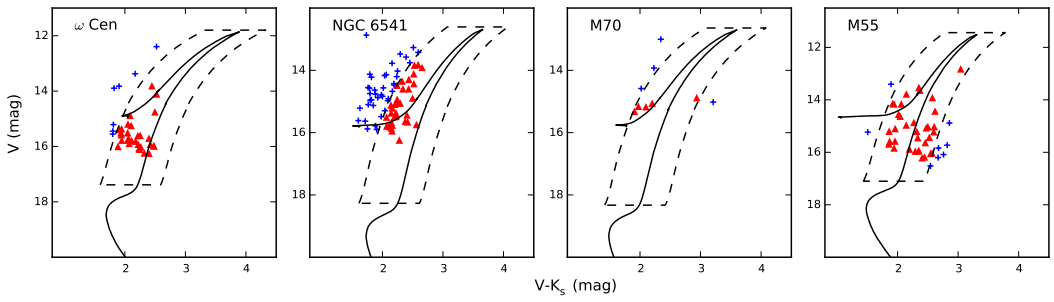

Figure 5. V versus V-K$_s$ CMD of candidate stars around target globular clusters. The solid black line shows the PARSEC isochrone for the cluster. The dashed black line shows the boundary for candidate selection based on V versus V-K$_s$ photometry. The stars are colour-coded with stars inside the V versus V-K$_s$ limits box as red triangles and stars outside the limits as blue crosses.

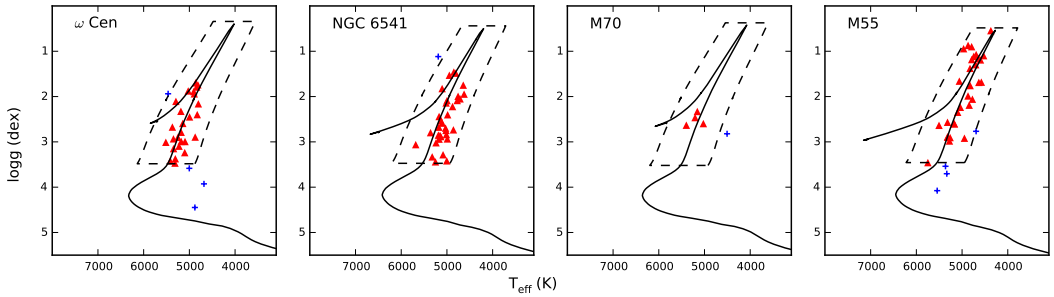

Figure 6. log g versus T$_{\rm eff}$ diagram of candidate stars around target globular clusters. The solid black line is the PARSEC isochrone for the cluster. The dashed black line shows the boundary for candidate selection based on the log g versus T$_{\rm eff}$ limits box. The stars are colour-coded with stars inside the log g versus T$_{\rm eff}$ limits box as red triangles and stars outside the limits as blue crosses.

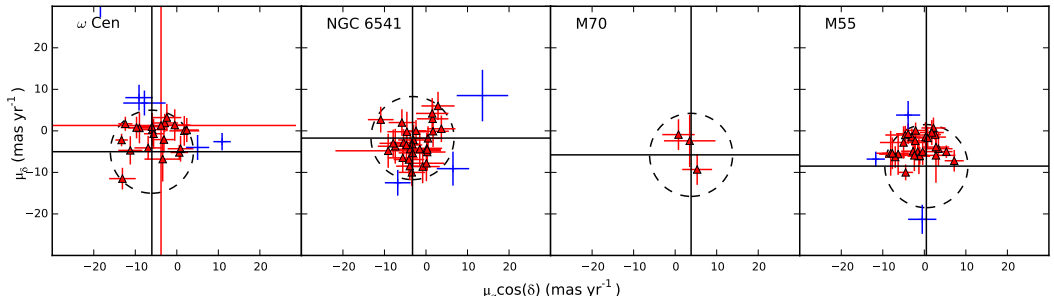

Figure 7. Absolute proper motions of the candidate stars of target globular clusters. Red triangles denote stars with proper motions within 10 mas yr^{-1} of the cluster proper motion. Blue crosses denote stars that have proper motions more than 10 mas yr^{-1} different from the cluster proper motion (there are also several stars outside the plot limits). The error bars show the tabulated UCAC4 mean errors. The vertical and horizontal black lines indicate the cluster proper motion and the black dashed circle indicates the 10 mas yr^{-1} limit.

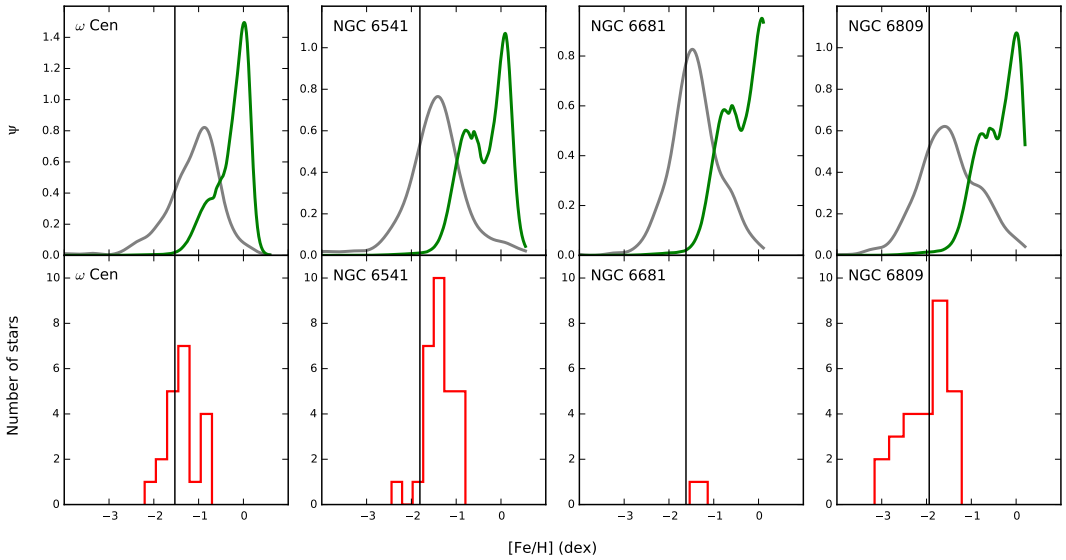

Figure 8. Top panels: Gray: Kernel density estimations of the [Fe/H] distributions of all the observed stars within a radius of 5° of the target clusters central position. Green: Kernel density estimations of the predicted [Fe/H] distributions of the Milky Way model generated by the Galaxia code (Sharma et al. 2011). Bottom panels: Histograms of the [Fe/H] distributions of the candidate halo stars for the target clusters. The vertical black line indicates the cluster [Fe/H] (Harris 1996) (2010 edition) catalog.

Table 2. Candidate selection

Stars within	5° of cluster centre	V_r limits	photometric limits	T_{eff} and log g limits	proper motion limits	[Fe/H] limits
ω Cen (NGC 5139)	756	89	30	26	20	20[1]
NGC 6541	502	86	34	33	29	6
M70 (NGC 6681)	226	21	5	4	3	1
M55 (NGC 6809)	689	75	35	31	27	6

Notes.[1] [Fe/H] was not used to eliminate candidate stars for ω Cen

AAT Data Archive[2]. Using the original spectra we measured (1) V_r and [Fe/H] using the Ca II triplet lines as a verification of AEGIS catalogue values (see Subsection 5.1 and Subsection 5.2), and (2) CH and CN line indices to provide additional parameters to confirm or reject stars as cluster members (see Subsection 5.3).

We used the standard AAO 2dF data reduction pipeline (2dfdr) version 6.28 with the default configuration files appropriate for each grating. 2dfdr automatically performs bias subtraction using the overscan, tramline fitting using the fibre flat, wavelength calibration using the arc exposure, extraction of spectra, sky subtraction using fibres assigned to sky positions, and the combination of the individual exposures of each star. We eliminated spectra with low (≤ 5) S/N ratios from the analysis. For individual spectra, we deleted and interpolated across points with large ($\geq 10^6$) values of variance (as calculated by 2dfdr) using Python code written for the reduction and analysis. In a few cases we also used the IRAF task `splot` to manually remove anomalous spectral features. An example of the blue and red arm AAOmega spectra for one of the ω Cen candidate members (AEGIS catalogue ID 2617_1_351, 2MASS identification 13294957-4321148) is shown in Figure 9.

[2] `http://site.aao.gov.au/arc-bin/wdb/aat_database/observation_log/make`

Table 4 contains V_r, [Fe/H] and spectral indices measured from spectra for candidate stars.

Table 3. Candidate cluster halo stars

2MASS ID	AEGIS catalogue ID	RA (degrees)	Dec (degrees)	V_r ($km\,s^{-1}$)	V (mag)	K_s (mag)	T_{eff} (K)	log g (dex)	R (arcmin)	$\mu_\alpha cos(\delta)$ (mas yr^{-1})	μ_δ (mas yr^{-1})	[Fe/H] (dex)
ω Cen (NGC 5139)												
13325691-4348382	2617_1_017	203.237000	-43.811001	193.9	16.0	13.5	4839	1.8	229.4	-0.5	1.4	-1.45
13301033-4400416	2617_1_058	202.542999	-44.012001	271.0	16.0	13.5	4804	2.2	211.0	-5.9	0.3	-1.07
13295909-4422479	2617_1_081	202.496002	-44.380001	223.7	15.7	13.3	4862	1.7	188.9	-2.9	1.9	-1.87
13284901-4401013	2617_1_111	202.203995	-44.016998	273.2	15.5	13.6	5314	3.5	208.8	-11.2	-4.7	-1.22
13240373-4320218	2617_1_215	201.016006	-43.340000	213.0	14.8	12.3	4873	2.9	250.0	0.6	-5.2	-1.52
13242022-4311115	2617_1_229	201.084000	-43.187000	246.2	16.0	13.8	4813	1.7	258.8	-3.1	-2.1	-1.69
13273946-4316289	2617_1_265	201.914001	-43.275002	213.5	15.9	13.7	5179	3.0	252.4	-5.6	-0.7	-1.45
13281225-4241490	2617_1_293	202.050995	-42.696999	278.8	15.2	13.1	5515	3.0	287.3	-12.4	1.7	-0.74
13282501-4237381	2617_1_296	202.104004	-42.626999	187.1	15.8	13.8	5418	3.4	291.7	-13.1	-11.5	-0.89
13291663-4328179	2617_1_335	202.319000	-43.472000	215.7	16.2	13.9	5101	3.2	241.9	1.8	0.0	-0.71
13294957-4321148	2617_1_351	202.457001	-43.354000	222.9	13.8	11.4	4904	1.9	249.6	-13.3	-2.2	-1.46
13313982-4314192	2617_1_365	202.916000	-43.238998	198.4	16.2	13.8	4893	1.9	259.6	-3.4	-6.8	-1.89
13303920-4324422	2617_1_371	202.662994	-43.411999	189.1	15.8	13.7	5226	3.1	247.4	-9.0	0.7	-1.43
13440923-4646533	2730_1_108	206.037994	-46.782001	219.0	16.1	13.9	5025	1.9	182.1	-3.8	1.3	-2.20
13434667-4629556	2730_1_120	205.945007	-46.499001	195.1	15.7	13.6	5294	2.1	183.5	0.9	-4.3	-1.33
13414597-4611521	2730_1_167	205.442001	-46.198002	205.0	14.1	11.6	4828	2.4	171.8	-9.7	0.8	-1.20
13393344-4554306	2730_1_201	204.889008	-45.909000	245.7	15.2	13.1	5185	2.3	161.7	2.4	0.2	-1.53
13410344-4549131	2730_1_211	205.264008	-45.820000	239.0	15.8	13.7	5348	2.9	177.5	-2.4	3.2	-1.37
13440360-4547255	2730_1_262	206.014999	-45.790001	187.5	15.6	13.3	4996	2.4	204.7	-6.0	1.0	-1.52
13472153-4502479	2730_1_329	206.839996	-45.047001	194.7	15.5	13.5	5372	2.7	258.4	-6.9	-4.1	-0.70
NGC 6541												
18154675-3931539	2406_1_138	273.945007	-39.532001	-195.7	15.8	13.7	4849	1.5	265.5	-7.4	-3.7	-1.68
18221874-4152282	2525_1_038	275.578003	-41.874001	-139.6	15.1	12.8	5133	2.5	192.0	-3.9	-8.5	-1.65
18195922-4134263	2525_1_043	274.997009	-41.574001	-196.7	15.4	13.2	5105	1.8	184.0	-1.5	-4.4	-1.69
18140795-4140225	2525_1_171	273.532990	-41.673000	-156.2	15.7	13.2	5012	2.8	139.7	-3.8	-4.4	-1.83
18141057-4059179	2525_1_226	273.544006	-40.987999	-145.7	15.1	12.8	5030	2.7	177.2	-3.2	-5.3	-1.73
18152617-4036395	2525_1_259	273.859009	-40.611000	-139.7	14.4	11.9	4775	2.1	203.6	-5.4	-2.8	-1.69
M70 (NGC 6681)												
18280626-3356317	2157_1_258	277.026001	-33.942001	207.3	15.2	13.1	5157	2.3	214.1	3.5	-2.4	-1.54
M55 (NGC 6809)												
19173299-3101242	2031_1_284	289.386993	-31.023001	179.1	14.6	12.6	5318	2.6	288.6	2.6	-0.9	-1.93
19182697-3056159	2031_1_302	289.612000	-30.938000	151.4	13.8	11.6	5060	1.7	277.2	-2.2	-2.4	-1.85
19205914-3145450	2031_1_398	290.246002	-31.761999	169.1	14.1	12.2	5504	2.6	248.1	-8.1	-5.4	-1.75
19593502-3157115	2035_1_188	299.895996	-31.952999	183.9	15.8	13.9	5276	3.0	257.5	-3.9	-0.7	-1.99
19454777-3403327	2164_1_008	296.449005	-34.058998	169.7	15.9	13.6	5037	2.2	199.6	0.3	-1.5	-2.11
19412385-3402099	2164_1_207	295.348999	-34.035999	168.7	15.6	13.2	4744	1.1	185.1	-2.4	-5.9	-1.76

Notes. Values are from the AEGIS catalogue except for V_r, which is measured from AAOmega red arm spectra. The 2MASS ID is from Skrutskie et al. (2006) and the proper motions $\mu_\alpha cos(\delta)$ and μ_δ are from Kharchenko et al. (2013). R = radial distance from cluster centre.

5.1 Radial velocity from the Ca II triplet lines in the red arm spectra

The Ca II triplet absorption lines are the strongest features in the near-infrared spectra of cool G, K, and M-type giants and dwarfs, even in low-metallicity halo stars, and are ideal for measuring radial velocities. We used a Monte Carlo method to measure V_r from the Ca II triplet lines in the red arm spectra. We produced 100 different realizations of the spectra by adding a value – drawn from a Gaussian distribution with a standard deviation equal to the square root of the variance calculated by 2dfdr at that wavelength point – to each flux point.

We normalised each realization of the spectrum by iteratively fitting a fifth-degree Chebyshev polynomial with SCIPY's CHEBFIT function. We rejected flux values if they were 0.1σ below or 0.5σ above the fit, and stopped the iteration when 1000 spectral points remained. We refined the normalisation by making a linear fit to the mean flux values in the five continuum regions of Cenarro et al. (2001) using the method of Carrera et al. (2013). We located the Ca II triplet lines in each spectrum and fitted each line with a Voigt function (a convolution of Gaussian and Lorentzian functions) using VOIGT1D from ASTROPY (Astropy Collaboration et al. 2013). We found the best fitting Voigt function using a least-squares fit from the Levenberg-Marquardt algorithm implemented by LEVMARLSQFITTER from ASTROPY. We used the central wavelength of the Voigt function for each Ca II triplet line to calculate V_r and chose the median of these values, corrected to the heliocentric reference frame, as the V_r for each realization.

We adopted the median of the 100 calculated values as the star's heliocentric V_r and the uncertainty as half the range between the 16^{th} and 84^{th} percentile values of V_r.

Table 4. Candidate cluster halo stars – AAOmega measurements

2MASS ID	AEGIS catalogue ID	V_r ($km\,s^{-1}$)	$\sigma(V_r)$ ($km\,s^{-1}$)	[Fe/H] (dex)	σ([Fe/H]) (dex)	S(3839)	σS(3839)	S_2(CH)	σS_2(CH)	CH(4300)	σCH(4300)
ω Cen (NGC 5139)											
13325691-4348382	2617_1_017	193.9	6.3	-	-	0.06	0.02	1.98	0.04	1.14	0.02
13301033-4400416	2617_1_058	271.0	3.2	-	-	-0.08	0.23	1.99	0.07	1.23	0.06
13295909-4422479	2617_1_081	223.7	0.7	-	-	-0.27	0.04	1.71	0.02	0.99	0.01
13284901-4401013	2617_1_111	273.2	1.4	-	-	-0.12	0.02	1.81	0.01	1.07	0.01
13240373-4320218	2617_1_215	213.0	65.3	-	-	-0.06	0.06	1.90	0.02	1.12	0.01
13242022-4311115	2617_1_229	246.2	24.8	-	-	-0.63	0.07	1.63	0.03	0.88	0.05
13273946-4316289	2617_1_265	213.5	0.9	-	-	-0.31	0.02	1.80	0.01	1.05	0.00
13281225-4241490	2617_1_293	278.8	0.7	-	-	-0.22	0.02	1.74	0.01	1.00	0.00
13282501-4237381	2617_1_296	187.1	4.0	-	-	-0.23	0.02	1.85	0.01	1.03	0.02
13291663-4328179	2617_1_335	215.7	1.4	-	-	0.02	0.03	1.87	0.01	1.07	0.01
13294957-4321148	2617_1_351	222.9	0.2	-1.45	0.01	-0.18	0.00	1.81	0.00	1.04	0.00
13313982-4314192	2617_1_365	198.4	1.0	-	-	-0.27	0.02	1.81	0.01	1.05	0.00
13303920-4324422	2617_1_371	189.1	1.8	-	-	-0.30	0.03	1.82	0.01	1.03	0.01
13440923-4646533	2730_1_108	219.0	0.7	-	-	-0.32	0.02	1.71	0.01	1.04	0.01
13434667-4629556	2730_1_120	195.1	0.6	-	-	-0.28	0.01	1.69	0.01	1.02	0.01
13414597-4611521	2730_1_167	205.0	0.3	-0.88	0.01	-0.06	0.02	1.86	0.00	1.15	0.00
13393344-4554306	2730_1_201	245.7	0.5	-	-	-0.36	0.02	1.81	0.01	1.11	0.01
13410344-4549131	2730_1_211	239.0	1.6	-	-	-0.31	0.02	1.75	0.01	1.09	0.00
13440360-4547255	2730_1_262	187.5	0.7	-	-	-0.33	0.02	1.83	0.01	1.13	0.01
13472153-4502479	2730_1_329	194.7	1.0	-	-	-0.10	0.02	1.83	0.01	1.14	0.00
NGC 6541											
18154675-3931539	2406_1_138	-195.7	10.5	-	-	0.37	0.12	1.79	0.05	1.12	0.02
18221874-4152282	2525_1_038	-139.6	1.1	-1.39	0.11	-0.40	0.06	1.65	0.01	1.03	0.01
18195922-4134263	2525_1_043	-196.7	0.9	-	-	-0.25	0.03	1.67	0.02	1.07	0.02
18140795-4140225	2525_1_171	-156.2	0.6	-	-	-0.08	0.05	1.70	0.02	1.14	0.01
18141057-4059179	2525_1_226	-145.7	0.7	-1.49	0.09	-0.18	0.04	1.72	0.01	1.11	0.00
18152617-4036395	2525_1_259	-139.7	0.5	-1.25	0.02	-0.15	0.04	1.69	0.02	1.10	0.01
M70 (NGC 6681)											
18280626-3356317	2157_1_258	207.3	0.7	-1.55	0.03	-0.27	0.01	1.83	0.00	1.11	0.01
M55 (NGC 6809)											
19173299-3101242	2031_1_284	179.1	0.2	-	-	-0.37	0.01	1.68	0.00	0.99	0.00
19182697-3056159	2031_1_302	151.4	0.1	-1.78	0.00	-0.34	0.01	1.63	0.00	0.94	0.00
19205914-3145450	2031_1_398	169.1	0.1	-2.35	0.00	-0.31	0.01	1.70	0.00	1.05	0.00
19593502-3157115	2035_1_188	183.9	0.8	-	-	-0.36	0.02	1.72	0.01	0.99	0.01
19454777-3403327	2164_1_008	169.7	0.5	-	-	-0.24	0.06	1.72	0.01	1.01	0.01
19412385-3402099	2164_1_207	168.7	0.4	-	-	-0.22	0.01	1.75	0.01	1.03	0.00

Notes. S(3839), S_2(CH), and CH(4300) are the spectral indices measured from the AAOmega blue arm spectra. σS(3839), σS_2(CH), and σCH(4300) are the corresponding uncertainties in the measurements.

Table 4 and Table 3 contain our calculated V_r and uncertainties, which we used for the candidate selection process (see Subsection 4.1).

5.2 Metallicity from the Ca II triplet lines in the red arm spectra

The Ca II triplet lines have been used extensively in globular cluster studies to estimate the metallicity of member stars (e.g. Armandroff & Da Costa 1991). A number of Ca II triplet empirical relations have been developed by different authors (e.g. Starkenburg et al. 2010; Carrera et al. 2013; Yong et al. 2014). They connect a linear combination of two or three of the equivalent widths (EWs) of the Ca II triplet lines and the luminosity of the star. The luminosity of the star is commonly obtained from the V magnitude of the star relative to the V magnitude of the HB of the cluster ($V - V_{HB}$), but other indicators have also been used. In this work we used the calibration of Carrera et al. (2013):

$$\begin{aligned}[\mathrm{Fe/H}] &= 3.45 \pm 0.04 \\ &+ (0.11 \pm 0.02 \times (V - V_{HB})) \\ &+ (0.44 \pm 0.006 \times \Sigma W) \\ &- (0.65 \pm 0.12 \times \Sigma W^{-1.5}) \\ &+ (0.03 \pm 0.003 \times \Sigma W \times (V - V_{HB})) \end{aligned} \quad (1)$$

where

$$\Sigma W = EW_{8498} + EW_{8542} + EW_{8662} \quad (2)$$

and EW_{8498}, EW_{8542}, and EW_{8662} are the measured EWs of the 8498, 8542 and 8662 Å Ca II triplet lines, respectively.

We chose this calibration as it covers a wide range of [Fe/H] and is valid for a range ~5 mag in V–V_{HB} luminosities

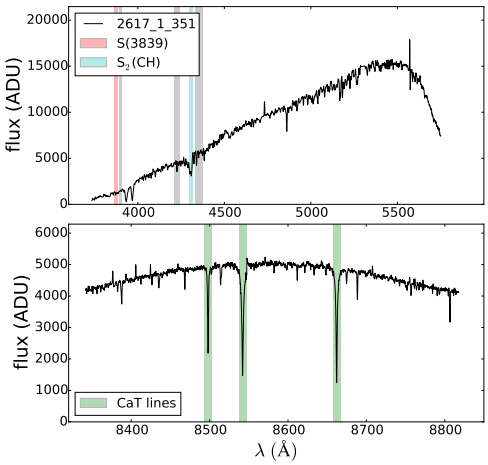

Figure 9. Top panel: Blue arm AAOmega spectrum of one of the ω Cen candidate members: AEGIS catalogue ID 2617_1_351, 2MASS identification 13294957-4321148. The coloured regions show the wavelength ranges used for the calculation of the spectral indices, the closest gray regions to each coloured region show the ranges used for measurement of the continuum for that index. The CH(4300) index is not shown as it overlaps the S_2(CH) index. Bottom panel: Red arm spectrum of the same star. The coloured regions show the Ca II triplet (CaT)

absorption lines.

fainter than the tip of the RGB, and brighter than the cluster HB. As with our measurements of V_r, we used a Monte Carlo method to measure the EWs of the Ca II triplet lines from the same 100 realizations of the normalized red arm spectra. For stars brighter than the HB, we numerically integrated the Voigt fit to each Ca II triplet line (the Voigt function has no analytical integral) using INTEGRATE.QUAD from SciPy (Jones 2001) to measure the EW. We calculated the [Fe/H] from equations 1 and 2 using these EW values for each realization and, assuming the stars are cluster members, V_{HB} from the Harris (1996) (2010 edition) catalog for the cluster. The [Fe/H]s and uncertainties were calculated using the same method as for V_r using the 100 calculated values.

As can be seen in Figure 5, only some of the stars in each sample are brighter than the cluster HB. For ω Cen and M55, in particular, this is a small fraction of the total. In the final candidate sample, there were only eight stars, divided between our four target clusters, for which we were able to calculate [Fe/H] from the Ca II triplet lines. The measured [Fe/H] values for six of the eight stars are within ±0.2 dex of those from the AEGIS catalogue, but with such a small sample it is difficult to make meaningful comparisons. The measured [Fe/H] values and uncertainties are shown in Table 4.

5.3 Spectral indices from the blue arm spectra

We used the low resolution blue spectra to calculate spectral indices to measure the strength of CN and CH molecular bands. We measured three spectral indices: a CN index (S(3839) from Harbeck et al. (2003)) and two CH indices (CH(4300) from Harbeck et al. (2003), and S_2(CH) from Martell et al. (2008)):

$$\mathrm{S(3839)} = -2.5 \log \frac{F_{3861-3884}}{F_{3894-3910}}, \quad (3)$$

$$\mathrm{CH(4300)} = -2.5 \log \frac{F_{4285-4315}}{0.5F_{4240-4280} + 0.5F_{4390-4460}} \quad (4)$$

$$\mathrm{S_2(CH)} = -2.5 \log \frac{F_{4297-4317}}{F_{4212-4242} + F_{4330-4375}} \quad (5)$$

$$(6)$$

where

$$F_{A-B} = \int_A^B F(\lambda) d\lambda. \quad (7)$$

As with our measurements of V_r and [Fe/H], we used a Monte Carlo method to measure the indices in the blue arm of the spectra. We used 100 different realizations of the spectra produced using the same method as for the red arm spectra. The spectral indices and the uncertainties were calculated using the same method as for V_r using the 100 calculated values. Table 4 contains our calculated indices and their uncertainties and they are plotted against J magnitudes in Figure 10.

The typical behaviour of CN and CH indices in globular cluster stars is complex. It is generally bimodal in CN (e.g., Norris et al. 1981), although some globular clusters such as NGC 1851 show multimodal behaviour (Campbell et al. 2012; Simpson et al. 2017). CN and CH band strengths are anticorrelated (e.g., Norris & Freeman 1982). The band strengths are modulated by carbon and nitrogen abundances as well as the overall metallicity and the evolutionary state of the star (e.g., Martell et al. 2008).

The carbon and nitrogen abundance variations that drive the band strength bimodality and anticorrelation are part of a larger pattern of light-element abundance variations (e.g. Carretta et al. 2010a, though the literature on this topic is extensive). Correlations between CN strength and Na and Al were found by Cottrell & Da Costa (1981) and an anticorrelation between CN and Na was found by Sneden et al. (1992). The CN-CH anti-correlation corresponds with the anti-correlations between O-Na and Mg-Al (Gratton et al. 2001; Carretta et al. 2009b). Within each globular cluster, roughly half of the stars have relatively weak CN bands and scaled-Solar abundance patterns, and the other half have relatively strong CN bands and enhancements in [N/Fe], [Na/Fe] and [Al/Fe] along with depletions in [C/Fe], [O/Fe] and [Mg/Fe].

Between 30 – 70 percent (Pancino et al. 2010; Carretta et al. 2009a) of stars in a given globular cluster exhibit light-element abundance anticorrelations, with the remaining stars similar to halo field stars of the same metallicity. This behaviour, only prevalent in globular cluster stars, strongly resembles the products of high-temperature proton-capture nucleosynthesis. This has driven globular cluster formation scenarios (e.g. D'Ercole et al. 2010; Decressin et al. 2010; Kruijssen 2015) toward early self-enrichment between

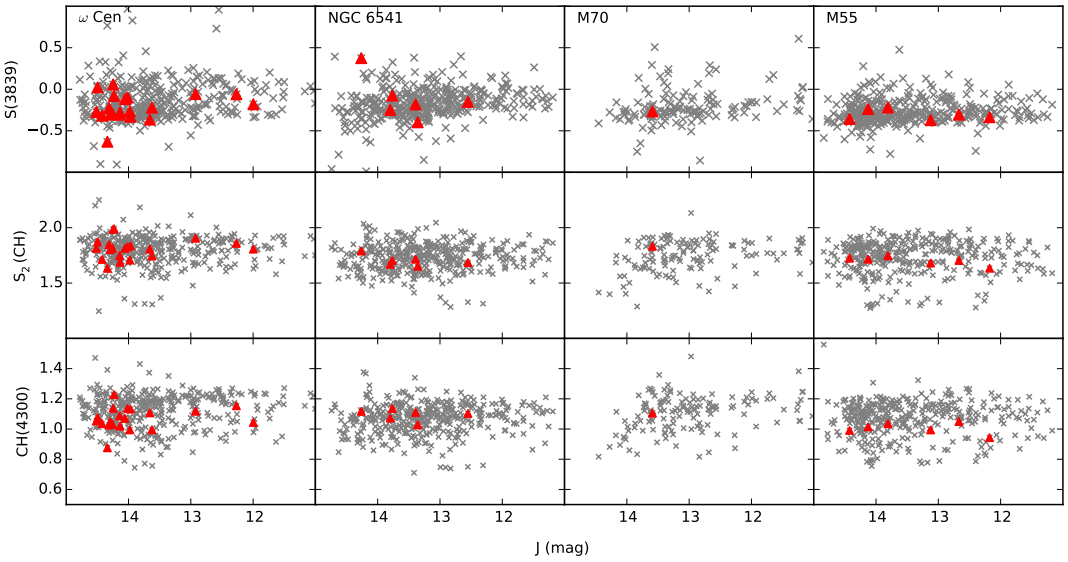

Figure 10. S(3839), S_2(CH) and CH(4300) indices versus apparent J magnitude for our target cluster stars. Red triangles denote candidate extratidal stars. Gray crosses show all stars within 5° of the cluster centres for which we measured S(3839).

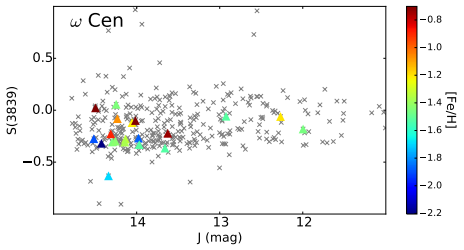

Figure 11. S(3839) versus apparent J magnitude for ω Cen stars. Triangles denote candidate extratidal stars colour coded by metallicity. Gray crosses show all stars within 5° of the cluster centres for which we measured S(3839).

multiple generations of stars, with chemical feedback from the later evolutionary phases of some or all of the more massive (≥ 3 $M_\odot$) cluster stars.

As a result, the CN and CH indices can be used as a confirmation of a connection between the candidate stars and a globular cluster, but cannot be used to reject candidate stars. If the stars are CN-strong relative to the field at a fixed metallicity, then that is an indication that they carry "second-generation" light element abundances and are likely to have formed within the globular cluster. This indication could be strengthened with the use of further light-element abundances, as in Lind et al. (2015) and Martell et al. (2016). If the stars are not CN-strong relative to the field, then their band strengths are consistent with either forming as "first-generation" globular cluster stars or as ordinary field stars, and light-element abundances cannot distinguish between the two possibilities.

ω Cen offers the best demonstration of how we might use CN and CH band strengths as criteria for our candidates as it has the largest number of candidates. Figure 11 shows S(3839) versus apparent J magnitude for the candidate ω Cen stars and the field stars in the same region of the sky. The general upward trend in band strength with rising luminosity is primarily driven by increased formation of CN molecules in the atmospheres of cooler stars and not by any significant change in the nitrogen abundance. The broad metallicity range in ω Cen can be seen as a vertical gradient in the colour of the points. Within a narrow metallicity range (-1.6≤[Fe/H]≤-1.4 dex is a good illustration of this), the band strengths are bimodally distributed, representing a primordial offset between the first- and second-generation stars. We consider the relatively CN-strong ω Cen candidates to be more likely to be associated with the cluster as a result of this analysis, but (as discussed above) the band strengths for CN-weak stars do not add information that would allow us to raise or lower the likelihood of their association with the cluster.

There are no clear CN-strong subgroups in the candidate stars corresponding to any of the other three clusters,

although the numbers are small. As a result, the spectral index measurements do not add any weight to the possibility that they are cluster halo stars. The faintest candidate in NGC 6541 has a high CN index but does not have a correspondingly low CH index. All spectra were visually inspected, the spectrum of this star leads us to suspect that noise in the continuum band of the S(3839) index is likely artificially inflating its value, and that it is not reflective of real abundance behaviour.

6 SPATIAL DISTRIBUTION

Figure 12 shows the on-sky distribution of observed and candidate stars for the target globular clusters in equatorial coordinates. The cluster proper motion and the directions to the Galactic centre and the Galactic plane are shown in the plots for orientation. The sparse sightlines of the survey preclude any conclusion regarding the orientation of any of the candidate cluster members with respect to their orbits.

For ω Cen there are 20 candidate ex-member stars outside the adopted tidal radius of 48.4 arcmin at distances from the cluster centre ranging from ∼3 to ∼6 times the tidal radius. For NGC 6541 there are six stars at distances from ∼11 to ∼22 times the tidal radius of 13.0 arcmin. For M70 there is one star at a distance of ∼23 times the tidal radius of 9.5 arcmin. For M55 there are six stars at distances from ∼12 to ∼19 times the tidal radius of 15.3 arcmin.

7 CLUSTER MASS LOSS AND DESTRUCTION RATES

It is of interest to compare the destruction rate implied by these stars, assuming that they have indeed escaped from their parent clusters, with those from simulations such as Gnedin & Ostriker (1997) and Moreno et al. (2014).

The simulations of Gnedin & Ostriker (1997) included evaporation and disk and bulge gravitational shocks to calculate destruction rates of globular clusters. They simulated a significant fraction (119) of the ∼150 known Galactic globular clusters. They used two different Galactic models and an isotropic kinematic model for the Galactic globular cluster system. They concluded that the present day globular cluster population is a fraction of the initial population and that the Galactic bulge and halo contain a large proportion of stars that originate in globular clusters. They also found that that more than half of the existing globular clusters will not survive the next Hubble time and that the present day destruction time was similar to the typical age of a globular cluster. Depending on the models used, they calculated destruction rates of 1.60–3.43$\times10^{-11}$, 2.42–6.42$\times10^{-11}$, 7.09–14.8 $\times$ 10^{-11}, and 6.83–7.52 $\times$ 10^{-11} yr^{-1} for ω Cen, NGC 6541, M70, and M55, respectively.

Moreno et al. (2014) calculated orbits, tidal radii and destruction rates due to bulge-bar and disk shocking an axisymmetric Galactic gravitational potential and a Galaxy-like barred spiral potential. They included real orbits, six-dimensional positions and velocities and three-dimensional (3D) spiral arms. They calculated the destruction rates for a total of 63 globular clusters, including two of our target clusters: 4.3–16.3$\times10^{-11}$ yr^{-1} for ω Cen and 6.0–33.2$\times10^{-12}$ yr^{-1} for M55, depending on the models used.

To estimate the observed cluster fractional mass loss we used the ratio of the total cluster extratidal halo stars V luminosity to the integrated cluster V luminosity (from the cluster integrated V magnitude V_t in Table 1). The observed cluster fractional mass losses are 0.00047, 0.00182, 0.00124, and 0.00285 for ω Cen, NGC 6541, M70, and M55 respectively.

We then estimated the time taken for a star to move outside our 5° search area. Küpper et al. (2010) equation (18) gives the relative velocity v_c of escaped stars for clusters in circular orbits in the Galactic disk, which we used as an estimate for the space velocity:

$$v_c \simeq \pm 2\Omega x_L = \pm(4GM\Omega)^{1/3} \quad (8)$$

where Ω is the Galactic orbital angular velocity of the cluster, x_L is the cluster tidal radius, G is the gravitational constant and M is the cluster mass. This yields relative velocities of ±12.9, ±9.2, ±8.2, and ±6.7 km s^{-1}. As stars can escape in any direction, the mean relative velocities perpendicular to our line-of-sight (i.e. the proper motions) are calculated by multiplying the relative velocities by $2/\pi$ to give ±8.2, ±5.9, ±5.2, and ±4.2 km s^{-1}. Extratidal stars would move 5° from the clusters' central positions in 54.1, 108.9, 147.6, and 108.5 Myr at these velocities.

We then adjusted for sample completeness: (1) AEGIS is not spatially complete (see Figure 12) over the area of sky we searched and (2) AEGIS is not photometrically complete to the faintness limit of the RGB for these clusters. We estimated completeness by comparing AEGIS stars to samples of stars from the UCAC4 catalog (Zacharias et al. 2013). UCAC4 contains V magnitudes from the APASS catalog (Henden et al. 2009), which quotes current completeness down to V=16 mag. We selected UCAC4 stars outside the cluster tidal radius and inside the V versus V-K$_s$ AEGIS selection function boundaries (Figure 1), with a revised limit of V < 16 mag, and compared them to a similarly selected sample of AEGIS stars. This gave AEGIS completeness of 0.0025, 0.00158, 0.00074, and 0.00302 for our final candidate cluster extratidal halo samples.

We divided the fractional mass losses by (1) the time taken for the cluster extratidal halo stars to move outside our search area, and (2) completeness, to give the final cluster destruction rates. These are 3.49×10^{-9}, 1.06×10^{-8}, 1.14×10^{-8}, and 8.69×10^{-9} yr^{-1} for ω Cen, NGC 6541, M70, and M55, respectively.

We assumed/estimated the following in this calculation: (1) It is likely that the mass-to-light ratios of the cluster and the observed extratidal stars are different. The integrated cluster luminosity includes contributions from both giant and dwarf cluster members. However, the AEGIS survey would not detect dwarfs at cluster distances, so the observed cluster fractional mass losses are likely underestimated. This would translate to an underestimate of the destruction rate. (2) The AEGIS completeness is an estimate. (3) Some of the stars that we include in our lists of candidates might be field stars rather than ex-members of the cluster, so this would lead to an overestimate of cluster destruction rates. We defer discussion of this to Section 8. (4) Küpper et al. (2010) Equation (18) applies to escaped stars for clusters in circular orbits in the disk. If the actual velocities are lower, then

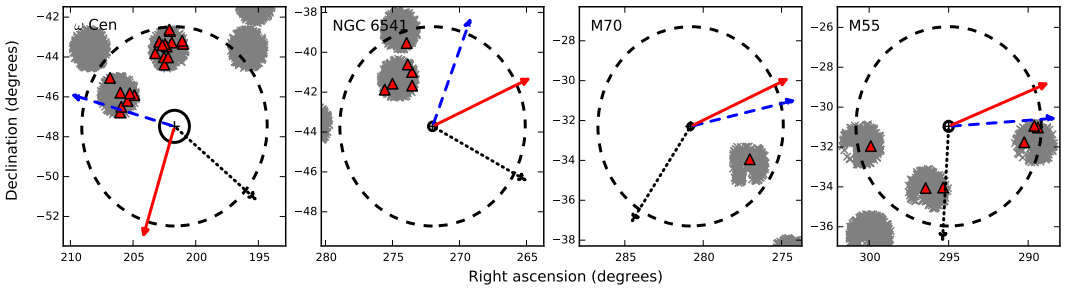

Figure 12. Spatial distribution of AEGIS catalogue stars around the target globular cluster position. Gray crosses show all observed AEGIS stars, red triangles denote candidate extratidal cluster halo stars. The black cross and solid circle show the centre position and the tidal radius, the black dashed circle is at a 5° radius from the cluster centre position. The black dotted arrow indicates the direction of the cluster proper motion, the blue dashed arrow is the direction to the Galactic centre and the solid red arrow is the direction perpendicular to the Galactic plane.

the calculated mass loss rates would be an overestimate and vice versa. (5) We have assumed a constant relative velocity of escaped stars. There is some evidence that the velocities of escaped stars may vary along the tidal tails of globular clusters (e.g. Odenkirchen et al. 2009; Kuzma et al. 2015).

Given those limitations in our estimates, the destruction rate for all our target clusters are ~2 orders of magnitude larger than predicted by both sets of models, except for M55, for which it is ~3 orders of magnitude greater than the rate calculated by Moreno et al. (2014).

8 DISCUSSION AND CONCLUSIONS

The final list of candidate halo stars for the clusters is presented in Table 3.

There are a number of parameters that can be used to differentiate stellar cluster members from field stars. Candidate cluster members appear as a clump of stars in the parameter space of [(l,b), V_r, photometry, T_{eff}, log g, [Fe/H], [X/Fe]]. Cluster members occupy a well-defined region of this space because they inherit characteristics from their common origin.

In previous studies we found candidate extratidal members around three other globular clusters with evidence of extratidal stellar halos: NGC 1851 (Navin et al. 2015; Simpson et al. 2017), and M3 and M13 (Navin et al. 2016).

We reduced and analysed original AAOmega spectra of 1149 stars for our study of NGC 1851. We identified four candidate extratidal cluster halo red giant stars at distances up to ~3.1 times the tidal radius. We confirmed their identity from measurements of spectral indices in Simpson et al. (2017), where we also estimated the destruction rate for NGC 1851 using the method adopted in this paper. We found that the destruction rate is comparable to that calculated by Gnedin & Ostriker (1997), but considerably higher than that of Moreno et al. (2014) (there are significant differences in the predicted rates).

For our study of M3 and M13 we used the LAMOST (Zhao et al. 2006) Data Release 1 (Luo et al. 2015) as our dataset (Navin et al. 2016). In M3 we identified eight candidate cluster halo stars, at distances up to ~10.2 times the tidal radius, while in M13 we found 12 candidates at distances up to ~13.8 times the tidal radius. We estimated the destruction rates for both these clusters and found discrepancies between observed and predicted rates similar to those we found in this study, i.e. ~1–3 orders of magnitude larger than the destruction rates calculated by Gnedin & Ostriker (1997) and Moreno et al. (2014). However, we note that these stars are not confirmed ex-members and high-resolution spectroscopic observations are needed to match the chemical abundances of these stars with their putative parent clusters.

In this study, the AEGIS survey catalogue contained most of the parameters needed to select extratidal cluster halo red giant stars from field stars. We supplemented these as required from other sources and from our own measurements of V_r, [Fe/H], and spectral indices by reducing and analysing the original AAOmega spectra. We chose clusters with a high $|V_r| > 100$ km s^{-1} to make it a clear discriminant, but we used all available parameters to give more confident member/non-member discrimination. We identified candidate halo stars around four other globular clusters (ω Cen, NGC 6541, M70, and M55).

Although these candidate extratidal stars lie at significant distances outside the cluster radius, this is not without precedent. Tidal tails around known globular clusters have been mapped photometrically out to ~18.5° from Palomar 5 (Grillmair & Dionatos 2006a) and ~45° from NGC 5466 (Grillmair & Johnson 2006). There are also streams with unknown progenitors that were likely now-disrupted globular clusters, such as the 63° long GD-1 (Grillmair & Dionatos 2006b) and the Acheron, Cocytos, and Lethe streams (Grillmair 2009) spanning 34 – 84°. Individual extratidal stars have been identified spectroscopically across ~17° (Ishigaki et al. 2016) and ~20° of the tails (Kuzma et al. 2015) of Palomar 5. Anguiano et al. (2016) found evidence of the association of four stars with the halo globular cluster NGC 3201 spread up to 60° from the cluster centre. As mentioned above, we found extratidal stars around M13 at distances up to 13.8 times the tidal radius, subject to future confir-

mation. Nevertheless, we recognise that some of the stars we include as candidates might be field stars rather than extratidal stars from the cluster. This is particularly so for ω Cen where we were unable to use [Fe/H] as a discriminant because it is not a mono-metallic cluster.

We also find that the globular cluster destruction rates corresponding to the observed mass loss for all four of these clusters are significantly higher (~2 orders of magnitude) than theoretical studies predict. There are also significant differences in the rates predicted from models so there may also be progress to be made there. There are a number of implications if these destruction rates are correct, and other globular clusters are also found to have higher destruction rates than predicted. It may imply that the current number of globular clusters is a small fraction of the original population and that the initial masses of globular clusters were higher than we currently expect, or the initial mass functions may be different. It may also imply that the proportion of Galactic halo stars contributed by globular clusters is larger. It is also possible that there has been some recent change in the Milky Way that has increased the destruction rate of globular clusters.

We present evidence for extratidal cluster halo stars around the globular clusters ω Cen (NGC 5139), NGC 6541, M70 (NGC 6681) and M55 (NGC 6809) in the AEGIS Survey catalogue. ω Cen has 20 candidate extratidal cluster halo stars at distances up to ~6 times the tidal radius, NGC 6541 has six candidates at distances up to ~20 times the tidal radius, M70 has one candidate at a distance of ~22 times the tidal radius, and M55 has six candidate extratidal cluster halo stars at distances up to ~19 times the tidal radius. Similar to our previous studies of NGC 1851, M3 and M13, the destruction rates corresponding to the observed mass loss are considerably higher than theoretical studies predict. Further investigation is required to reconcile the discrepancies between our observed and predicted destruction rates. It is important to resolve this to constrain theoretical studies of globular cluster destruction and the contribution of globular clusters to the Galaxy's stellar halo.

ACKNOWLEDGEMENTS

Based on data acquired through the Australian Astronomical Observatory, via program AAT/11B/20 and 13A/22. SLM and DBZ acknowledge the financial support from the Australian Research Council through grants DE140100598 and FT110100793, respectively. We would like to thank Andy Casey for help with the interpretation of the AEGIS data.

This research made use of NASA's Astrophysics Data System and the VizieR catalogue access tool, CDS, Strasbourg, France. This research made use of Astropy, a community-developed core Python package for Astronomy (Astropy Collaboration et al. 2013); the IPython package (Pérez & Granger 2007); SciPy (Jones 2001); TOPCAT, an interactive graphical viewer and editor for tabular data (Taylor 2005); IRAF is distributed by the National Optical Astronomy Observatory, which is operated by the Association of Universities for Research in Astronomy (AURA) under cooperative agreement with the National Science Foundation (Tody 1993); PyRAF is a product of the Space Telescope Science Institute, which is operated by AURA for NASA.

We acknowledge with thanks the variable star observations from the AAVSO International Database contributed by observers worldwide and used in this research. This publication makes use of data products from the Two Micron All Sky Survey, which is a joint project of the University of Massachusetts and the Infrared Processing and Analysis Center/California Institute of Technology, funded by the National Aeronautics and Space Administration and the National Science Foundation. Funding for RAVE has been provided by: the Australian Astronomical Observatory; the Leibniz-Institut fuer Astrophysik Potsdam (AIP); the Australian National University; the Australian Research Council; the French National Research Agency; the German Research Foundation (SPP 1177 and SFB 881); the European Research Council (ERC-StG 240271 Galactica); the Istituto Nazionale di Astrofisica at Padova; The Johns Hopkins University; the National Science Foundation of the USA (AST-0908326); the W.M. Keck foundation; the Macquarie University; the Netherlands Research School for Astronomy; the Natural Sciences and Engineering Research Council of Canada; the Slovenian Research Agency; the Swiss National Science Foundation; the Science & Technology Facilities Council of the UK; Opticon; Strasbourg Observatory; and the Universities of Groningen, Heidelberg and Sydney. The RAVE web site is at `https://www.rave-survey.org`.

REFERENCES

Anguiano B., et al., 2015, MNRAS, 451, 1229
Anguiano B., et al., 2016, MNRAS, 457, 2078
Armandroff T., Da Costa G., 1991, AJ, 101, 1329
Astropy Collaboration et al., 2013, A&A, 558, A33
Balbinot E., Gieles M., 2017, preprint, (`arXiv:1702.02543`)
Bedin L. R., Piotto G., Anderson J., Cassisi S., King I. R., Momany Y., Carraro G., 2004, ApJ, 605, L125
Beers T. C., Chiba M., Yoshii Y., Platais I., Hanson R. B., Fuchs B., Rossi S., 2000, AJ, 119, 2866
Bekki K., Freeman K. C., 2003, MNRAS, 346, L11
Bica E., Ortolani S., Barbuy B., 2016, Publ. Astron. Soc. Australia, 33, e028
Bressan A., Marigo P., Girardi L., Salasnich B., Dal Cero C., Rubele S., Nanni A., 2012, MNRAS, 427, 127
Bullock J. S., Johnston K. V., 2005, ApJ, 635, 931
Campbell S. W., et al., 2012, ApJ, 761, L2
Carrera R., Pancino E., Gallart C., del Pino A., 2013, MNRAS, 434, 1681
Carretta E., et al., 2009a, A&A, 505, 117
Carretta E., Bragaglia A., Gratton R., Lucatello S., 2009b, A&A, 505, 139
Carretta E., Bragaglia A., Gratton R., D'Orazi V., Lucatello S., 2009c, A&A, 508, 695
Carretta E., Bragaglia A., Gratton R. G., Recio-Blanco A., Lucatello S., D'Orazi V., Cassisi S., 2010a, A&A, 516, A55
Carretta E., et al., 2010b, ApJ, 714, L7
Casey A. R., Keller S. C., Ness M. K., Aegis Collaboration Skymapper Team 2012, in Aoki W., Ishigaki M., Suda T., Tsujimoto T., Arimoto N., eds, Astronomical Society of the Pacific Conference Series Vol. 458, Galactic Archaeology: Near-Field Cosmology and the Formation of the Milky Way. p. 413
Cenarro A., Cardiel N., Gorgas J., Peletier R., Vazdekis A., et al., 2001, MNRAS, 326, 959
Chen C. W., Chen W. P., 2010, ApJ, 721, 1790

Cottrell P. L., Da Costa G. S., 1981, ApJ, 245, L79
D'Ercole A., D'Antona F., Ventura P., Vesperini E., McMillan S. L. W., 2010, MNRAS, 407, 854
Da Costa G. S., Coleman M. G., 2008, AJ, 136, 506
Decressin T., Baumgardt H., Charbonnel C., Kroupa P., 2010, A&A, 516, A73
Dinescu D. I., 2002, in van Leeuwen F., Hughes J. D., Piotto G., eds, Astronomical Society of the Pacific Conference Series Vol. 265, Omega Centauri, A Unique Window into Astrophysics. p. 365 (arXiv:astro-ph/0112364)
Dinescu D., Girard T., van Altena W., 1999, AJ, 117, 1792
Erkal D., Koposov S. E., Belokurov V., 2016, preprint, (arXiv:1609.01282)
Fernández Trincado J. G., Vivas A. K., Mateu C. E., Zinn R., 2013, Mem. Soc. Astron. Italiana, 84, 265
Frinchaboy P. M., Majewski S. R., 2008, AJ, 136, 118
Gilmore G., Wyse R. F. G., Norris J. E., 2002, ApJ, 574, L39
Gnedin O., Ostriker J., 1997, ApJ, 474, 223
Gratton R. G., et al., 2001, A&A, 369, 87
Gratton R. G., Carretta E., Claudi R., Lucatello S., Barbieri M., 2003, A&A, 404, 187
Gratton R. G., Carretta E., Bragaglia A., 2012, A&ARv, 20, 50
Grillmair C. J., 2009, ApJ, 693, 1118
Grillmair C. J., Dionatos O., 2006a, ApJ, 641, L37
Grillmair C. J., Dionatos O., 2006b, ApJ, 643, L17
Grillmair C. J., Johnson R., 2006, ApJ, 639, L17
Grillmair C. J., Freeman K. C., Irwin M., Quinn P. J., 1995, AJ, 109, 2553
Harbeck D., Smith G. H., Grebel E. K., 2003, AJ, 125, 197
Harris W., 1996, AJ, 112, 1487
Henden A. A., Welch D. L., Terrell D., Levine S. E., 2009, BAAS, 41, 669
Ibata R., Gilmore G., Irwin M., 1995, MNRAS, 277, 781
Ishigaki M. N., Hwang N., Chiba M., Aoki W., 2016, ApJ, 823, 157
Johnson C. I., Pilachowski C. A., 2010, ApJ, 722, 1373
Jones E., 2001, SciPy: Open source scientific tools for Python, http://www.scipy.org/
Keller S. C., et al., 2007, Publ. Astron. Soc. Australia, 24, 1
Kharchenko N. V., Piskunov A. E., Schilbach E., Röser S., Scholz R.-D., 2013, A&A, 558, A53
Kiss L. L., Székely P., Bedding T. R., Bakos G. Á., Lewis G. F., 2007, ApJ, 659, L129
Koposov S., Rix H., Hogg D., 2010, ApJ, 712, 260
Kruijssen J. M. D., 2015, MNRAS, 454, 1658
Kunder A., et al., 2016, preprint, (arXiv:1609.03210)
Küpper A. H. W., Kroupa P., Baumgardt H., Heggie D. C., 2010, MNRAS, 401, 105
Küpper A., Balbinot E., Bonaca A., Johnston K., Hogg D., Kroupa P., Santiago B., 2015, ApJ, 803, 80
Kuzma P. B., Da Costa G. S., Keller S. C., Maunder E., 2015, MNRAS, 446, 3297
Law D. R., Majewski S. R., 2010, ApJ, 718, 1128
Law D. R., Majewski S. R., Skrutskie M. F., Carpenter J. M., Ayub H. F., 2003, AJ, 126, 1871
Lee J., Carney B. W., 2001, in American Astronomical Society Meeting Abstracts. p. 1387
Lee Y., Joo J., Sohn Y., Rey S., Lee H., Walker A., 1999, Nature, 402, 55
Lee Y. S., et al., 2011, AJ, 141, 90
Leon S., Meylan G., Combes F., 2000, A&A, 359, 907
Lind K., et al., 2015, A&A, 575, 12
Luo A., et al., 2015, preprint, (arXiv:1505.01570)
Mackey A. D., Gilmore G. F., 2004, MNRAS, 355, 504
Majewski S. R., Nidever D. L., Smith V. V., Damke G. J., Kunkel W. E., Patterson R. J., Bizyaev D., Pérez A. E. G., 2012, ApJ, 747, L37
Marin-Franch A., et al., 2009, ApJ, 694, 1498
Martell S. L., Grebel E. K., 2010, A&A, 519, A14
Martell S. L., Smith G. H., Briley M. M., 2008, PASP, 120, 839
Martell S. L., Smolinski J. P., Beers T. C., Grebel E. K., 2011, A&A, 534, A136
Martell S., et al., 2016, ApJ, 825, 146
McLaughlin D. E., van der Marel R. P., 2005, ApJS, 161, 304
Merritt D., Meylan G., Mayor M., 1997, AJ, 114, 1074
Meza A., Navarro J. F., Abadi M. G., Steinmetz M., 2005, MNRAS, 359, 93
Mizutani A., Chiba M., Sakamoto T., 2003, ApJ, 589, L89
Moreno E., Pichardo B., Velázquez H., 2014, ApJ, 793, 110
Navin C., Martell S., Zucker D., 2015, MNRAS, 453, 531
Navin C. A., Martell S. L., Zucker D. B., 2016, ApJ, 829, 123
Norris J., Freeman K. C., 1982, ApJ, 254, 143
Norris J., Cottrell P. L., Freeman K. C., Da Costa G. S., 1981, ApJ, 244, 205
Noyola E., Gebhardt K., Bergmann M., 2008, ApJ, 676, 1008
O'Malley E. M., Gilligan C., Chaboyer B., 2017, preprint, (arXiv:1703.01915)
Odenkirchen M., et al., 2001, ApJ, 548, L165
Odenkirchen M., Grebel E. K., Kayser A., Rix H.-W., Dehnen W., 2009, AJ, 137, 3378
Olszewski E. W., Saha A., Knezek P., Subramaniam A., de Boer T., Seitzer P., 2009, AJ, 138, 1570
Pancino E., Rejkuba M., Zoccali M., Carrera R., 2010, A&A, 524, A44
Pérez F., Granger B., 2007, Computing in Science and Engineering, 9, 21
Robin A. C., Reylé C., Derrière S., Picaud S., 2003, A&A, 409, 523
Sharma S., Bland-Hawthorn J., Johnston K. V., Binney J., 2011, ApJ, 730, 3
Simpson J. D., Martell S. L., Navin C. A., 2017, MNRAS, 465, 1123
Skrutskie M., et al., 2006, ApJ, 131, 1163
Smith V. V., Suntzeff N. B., Cunha K., Gallino R., Busso M., Lambert D. L., Straniero O., 2000, AJ, 119, 1239
Sneden C., Kraft R. P., Prosser C. F., Langer G. E., 1992, AJ, 104, 2121
Starkenburg E., et al., 2010, A&A, 513, A34
Steinmetz M., et al., 2006, AJ, 132, 1645
Taylor M. B., 2005, in Shopbell P., Britton M., Ebert R., eds, Astronomical Society of the Pacific Conference Series Vol. 347, Astronomical Data Analysis Software and Systems XIV. p. 29
Tody D., 1993, in Hanisch R. J., Brissenden R. J. V., Barnes J., eds, Astronomical Society of the Pacific Conference Series Vol. 52, Astronomical Data Analysis Software and Systems II. p. 173
Webb J. J., Leigh N. W. C., 2015, MNRAS, 453, 3278
Williams M. E. K., et al., 2011, ApJ, 728, 102
Yong D., et al., 2014, MNRAS, 441, 3396
York D., et al., 2000, AJ, 120, 1579
Zacharias N., Finch C. T., Girard T. M., Henden A., Bartlett J. L., Monet D. G., Zacharias M. I., 2013, AJ, 145, 44
Zhao G., Chen Y.-Q., Shi J.-R., Liang Y.-C., Hou J.-L., Chen L., Zhang H.-W., Li A.-G., 2006, Chinese J. Astron. Astrophys., 6, 265

This paper has been typeset from a TEX/LATEX file prepared by the author.

5 Summary and conclusions

In this thesis work I studied 17 globular clusters and found candidate extratidal stars around seven of these. I used the extratidal stars identified to estimate the destruction rates for these seven clusters, and found that they are generally several orders of magnitude higher than predicted by current models of globular cluster destructon. Sky plots of the seven globular clusters and the candidate extratidal stars are shown in Figure 5.1, and Table 5.1 shows a summary of the final results.

5.1 Outline of work

This project began as a preliminary exploration of spectroscopic observations of the stars of a single globular cluster, NGC 1851, and surrounding stars. Observations had been obtained with the aim of completing a thorough abundance survey of member stars of NGC 1851 using the AAOmega spectrograph on the AAT. The wide 2° field of the 2dF fibre positioner, which feeds AAOmega, meant that fibres were available for allocation to targets well outside the tidal radius. The observing proposal therefore had a secondary aim of searching for ex-members surrounding the cluster to investigate previous reports of an extended stellar halo around NGC 1851. The surrounding stars were photometrically selected to be similar to RGB stars of NGC 1851 to maximise the likelihood of finding candidate extratidal stars.

This search revealed four likely extratidal stars, and showed that it was possible to match measured parameters of stars to those of a globular cluster to strongly associate individual extratidal stars with their parent cluster. These stars very likely formed in NGC 1851, subsequently escaped, and will eventually become stellar halo field stars. The results were published in Paper I (Navin et al., 2015), which appeared in the Monthly Notices of the Royal Astronomical Society in July 2015.

If extratidal stars could be observed and identified as ex-members of a particular globular cluster, this offered the prospect of directly calculating the current mass-loss rate of the cluster. These globular cluster mass-loss rates could be straightforwardly compared to the destruction rates predicted by various models of globular cluster destruction which, currently, are not well constrained observationally.

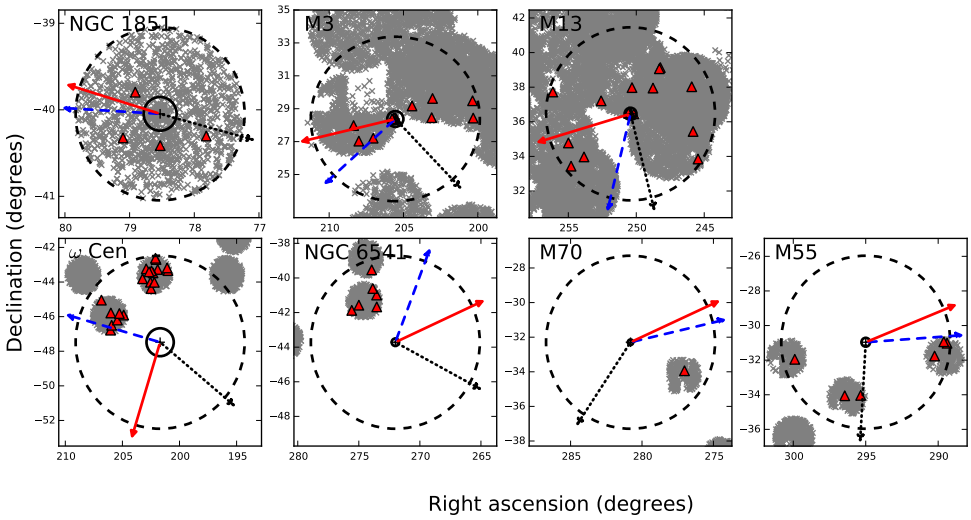

Figure 5.1: Spatial distribution of stars around the target globular cluster positions. The top left is NGC 1851, M3 and M13 are from LAMOST data, and ω Cen, NGC 6541, M55 and M70 on the bottom row are from AEGIS data. Gray crosses show all observed stars, red triangles denote candidate extratidal halo stars. The black cross and solid circle show the centre position and the tidal radius of the cluster. The black dashed circle is at a 1° radius from the cluster centre position for NGC 1851, the others are at a 5° radius. The black dotted arrow indicates the direction of the cluster proper motion, the blue dashed arrow is the direction to the Galactic centre and the solid red arrow is the direction perpendicular to the Galactic plane.

Table 5.1: Results summary

Globular cluster	Stars tested	Candidate extratidal stars	Mean relative velocity ($\mathrm{km\,s^{-1}}$)	Inferred cluster destruction rate ($\mathrm{yr^{-1}}$)	Model cluster destruction rate(s) ($\mathrm{yr^{-1}}$)
NGC 1851	1149	4	3.8	4.60×10^{-11}	1.24–1.27×10^{-11}
					8.31–10.3×10^{-16}
M3 (NGC 5272)	3879	8	3.8	8.04×10^{-11}	3.98–4.52×10^{-12}
					1.62–2.97×10^{-12}
M13 (NGC 6205)	7355	12	4.7	2.47×10^{-10}	1.02–1.47×10^{-11}
					6.2–10.4×10^{-14}
ω Cen (NGC 5139)	756	20	8.2	3.49×10^{-9}	1.60–3.43×10^{-11}
					4.3–16.3×10^{-11}
NGC 6541	502	6	5.9	1.06×10^{-8}	2.42–6.42×10^{-11}
M70 (NGC 6681)	226	1	5.2	1.14×10^{-8}	7.09–14.8×10^{-11}
M55 (NGC 6809)	689	6	4.2	8.69×10^{-9}	6.83–7.52×10^{-11}
					6.0–33.2×10^{-12}

Notes: The mean relative velocity is the velocity of extratidal stars with respect to the cluster calculated from Küpper et al. (2010). Model destruction rates on the first and second lines for each cluster are from Gnedin & Ostriker (1997) and Moreno et al. (2014), respectively.

To progress, the project needed to (1) develop a method of estimating the destruction rates from the masses of observed extratidal stars of clusters to compare with model predictions, and (2) obtain suitable data on a large enough sample of globular clusters to make a meaningful comparison with the models.

The destruction rate calculation depended on (1) being able to calculate the likely velocity of escaping stars, and (2) making reasonable estimates of completeness for the (likely small) samples of candidate extratidal stars. The first was estimated using equation 18 from Küpper et al. (2010) for the escape velocity of stars for globular clusters in circular orbits in the Galactic disk. The calculation for the destruction rate was implemented in Python code and is included in Appendix B Section 1. The completeness calculation was implemented using a simple photometric comparison of the stars in the sample with V magnitudes and B-V colours of stars from APASS (Henden et al., 2009) in the UCAC4 catalog (Zacharias et al., 2013). The sample of stars were selected from UCAC4 using the same selection function, as best as could be determined, used in the observations. With a quoted APASS completeness limit of V=16, this was found to be useful for all the target globular clusters and the observations, whether dedicated, as in the case of NGC 1851, or in the LAMOST and AEGIS surveys for the other clusters. The destruction rate calculations were first used in Paper II for the clusters M3 and M13, then in Paper III for NGC 1851, and finally in Paper VII for ω Cen, NGC 6541, M70 and M55.

The LAMOST survey (Zhao et al., 2006) was chosen to provide the data for the next part of the project. This survey had sufficient depth and sky-coverage to find likely RGB cluster members of northern hemisphere globular clusters. It also had a publicly available catalog, Data Release 1 (DR1), with stellar parameters obtained from a modified SDSS analysis pipeline. The survey was not complete in the sky areas near the target globular clusters, but it had a reasonably well defined selection function that meant that determining completeness should be straightforward. This search found extratidal stars that could be strongly associated with two globular clusters, eight for M3 and 12 for M13. In addition it recovered a number of stars in DR1 that had been previously identified as members of M3 and M13 in an independent paper (Zhang et al., 2015), providing support for the methods adopted in the paper. The most interesting result from this study, however, was not just the identification of candidate extratidal stars. When these stars were used to estimate the destruction rates of M3 and M13 using the method discussed above, it was found that they equated to destruction rates several orders of magnitude higher than those predicted by several models of globular cluster destruction (Gnedin & Ostriker, 1997, Moreno et al., 2014). Paper II (Navin et al., 2016) described this study and was published in the Astrophysical Journal in October 2016.

Once a method of calculating destruction rates had been developed for Paper II, it was also applied to the four extratidal stars of NGC 1851 found in Paper I. The destruction rate from the observations broadly agreed with the predictions of the models of Gnedin & Ostriker (1997), but was several orders of magnitude higher than those of Moreno et al. (2014). This result was included in Paper III, the main abundance study for NGC 1851, carried out by Dr Jeffrey Simpson. The four extratidal stars were also confirmed as ex-members of NGC 1851 in that paper.

The evidence for discrepancies between the models and the observations seemed to be accumulating and was intriguing. All three globular clusters studied up to this point in the project showed discrepancies between the observed and the predicted destruction rates, and generally the observed destruction rates were several orders of magnitude higher than predicted. However, given the assumptions and approximations in the translation of observed

mass-loss rate to destruction rate, and the small number of globular clusters investigated, it was certainly not conclusive.

The final search for extratidal members of globular clusters was carried out using data from the AEGIS survey. This investigation identified likely extratidal stars around four southern hemisphere globular clusters, 20 for ω Cen, six for NGC 6541, one for M70 and six for M55. When the destruction rates corresponding to the mass-loss rates observed were calculated, the results were striking. All four clusters showed 2–3 orders of magnitude higher rates than predicted by the models of both Gnedin & Ostriker (1997) and Moreno et al. (2014). Paper VII described this study and was submitted for publication to the Monthly Notices of the Royal Astronomical Society Journal in May 2017.

5.2 Future Work

There are several directions in which this research could be expanded and enhanced in the future.

The most obvious step is to increase the sample of globular clusters searched in order to make a more rigorous comparison with the models of globular cluster destruction. Although all seven of the globular clusters studied so far generally show significantly higher destruction rates then the models predict, they are still a small fraction of the Galactic globular cluster system population. An ideal dataset would include stars in and around all globular clusters in a photometrically complete and homogeneously reduced spectroscopic catalogue, and this is not currently available. However, some ongoing and future stellar spectroscopic surveys will provide, in sky-coverage, depth and completeness, a statistically significant subset of this ideal. On the other hand, a study of all the globular clusters of the Milky Way is almost certainly not necessary either. The constitution of a statistically meaningful sample of globular clusters representative of the range of possible destruction regime spaces (different Galactocentric and disk distances, sizes, masses, tidal radii, concentrations etc) needs to be determined.

There are several large stellar spectroscopic surveys that show promise as datasets. Membership of the GALAH (Galactic Archaeology with HERMES) survey collaboration (De Silva et al., 2015, Martell et al., 2017) provides access to the early data releases of (eventually) one million high-resolution stellar spectra optimised for chemical tagging. Other surveys that might be suitable include APOGEE (Allende Prieto et al., 2008), Gaia-ESO (Gilmore et al., 2012), and the WEAVE (Dalton et al., 2014) Galactic archaeology survey. Later data releases of LAMOST may also yield further results. In addition, data may be obtained through targeted observing proposals for specific globular clusters that might not be detected in surveys due to faintness or spatial limits, etc. There are already data in hand for several clusters that have not yet been analysed or studied.

The selection process used to identify likely extratidal stars has so far prioritised clusters with high radial velocities, as this enables a straightforward and convincing differentiation of cluster members and extratidal stars from field stars. However, the methods exploited in Paper II to determine V_r limits and membership probabilities are applicable to clusters with lower V_rs, so both the LAMOST and AEGIS catalogues may hold further useful data.

It may also be possible to place constraints on cluster destruction rates for globular clusters where no extratidal candidate stars are found, both in these and further studies. As the destruction rate (ν) of a cluster increases, the probability of getting 1,2,3,4... (i.e. $\geq$1) extratidal star detections [P($\geq$ 1 detection $\mid$ ν)] will also increase. If P($\geq$ 1 detection $\mid$ ν) is

greater than, say, 0.05 then there is a 95% probability that an extratidal star should have been detected. To calculate the minimum ν that gives P($\geq$ 1 detection | ν) > 0.05 (or, more simply, the minimum ν that gives P(0 detections | ν) < 0.05)), the Poisson distribution is likely to be a good model:

- the number of stars escaping from a globular cluster is discrete,
- the rate of stars escaping is constant for a reasonably long period, at least compared to the time intervals being considered (see below), and not too high,
- the probability of a star escaping in a small sub-interval is proportional to the length of the sub-interval, and
- each escape is independent of the time since the last escape

The Poisson distribution is given by:

$$P(k, \lambda) = \frac{\lambda^k \times e^{-\lambda}}{k!} \tag{5.1}$$

where λ = the average number of events per time interval, and k = the number of events occurring in a fixed time interval. The time interval of interest would be the time it takes for a star that has escaped from the globular cluster to drift (t_d) beyond our search radius (for clusters where extratidal stars have been found in this work, this has ranged from 54 to 228 Myr for a 5° radius). λ can be calculated from ν using the globular cluster mass, t_d, and completeness.

As a trial, these ideas were applied to M19 (NGC 6273) and Terzan 8, the two globular clusters for which no extratidal stars were detected in the AEGIS data. For both clusters, the destruction rate ν that gave P(0 detections | ν) < 0.05 was of the same order of magnitude as the ν predicted by the models (Gnedin & Ostriker, 1997, Moreno et al., 2014). So, if the model ν is correct, then there is a 95% probability that an extratidal star should have been detected. However, ν is very sensitive to the calculated completeness. As mentioned in Paper VII, both M19 and Terzan 8 are considerably fainter than the other clusters studied, and only the brightest part of the giant branches of these clusters is within the V magnitude faintness limit of the UCAC4 catalog used for estimating completeness. It is likely that completeness is overestimated by several orders of magnitude. Consequently, the ν giving P(0 detections | ν) < 0.05 could be one or two orders of magnitude higher than the ν predicted by the models and no stars would be detected. For brighter globular clusters where completeness can be more accurately estimated, this concept shows promise in applying constraints on globular cluster destruction rates. However, the issue of completeness will need a very careful treatment to confirm whether it is suitable for fainter clusters.

The Gaia survey (Gaia Collaboration, 2016) will also offer a wealth of valuable data for this research. Work on deblending and decontamination of the crowded fields found in globular clusters is ongoing, but it is expected that only the final Gaia data releases (with an anticipated public release in 2022-2023) will have the necessary treatment and quality for the fainter globular cluster stars. Eventually, for globular clusters at distances <15 kpc (~1/3 of known Milky Way globular clusters), parallaxes and systemic motions will be known to $\simeq$1% and $\ll$1% respectively, with larger errors for more distant globular clusters. These can be used to calculate more accurate globular cluster orbits. Proper motions of globular cluster member stars at distances <15 kpc will enable cluster mass measurements accurate to $\simeq$10%. Gaia will also measure V_r to within a few km s^{-1} for globular clusters at distances of 10 kpc or more. For all except the most distant known globular clusters, Gaia should provide photometry for at least some giant branch member stars (Pancino et al., 2017). This should be particularly useful in treating the completeness problem for fainter globular clusters discussed

above. Even with lower quoted accuracies and the crowded field problem, earlier data releases will still be extremely useful. Comparisons of proper motions of candidate extratidal stars in the surrounding area (where crowding is not a problem) can still be made with cluster proper motions. Accurate proper motions of member stars will enable the overall proper motion of the globular cluster as a group to be determined more accurately for comparisons. More accurate calculations of globular cluster orbits and masses will enable better determinations of the relative velocity of escaped stars and destruction rates.

There is also the prospect of applying data mining and machine learning techniques to automatically/objectively identify candidate extratidal stars in large datasets. There are a number of dimensionality reduction methods such as t-SNE and classification methods such as support vector machines, K-nearest-neighbour, and others, that could be investigated. Although they did not eventually form part of this thesis research, some promising initial investigations of these methods have been made that warrant further work on their applicability. The classifier that is chosen may vary with different datasets depending on the availability of labels for some of the data to form a training set, the number of measured and reduced data dimensions and the size of the dataset.

The calculation of destruction rates that has been used so far also needs consideration. In particular, the formula used for the calculation of the relative velocity of escaped stars is, as mentioned above, only applicable to globular clusters in circular orbits in the disk. For clusters with eccentric or inclined Galactic orbits, some research is necessary to find out how reasonable this adopted approximation is, or whether a more rigorous treatment is required. Certainly the relative escape velocities of stars would actually form a distribution function rather than the single value that has been used so far, so this concept also needs to be included.

5.3 Implications of the results

The final outcome of this and future work may be that the models of globular cluster destruction are consistent with the observed mass-loss rates for all or most clusters. The trend for the observed destruction rates to be higher than the models predict may simply be the result of small number statistics, as only a fraction of the Milky Way's globular cluster population has been studied. It may also fade as a consequence of eliminating or quantifying the assumptions and approximations used in the calculation of the destruction rates from the observations.

Alternatively the trend may continue for some or even most clusters, which would be an intriguing result. The simulations are complex, but the primary inputs are the kinematical and structural parameters for the clusters themselves, and the model used for the Galactic gravitational potential. If only some clusters show differences between the models and the observations, this would most likely be due to individual cluster parameters adopted for the simulations, which may change with better observations. If there are differences for a significant fraction of clusters, then the Galactic potential model or some aspects of the simulations themselves may require refinement.

The models predict the current destruction rate of globular clusters, i.e. the rate for present-day clusters evolving forward during the next Hubble time. This does not necessarily reflect the destruction rate from their formation until the present day. To estimate how many globular clusters have been destroyed since their formation (and the initial cluster masses) requires a lifetime function from which an historical mean or median rate can be derived. Gnedin & Ostriker (1997) considered the form of two possible lifetime functions, a constant mean destruction time (exponential decay) and a scale-free power law. The scale-free power

law function was favoured, as their models indicate that the time to destruction for the clusters that remain is of the same order as the age of the existing sample. For a scale-free power law function this would be true at any time since formation, but for a constant mean destruction time function this would only be true at the present-day. They concluded that the present-day population of globular clusters was a small fraction of those originally formed, and that a large fraction of the stars in the Galactic bulge and halo originated in globular clusters. While recognising that globular cluster destruction rates almost certainly change over time, there is also nothing special about the present-day. If the current destruction rates are indeed higher than the models predict, then this is also likely true at other epochs.

This points to globular cluster dynamical evolution scenarios requiring dramatic mass loss. It suggests that the initial masses of globular clusters were much more massive than they are at the present-day, which is in line with the high initial masses required to satisfy the mass-budget problem. It may also be an indication the currently understood initial mass function in the clusters needs refinement. It also follows that there is a significant fraction of the stars of the stellar halo that were contributed by globular clusters. Another possibility is that a high proportion of globular clusters are contributed by the ongoing accretion of dwarf galaxies (e.g. Mackey & Gilmore, 2004) with their retinue of globular clusters that are then subject to rapid dissolution.

It is challenging to estimate the magnitude of these effects. A naive interpretation is that there would initially be several orders of magnitude more globular clusters than currently believed, and/or that they were several orders of magnitude more massive, and that the vast majority of halo stars originate in globular clusters. There is evidence for extremely massive young clusters, and the most dense and massive are likely candidates to become the ancient globular clusters we observe today in the Milky Way (e.g. Portegies Zwart et al., 2010). Although the most massive young clusters in the Milky Way and Local Group galaxies seem to be $\sim 10^5$ $M_\odot$, large numbers of more massive clusters ($\gtrsim 10^6$ $M_\odot$) have also been detected in higher redshift galaxies (e.g. Linden et al., 2017). However, quantifying the effects would require detailed N-body simulations of the formation and evolution of various massive cluster populations in a Milky Way galactic model. This is a large, complex project in itself and an active area of research (e.g. Wang et al., 2016, Carlberg, 2017).

5.4 Final

The galaxy in which we live is the Milky Way or, simply, the Galaxy. It is a vast, ancient, complex and evolving system of stars, gas, dust and dark matter. A great deal is understood about the Milky Way, but there are still many unanswered questions, both large and small, to resolve. This thesis work, I believe, contributes to the resolution of one of those unanswered questions.

A

NGC 1851 project supplementary material

A.1 Uncertainties in the heliocentric radial velocities V_r

Multiple observations of the same target were used to estimate the V_r uncertainties for stars with both multiple and single observations. In these data there were from two to a maximum of four repeat observations of the same star. When the number of repeated observations is low, calculating statistics such as the standard deviation using the same methods as for large numbers of observations is inaccurate. Instead, an estimate of the standard deviation of V_r (σ_{V_r}) was calculated using the simplified statistics for small number of observations methods of Dixon & Massey (1951). The standard deviation σ_{V_r} of V_r is given by:

$$\sigma_{V_r} = R \times K_N \tag{A.1}$$

where R is the range of a set of N (= 2,3,...,10) observations and K_N is a deviation factor that depends on the number of observations (for our observations we require $K_2 = 0.89$, $K_3 = 0.59$ and $K_4 = 0.49$).

Figure A.1, not included in Paper I due to space considerations, shows the means of the σ_{V_r}s in bins for median continuum levels of the spectra of observed stars between the two strongest Ca II triplet lines measured in ADU. This plot was used to visualise the uncertainties in V_r (ΔV_r) based on the median continuum level of the spectra. As expected, the mean σ_{V_r} generally decreases as the continuum levels (and the signal-to-noise) of the spectra increases. At continuum levels from 0 to 200 ADU's the mean of the σ_{V_r} is 4.74 $\mathrm{km\,s^{-1}}$, dropping to 1.12 $\mathrm{km\,s^{-1}}$ in the 3000 to 4000 ADU bin. Above a continuum level of 4000 ADU there are only small numbers of stars in the bins (5 in the 4000 to 5000 ADU bin and 11 in the 5000 to 6000 ADU bin), so a standard $\sigma_{V_r} = 1.12$ $\mathrm{km\,s^{-1}}$ was adopted for all stars with continuum levels higher than 3000 ADUs.

For stars with single observations, their continuum level gave a corresponding mean σ_{V_r} which was then adopted as the uncertainty ΔV_r for that star's measured V_r. For stars with N multiple observations the mean continuum level of the N observations gave a corresponding mean σ_{V_r}, which was divided by $\sqrt{N}$ to give the adopted $\Delta V_r$for that star's measured V_r.

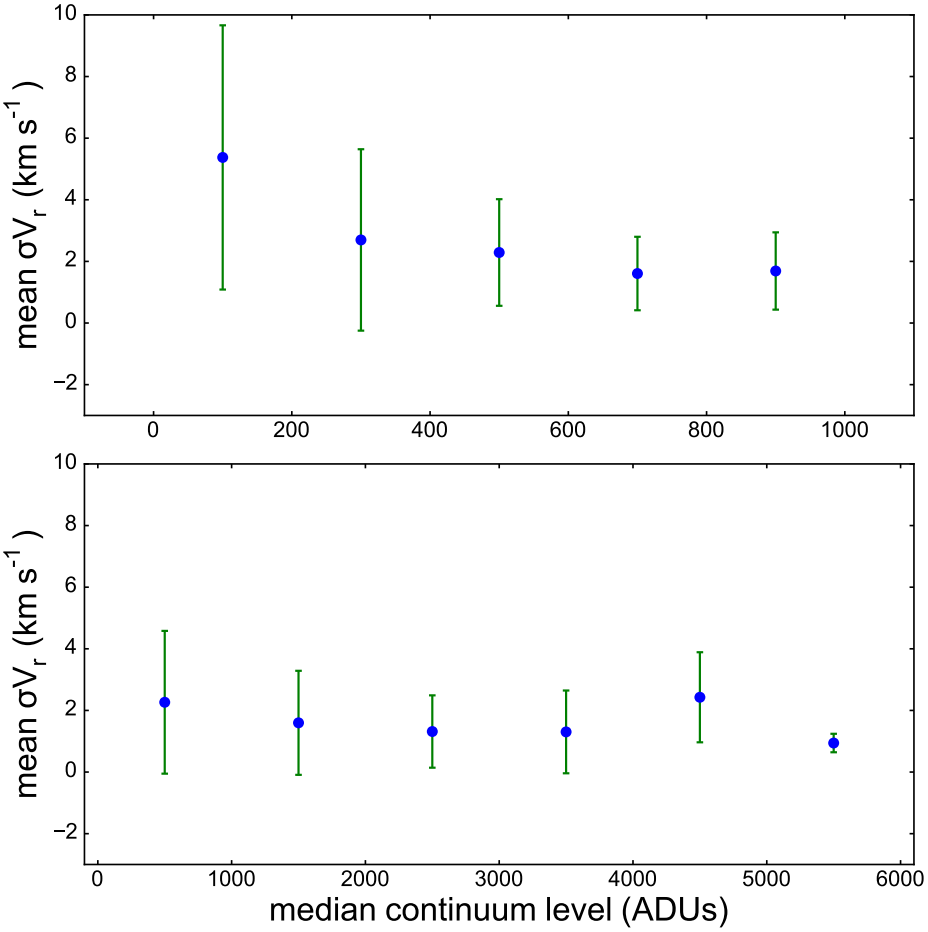

Figure A.1: Top panel: Means of the measured standard deviations of V_r (σ_{V_r}) in 200 ADU bins for spectra with median continuum levels from 0 to 1200 ADU's. Bottom panel: Means of σ_{V_r} in 1000 ADU bins for spectra with median continuum levels from 0 to 6000 ADU's. The error bars show the standard deviation of the σ_{V_r} s in each bin.

A.2 AAOmega spectra of NGC 1851 stars

The top panels show the blue channel AAOmega spectrum of the candidate members and extratidal halo stars of NGC 1851. The coloured regions show the wavelength ranges for the calculation of the primary spectral indices S(3839) and S_2(CH) used in the second paper on NGC 1851 (Simpson et al., 2017a). The closest grey regions to each coloured region show the ranges used for measurement of the continuum for that index. The other two indices used in the paper (HK′ and CH(4300)) are not shown as they overlap, or partially overlap, the S(3839) and S_2(CH) index, respectively. The bottom panel shows the red channel spectrum of the same star. The coloured regions show the CaT absorption lines used for measurements of V_r and [Fe/H]. All the spectra are shifted to the rest wavelength.

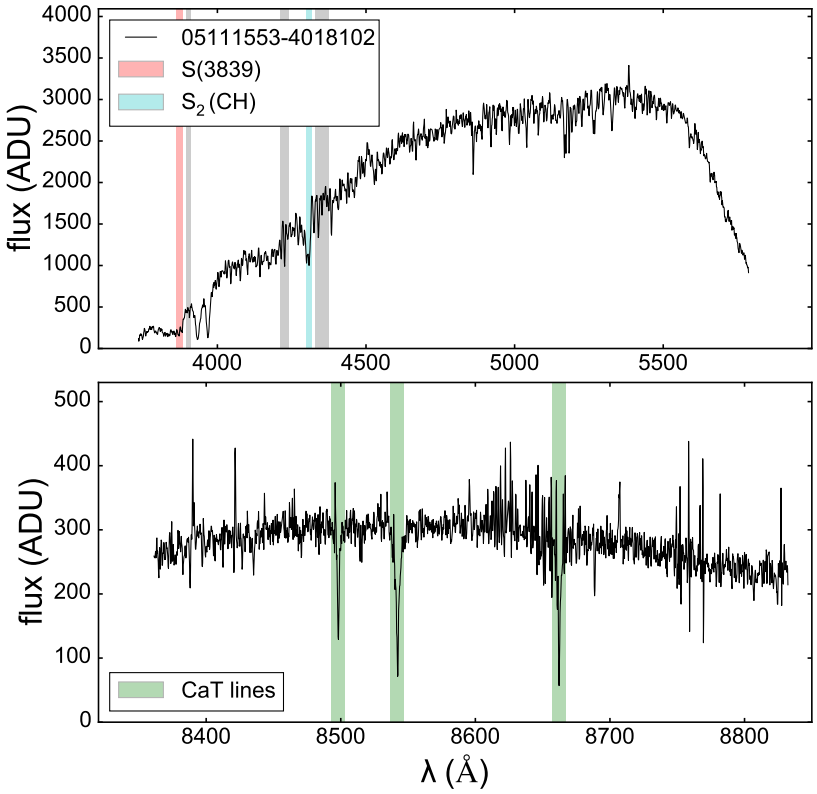

Figure A.2: 2MASS ID 05111553-4018102

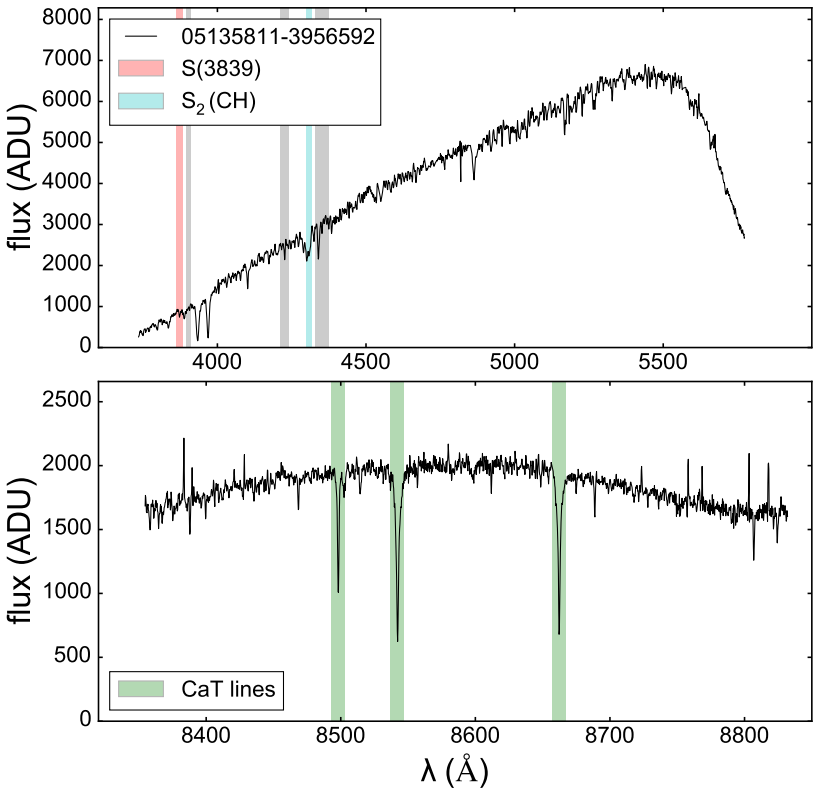

Figure A.3: 2MASS ID 05135811-3956592

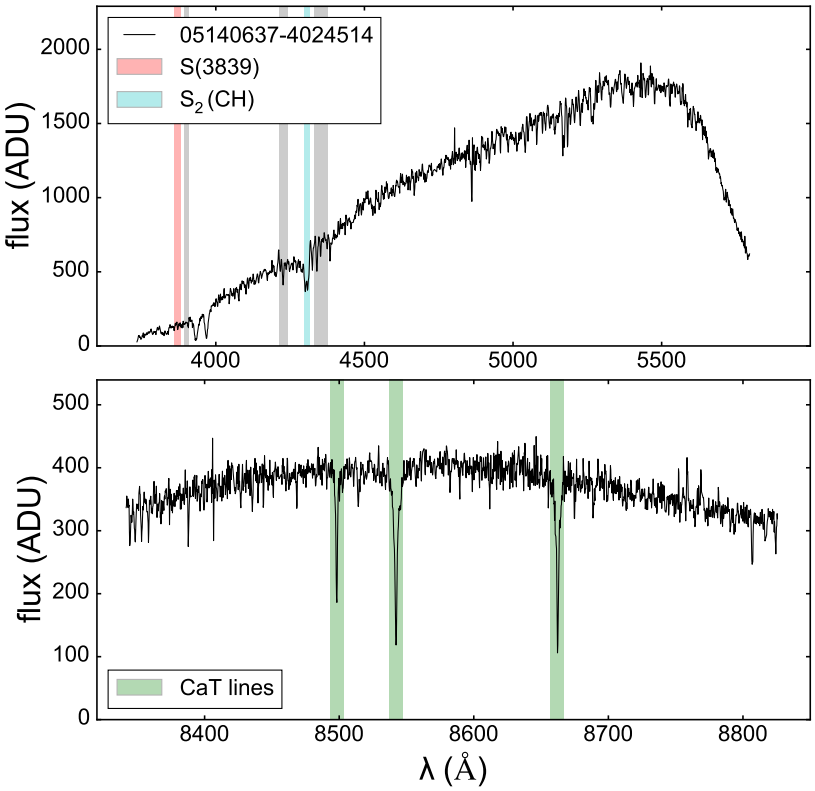

Figure A.4: 2MASS ID 05140637-4024514

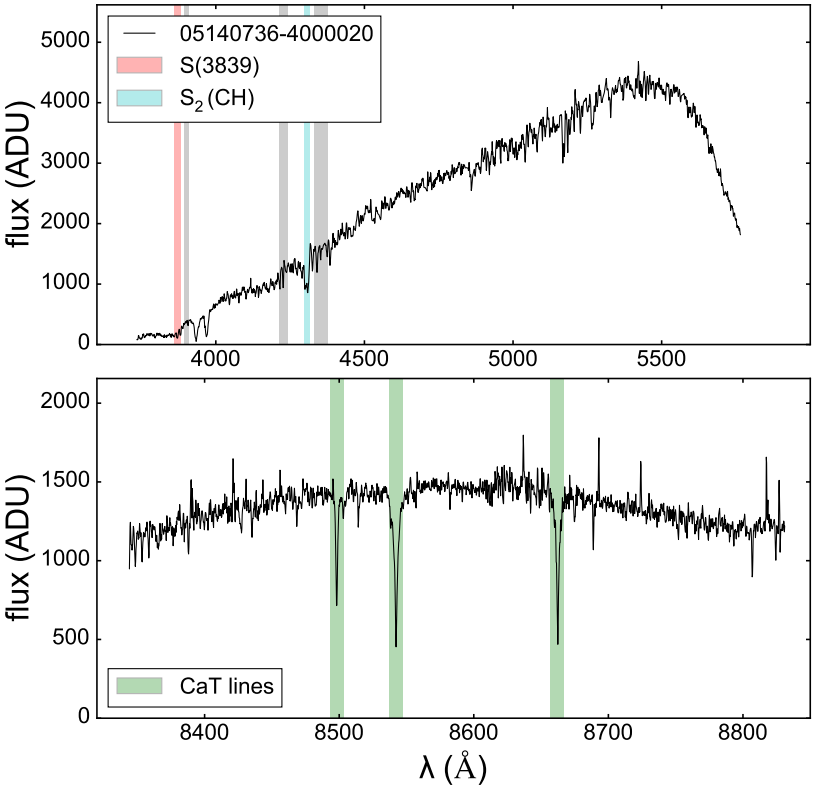

Figure A.5: 2MASS ID 05140736-4000020

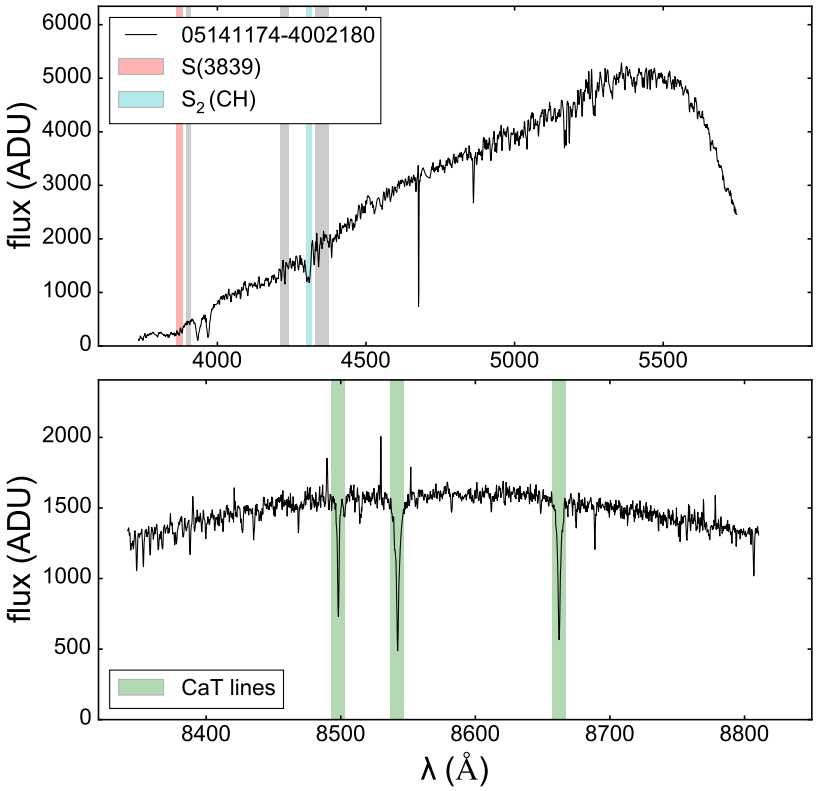

Figure A.6: 2MASS ID 05141174-4002180

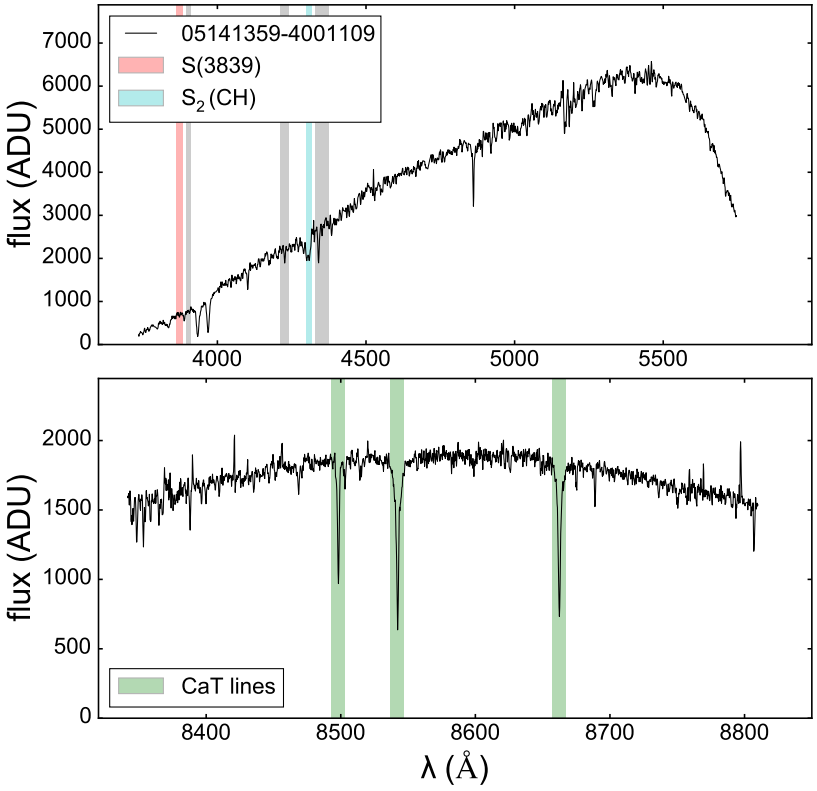

Figure A.7: 2MASS ID 05141359-4001109

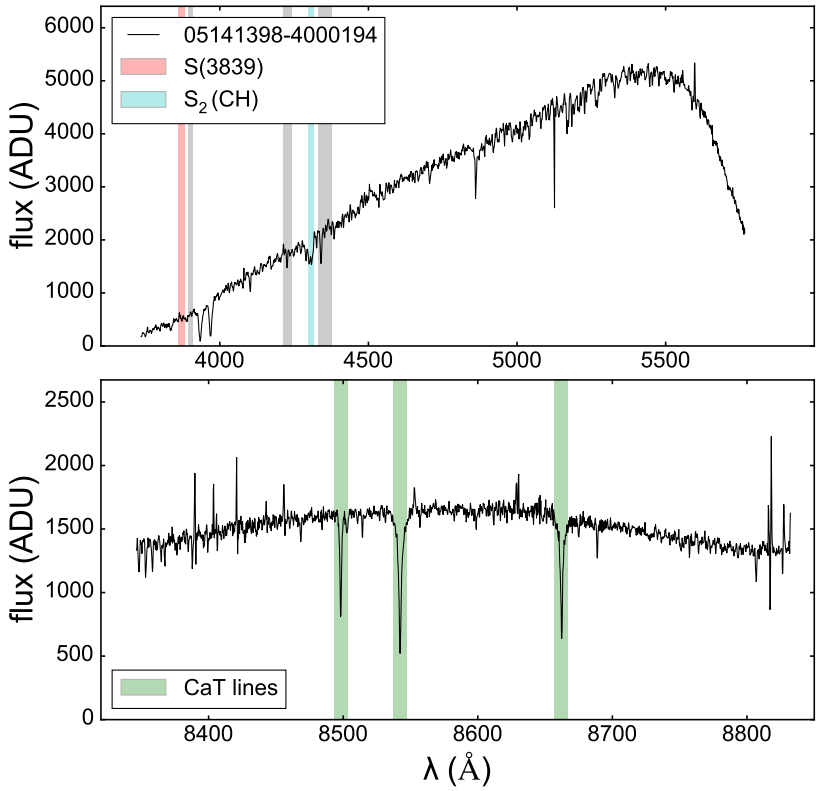

Figure A.8: 2MASS ID 05141398-4000194

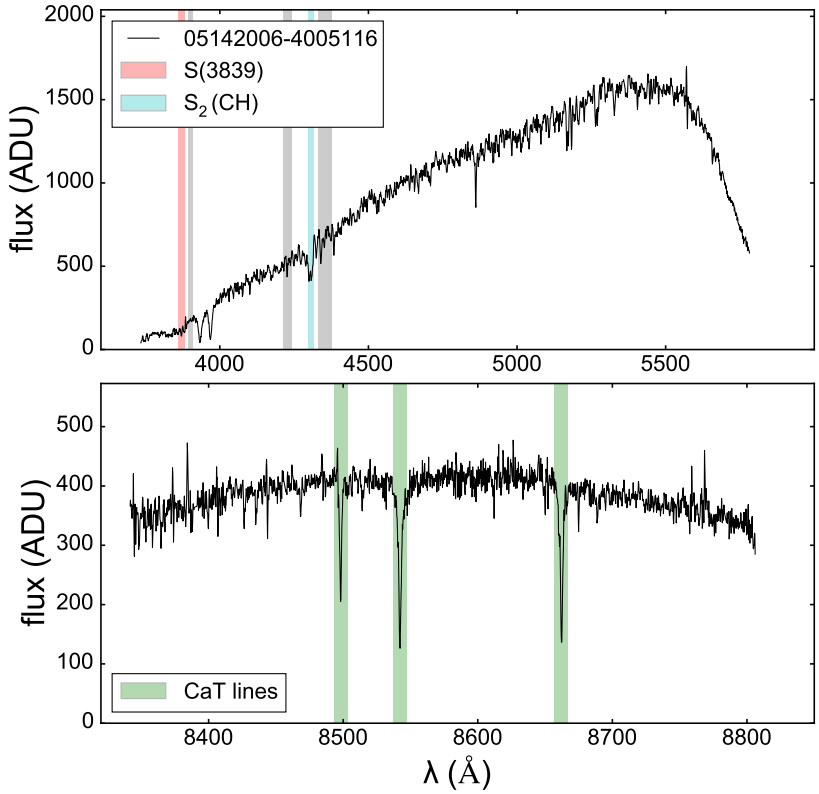

Figure A.9: 2MASS ID 05142006-4005116

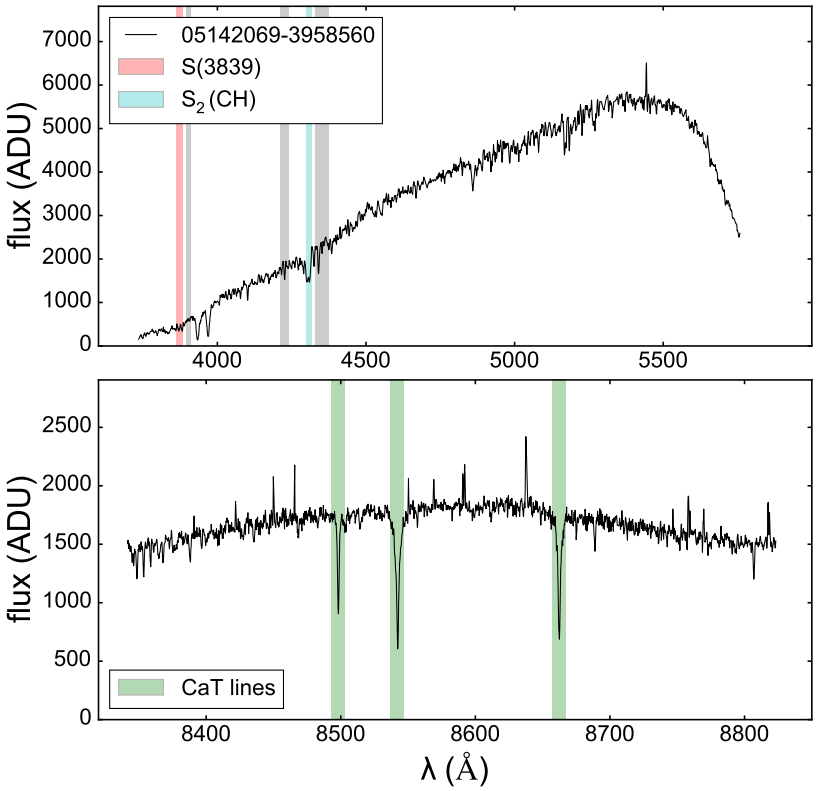

Figure A.10: 2MASS ID 05142069-3958560

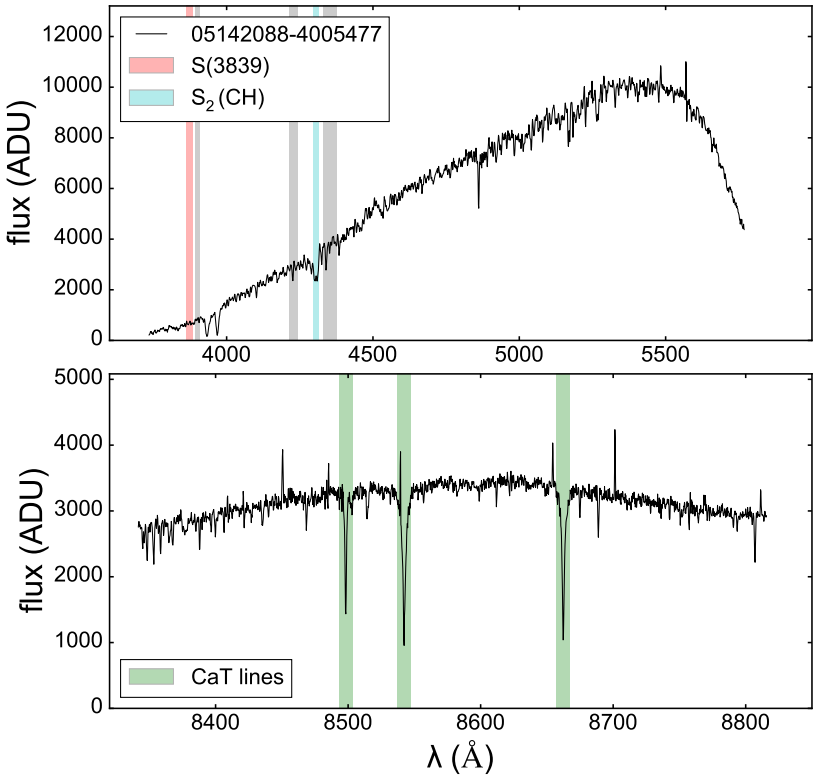

Figure A.11: 2MASS ID 05142088-4005477

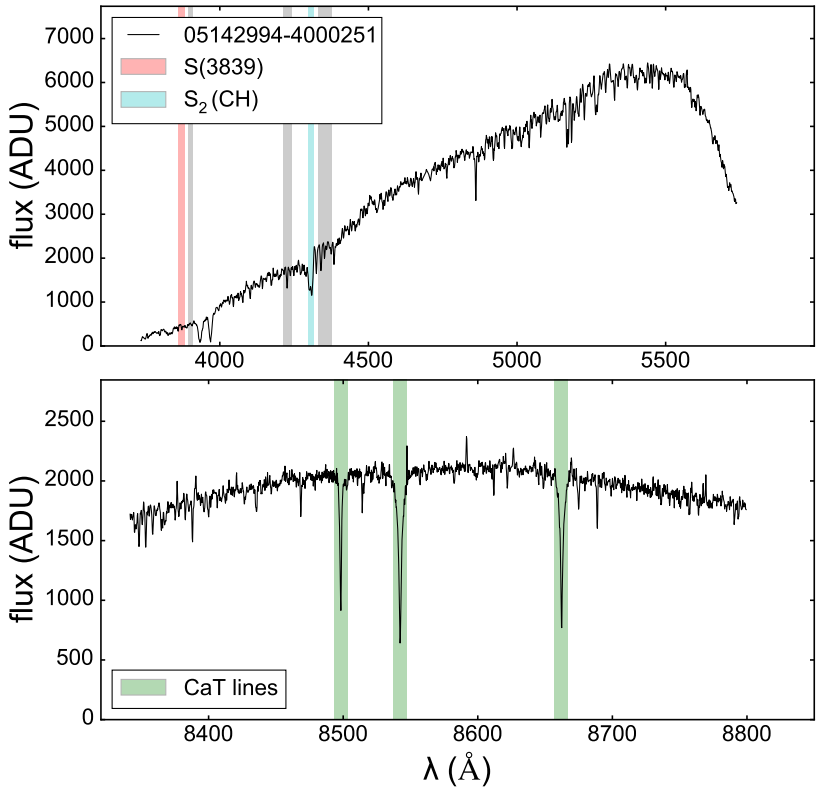

Figure A.12: 2MASS ID 05142994-4000251

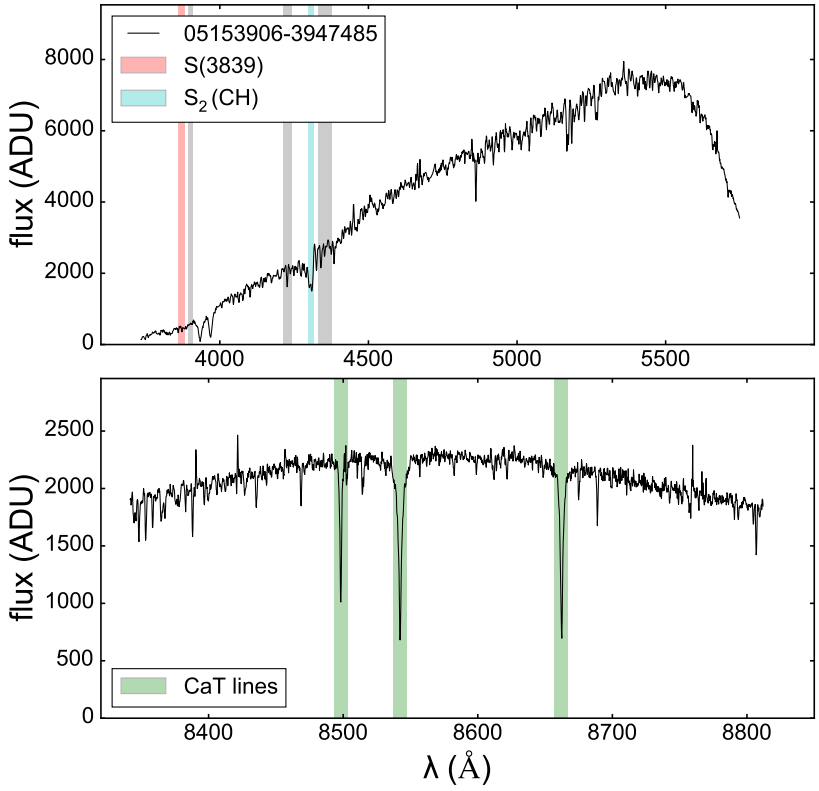

Figure A.13: 2MASS ID 05153906-3947485

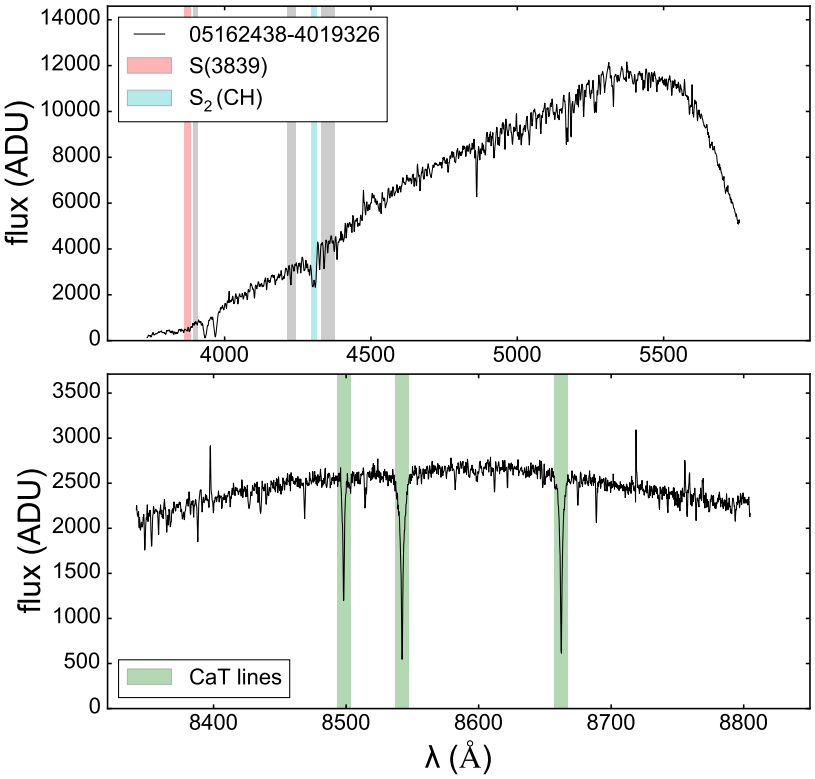

Figure A.14: 2MASS ID 05162438-4019326

A.3 Paper V

Pages 92-106 of this thesis have been removed as they contain published material under copyright. Removed contents published as:

Colin A. Navin, Sarah L. Martell, Daniel B. Zucker, (2016) New halo stars of the galactic globular clusters M3 and M13 in the LAMOST DR1 catalog, *The Astrophysical Journal*, Vol. 829, No. 2, 123, https://doi.org/10.3847/0004-637X/829/2/123.

B

LAMOST project supplementary material

B.1 Destruction rate calculation – Python script

```
def destruction_rate(halo_V_mag_array,
                     angular_drift_distance,
                     completeness,
                     GC_integrated_V_mag,
                     GC_tidal_radius,
                     GC_mass,
                     GC_mu_alpha_cos_delta, GC_mu_delta,
                     GC_Vr,
                     GC_R_Sun,
                     GC_R_gc):

    """
    Calculate the destruction rate of a globular cluster from the mass of
    observed extratidal halo stars

    ----------------------------------------------------------------------
    Arguments
    ----------
    halo_V_mag_array : numpy ndarray
        Array of V magnitudes for the sample of extratidal halo
        stars of the cluster
    angular_drift_distance : astropy.units.Quantity
        - u.deg
        Angular distance stars have to drift to pass outside search radius
        around the cluster
    completeness: float
        Ratio of the number of stars outside the cluster tidal radius in the
        sample of interest to the number of stars outside the cluster tidal
        radius in the similarly selected reference sample
    GC_integrated_V_mag: float
        - Integrated V magnitude of the cluster
        - from Harris, W. 1996, AJ, 112, 1487
    GC_tidal_radius : astropy.units.Quantity
```

```
    - u.arcmin
    - Tidal radius of the cluster
    - calculated from Harris, W. 1996, AJ, 112, 1487
GC_mass : astropy.units.Quantity
    - u.solMass
    - Mass of the cluster
    - from Harris, W. 1996, AJ, 112, 1487
GC_mu_alpha_cos_delta, GC_mu_delta : astropy.units.Quantity
    - u.milliarcsecond/u.yr
    - Proper motion of the cluster in RA and Dec
    - from Kharchenko et al, 2013, A&A, 558,53
GC_Vr : astropy.units.Quantity
    - u.km/u.s
    Radial velocity of the cluster
    - from Harris, W. 1996, AJ, 112, 1487
GC_R_Sun : astropy.units.Quantity
    - u.kpc
    - Distance of the cluster from the Sun
    - from Harris, W. 1996, AJ, 112, 1487
GC_R_gc : astropy.units.Quantity
    - u.kpc
    - Distance of the cluster from the Galactic centre
    - from Harris, W. 1996, AJ, 112, 1487

Returns
-------
halo_V_luminosity_total : float
    Integrated luminosity of extratidal halo stars, calculated from the sum
    of individual V magnitudes
halo_V_mag_total : float
    Integrated V magnitude of extratidal halo stars, calculated from the
    sum of individual V magnitudes
halo_to_cluster_V_luminosity_ratio : float
    Extratidal halo stars stars luminosity as a fraction of cluster
    luminosity
GC_mu : astropy.units.Quantity
    - u.milliarcsecond/u.yr
    - Total proper motion of the cluster, calculated from proper motions in
      RA and Dec
GC_Vt : astropy.units.Quantity
    - u.m/u.s
    - Cluster transverse velocity, calculated from total proper motion
GC_Vs : astropy.units.Quantity
    - u.km/u.s
    - Cluster space velocity, calculated from transverse and radial
      velocities
GC_V_omega : astropy.units.Quantity
    - u.rad/u.s
    - Cluster angular velocity around Galactic centre, calculated from
      space velocity
drift_velocity : astropy.units.Quantity
    - u.m/u.s
    - Tangential drift velocity of escaped stars, averaged over sphere to
      allow for stars escaping in any direction
    - calculated from Kupper et al 2010, MNRAS, 401, 105  equation (18)
linear_drift_distance : astropy.units.Quantity
    - u.m
    - Linear distance stars have to drift to pass outside search radius
```

```
      around cluster
drift_time : astropy.units.Quantity
    - u.Myr
    - Time required for stars to pass outside search radius around cluster
GC_destruction_rate : astropy.units.Quantity
    - 1/u.yr
    - Observed cluster destruction rate
GC_destruction_rate_adjusted : astropy.units.Quantity
    - 1/u.yr
    - Observed cluster destruction rate adjusted for sample completeness
"""

import numpy as np
import astropy.units as u
import math

# calculate halo stars luminosity as fraction of cluster luminosity
halo_V_luminosity_total = 0.0
for V_mag in halo_V_mag_array:
    halo_V_luminosity_total = (halo_V_luminosity_total
                                    + math.pow(10.0, -V_mag/2.512))
halo_V_mag_total = -2.512*math.log10(halo_V_luminosity_total)
halo_to_cluster_V_luminosity_ratio = math.pow(10.0,
                                              ((halo_V_mag_total
                                              - GC_integrated_V_mag)/-2.512))

# calculate cluster transverse velocity GC_Vt
# use small-angleapproximation
GC_mu = np.sqrt((GC_mu_alpha_cos_delta)**2+(GC_mu_delta)**2)
GC_Vt = (GC_mu*GC_R_Sun).to(u.m/u.s,
                            equivalencies=u.dimensionless_angles())

# calculate cluster space velocity GC_Vs
GC_Vs = np.sqrt(GC_Vt**2 + GC_Vr**2)

# calculate cluster angular velocity around Galactic centre GC_V_omega
# use small-angle approximation
GC_V_omega = ((GC_Vs/GC_R_gc).to(u.rad/u.s,
              equivalencies=u.dimensionless_angles()))

# calculate drift velocity from Kupper et al 2010, MNRAS, 401, 105
# equation (18),
# assume that formula for circular orbits in the Galactic disk applies
# use small-angle approximation
drift_velocity = ((4*const.G*GC_mass*GC_V_omega)**(1/3.0)).to(u.m/u.s,
                  equivalencies=u.dimensionless_angles())
# allow for stars escaping in any direction
drift_velocity = drift_velocity*2.0/math.pi

# calculate drift_distance, use small-angle approximation
linear_drift_distance = ((angular_drift_distance*GC_R_Sun)
    .to(u.m, equivalencies=u.dimensionless_angles()))

# calculate drift time for drift_distance
# assume that the drift velocity remains constant as the star escapes
# and drifts away
drift_time = linear_drift_distance/drift_velocity
```

```
    # calculate destruction rate
    # assume that the mass-to-light ratio is the same for the cluster and for
    # the extratidal halo stars
    GC_destruction_rate = halo_to_cluster_V_luminosity_ratio/drift_time
    GC_destruction_rate_adjusted = GC_destruction_rate/completeness

    return (halo_V_luminosity_total, halo_V_mag_total,
            halo_to_cluster_V_luminosity_ratio, GC_mu, GC_Vt, GC_Vs,
            GC_V_omega, drift_velocity, linear_drift_distance, drift_time,
            GC_destruction_rate, GC_destruction_rate_adjusted)
```

C

AEGIS project supplementary material

C.1 AAOmega spectra of candidate extratidal halo stars

The top panels show the blue channel AAOmega spectrum of the candidate extratidal halo stars of the clusters. The coloured regions show the wavelength ranges for the calculation of the primary spectral indices, S(3839) and S_2(CH), used in the paper. The closest grey regions to each coloured region show the ranges used for measurement of the continuum for that index. The CH(4300) index used in the paper is not shown as it overlaps the S_2(CH) index. The bottom panel shows the red channel spectrum of the same star. The coloured regions show the CaT absorption lines used for measurements of V_r and [Fe/H]. All the spectra are shifted to the rest wavelength.

C.1.1 ω Cen (NGC 5139)

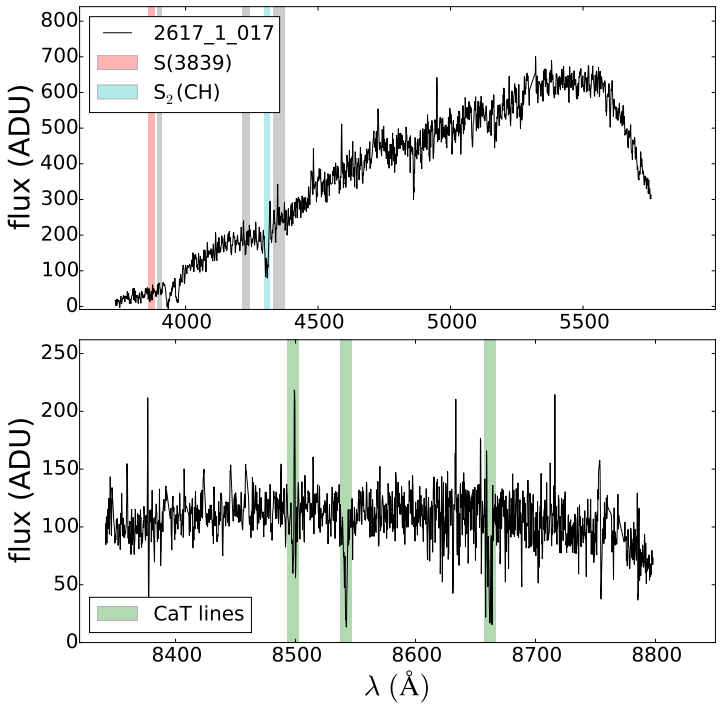

Figure C.1: AEGIS catalogue ID 2617_1_017, 2MASS ID 13325691-4348382

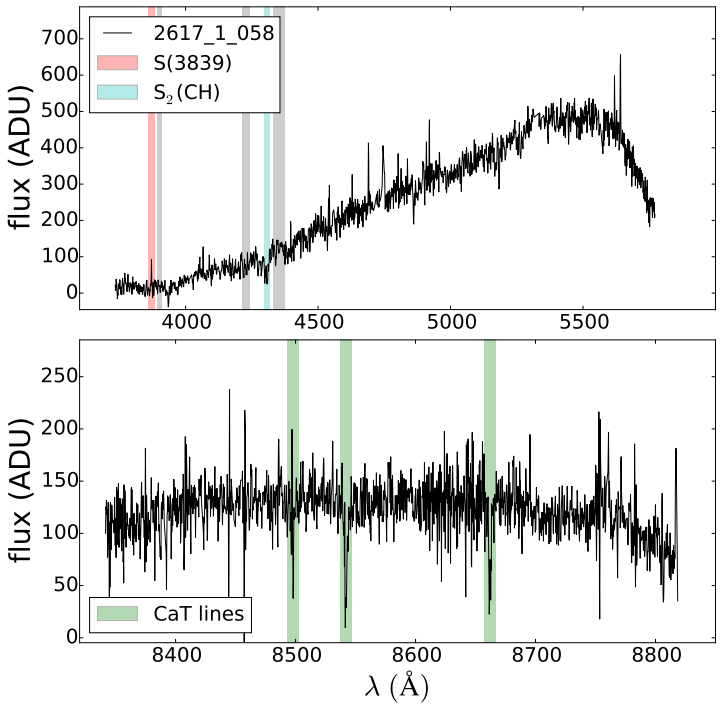

Figure C.2: AEGIS catalogue ID 2617_1_058, 2MASS ID 13301033-4400416

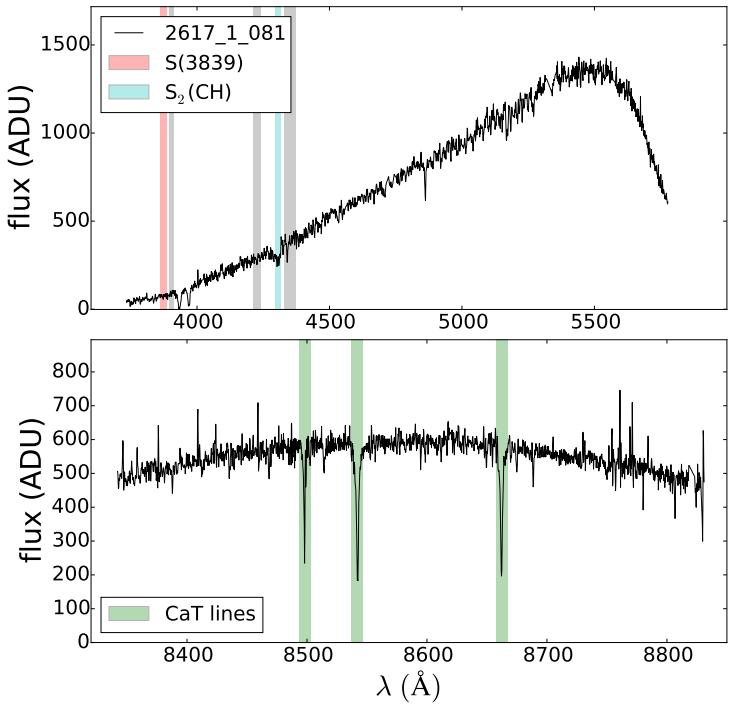

Figure C.3: AEGIS catalogue ID 2617_1_081, 2MASS ID 13295909-4422479

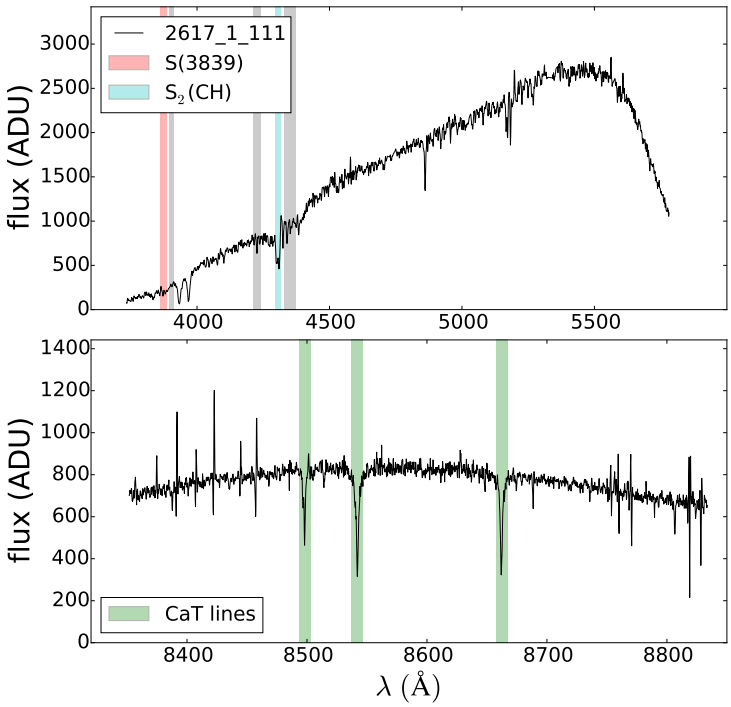

Figure C.4: AEGIS catalogue ID 2617_1_111, 2MASS ID 13284901-4401013

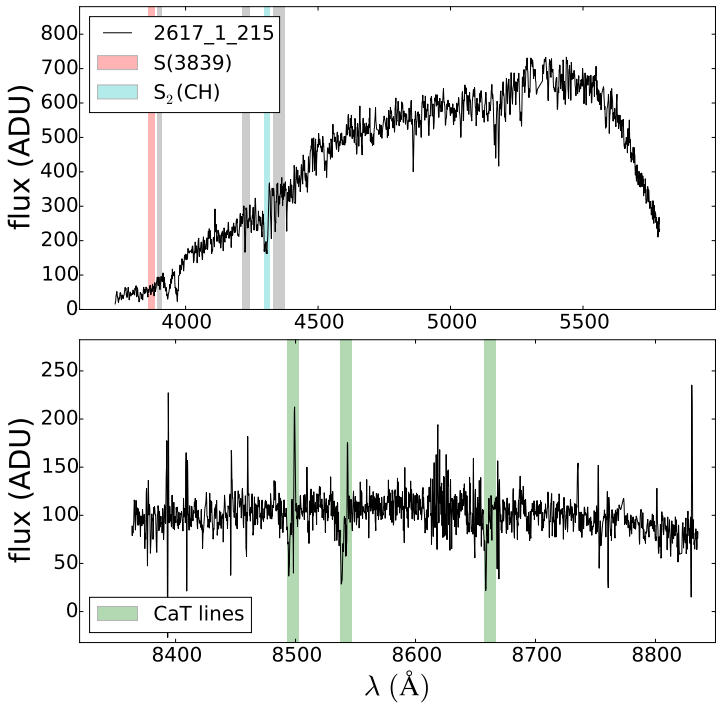

Figure C.5: AEGIS catalogue ID 2617_1_215, 2MASS ID 13240373-4320218

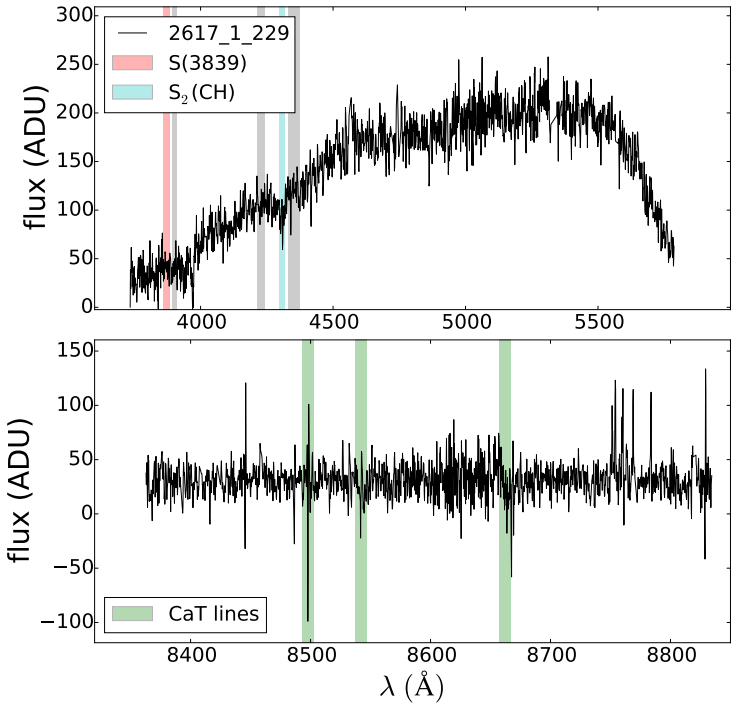

Figure C.6: AEGIS catalogue ID 2617_1_229, 2MASS ID 13242022-4311115

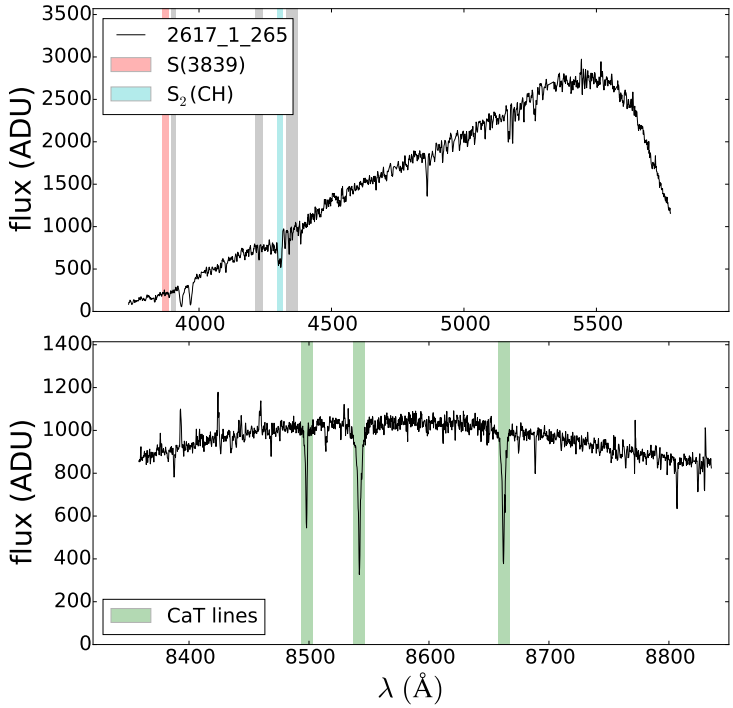

Figure C.7: AEGIS catalogue ID 2617_1_265, 2MASS ID 13273946-4316289

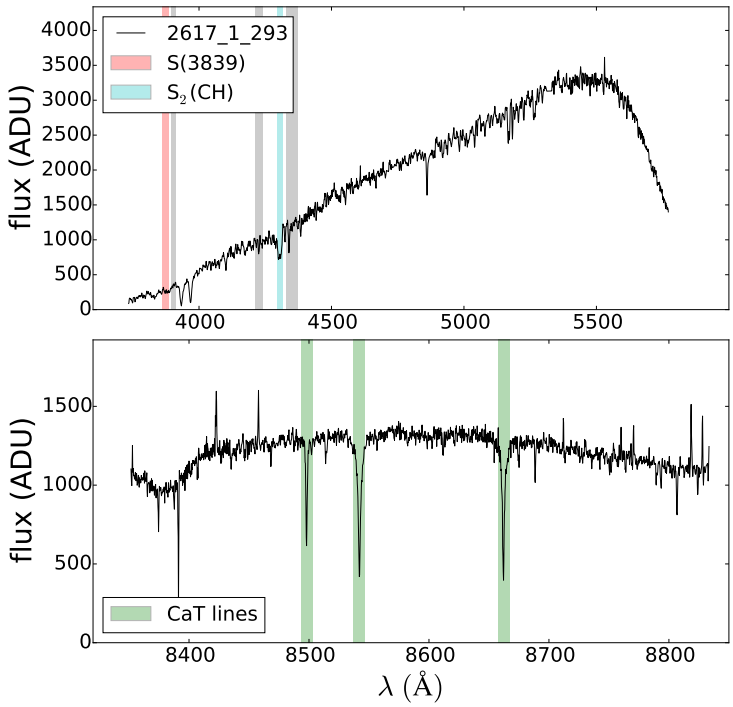

Figure C.8: AEGIS catalogue ID 2617_1_293, 2MASS ID 13281225-4241490

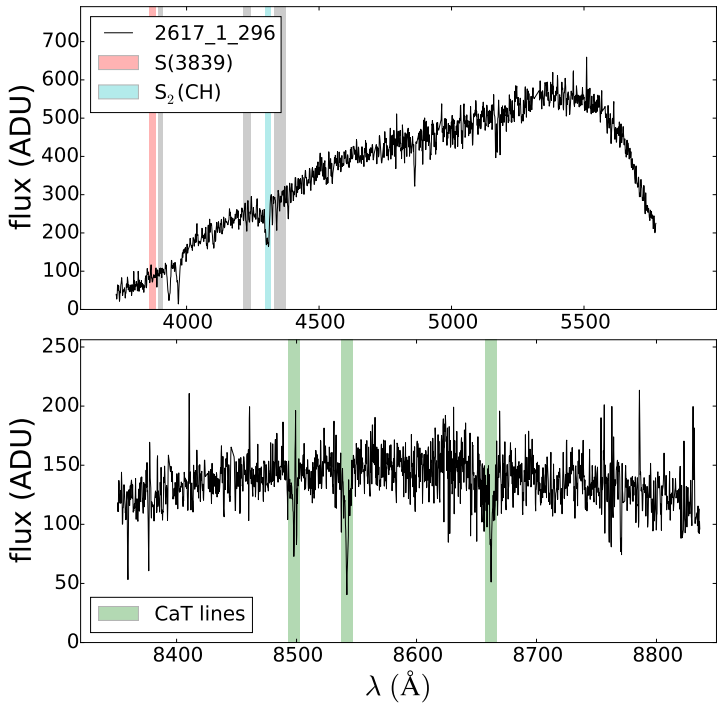

Figure C.9: AEGIS catalogue ID 2617_1_296, 2MASS ID 13282501-4237381

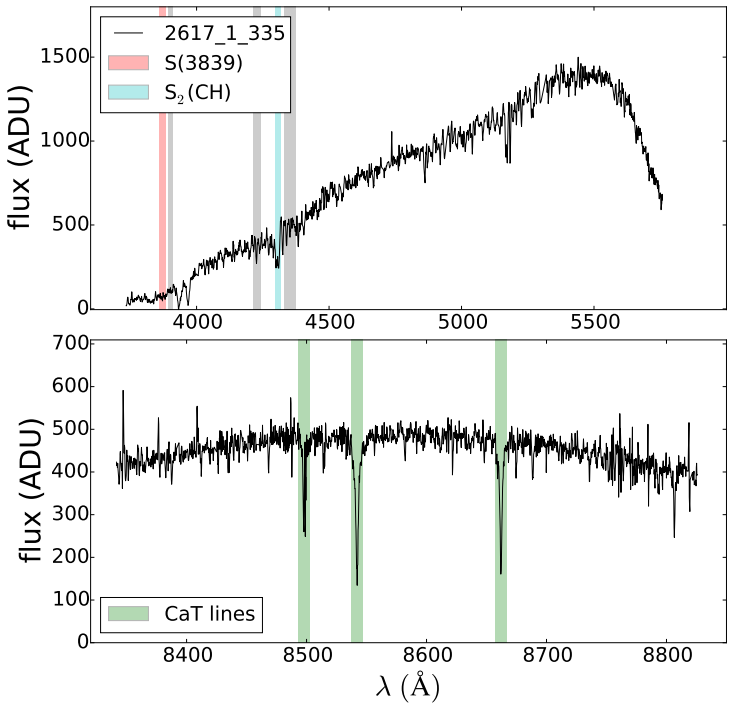

Figure C.10: AEGIS catalogue ID 2617_1_335, 2MASS ID 13291663-4328179

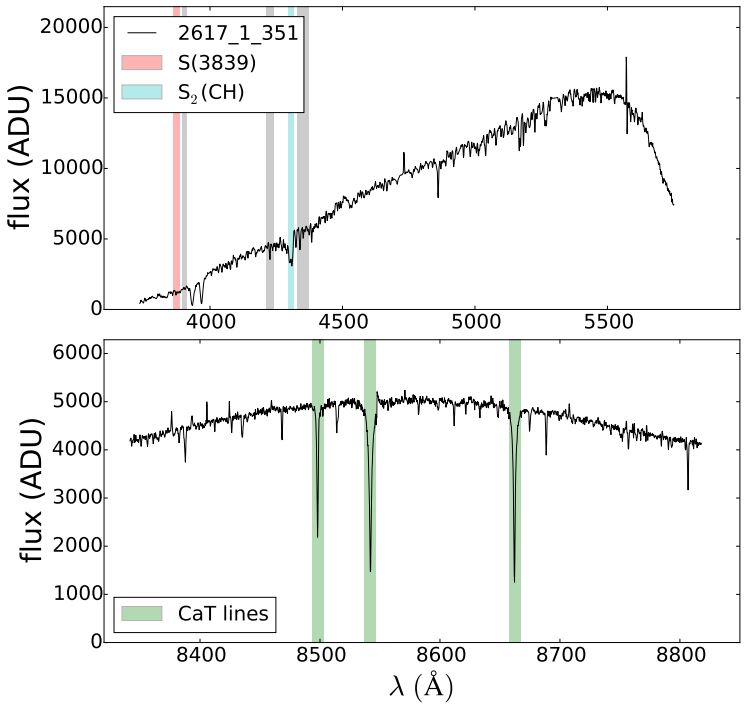

Figure C.11: AEGIS catalogue ID 2617_1_351, 2MASS ID 13294957-4321148

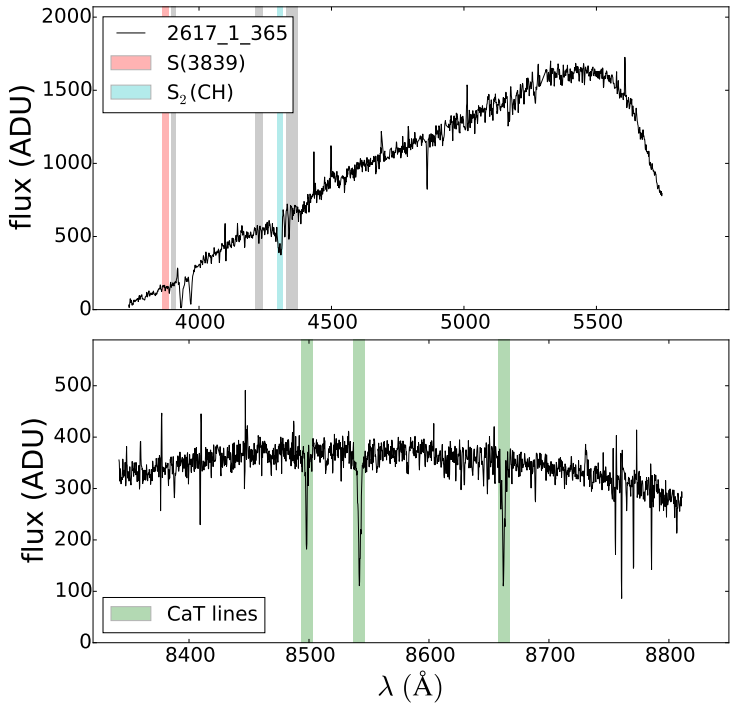

Figure C.12: AEGIS catalogue ID 2617_1_365, 2MASS ID 13313982-4314192

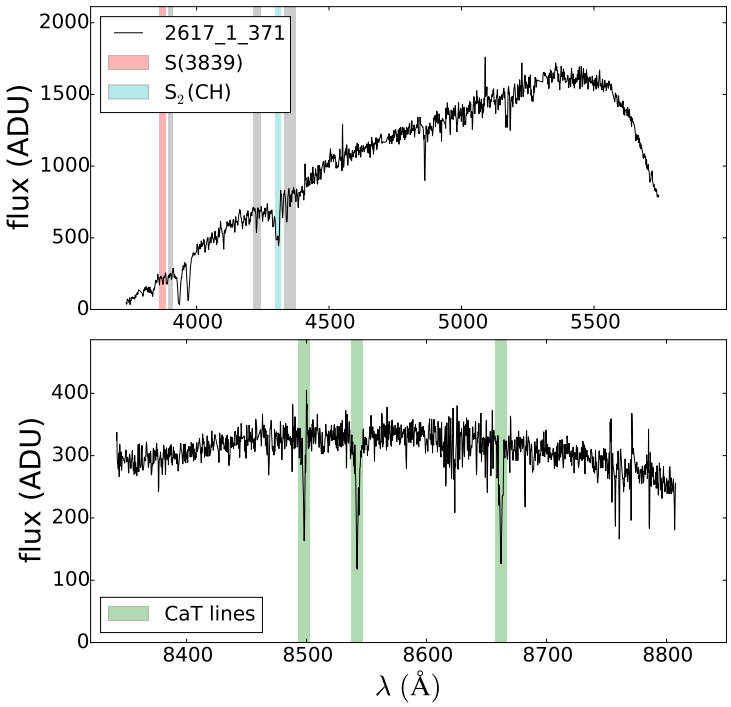

Figure C.13: AEGIS catalogue ID 2617_1_371, 2MASS ID 13303920-4324422

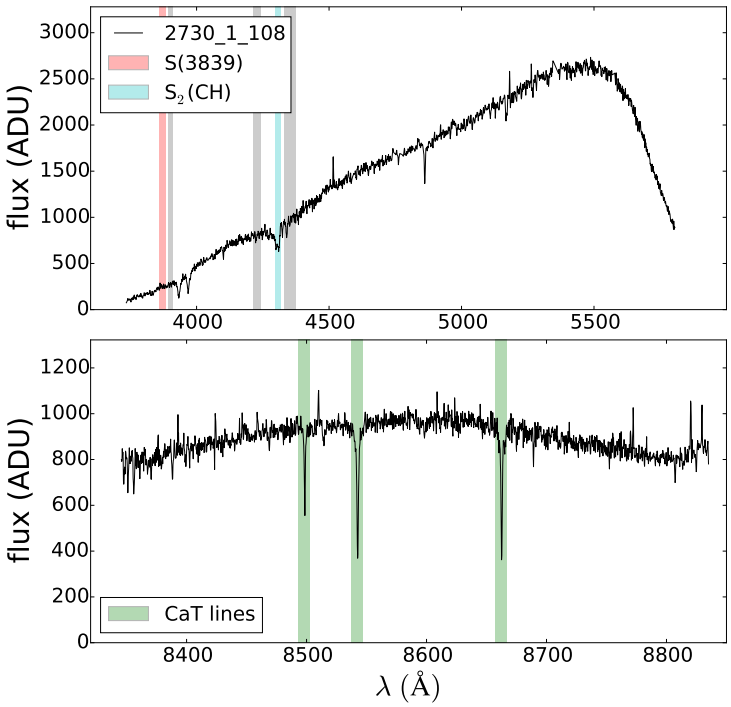

Figure C.14: AEGIS catalogue ID 2730_1_108, 2MASS ID 13440923-4646533

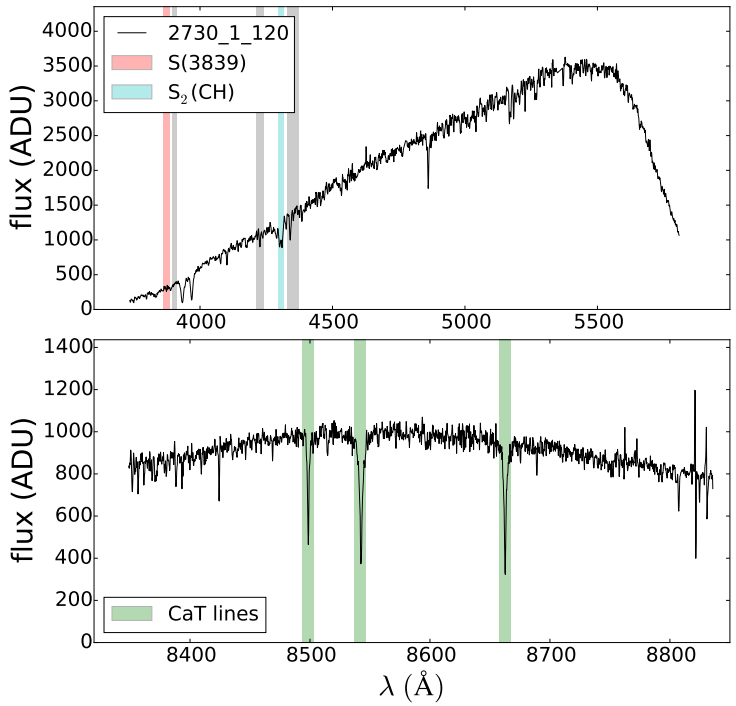

Figure C.15: AEGIS catalogue ID 2730_1_120, 2MASS ID 13434667-4629556

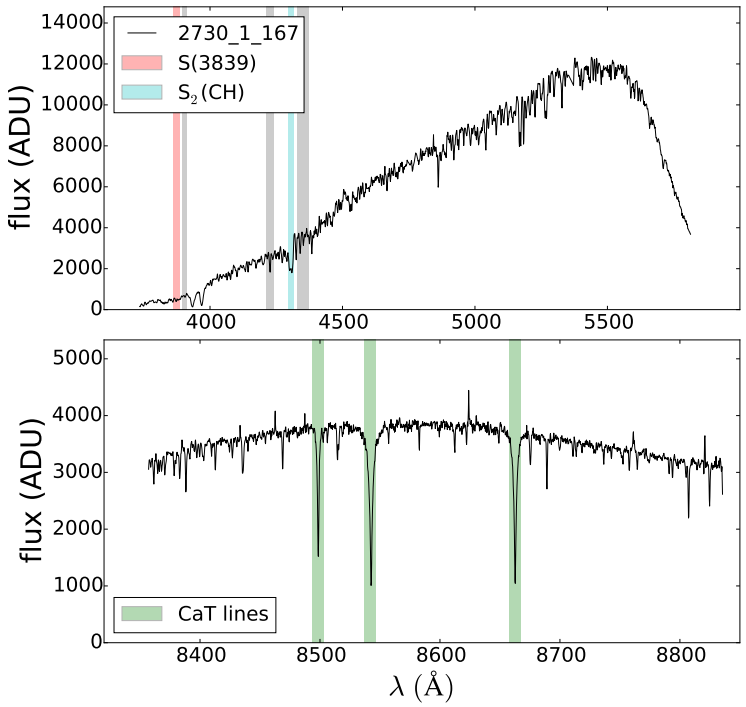

Figure C.16: AEGIS catalogue ID 2730_1_167, 2MASS ID 13414597-4611521

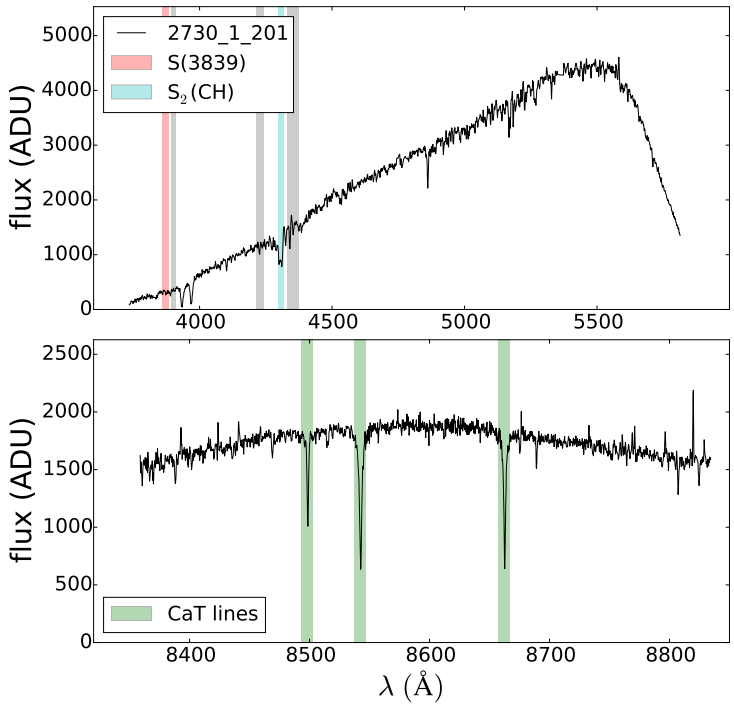

Figure C.17: AEGIS catalogue ID 2730_1_201, 2MASS ID 13393344-4554306

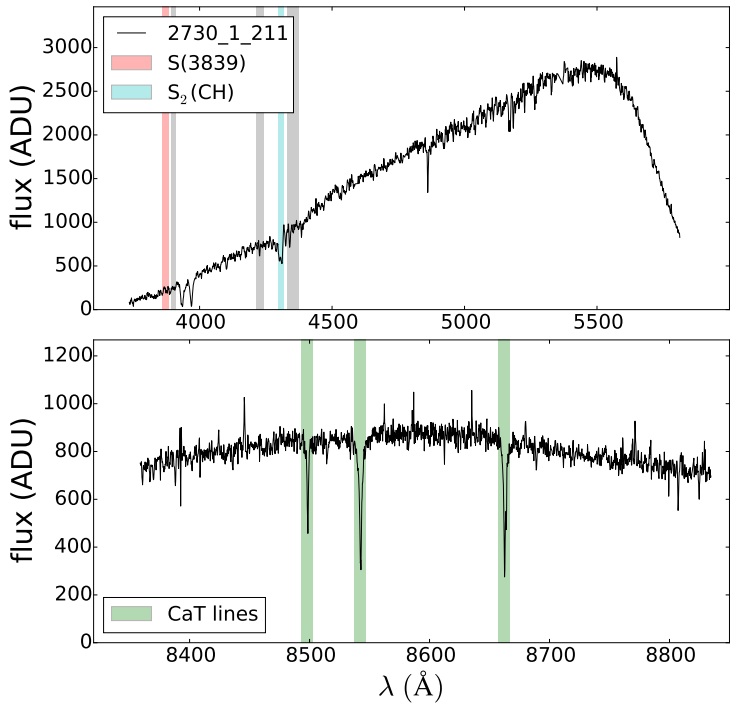

Figure C.18: AEGIS catalogue ID 2730_1_211, 2MASS ID 13410344-4549131

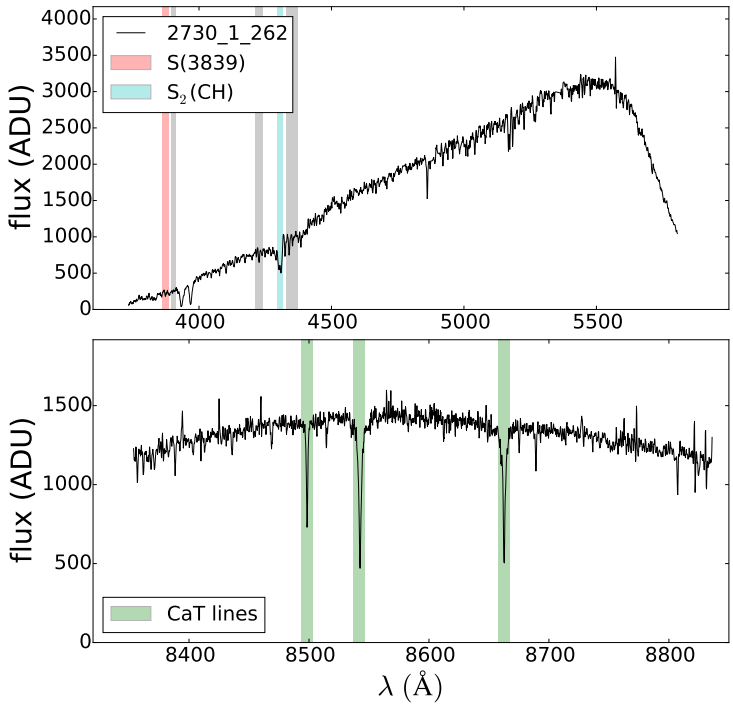

Figure C.19: AEGIS catalogue ID 2730_1_262, 2MASS ID 13440360-4547255

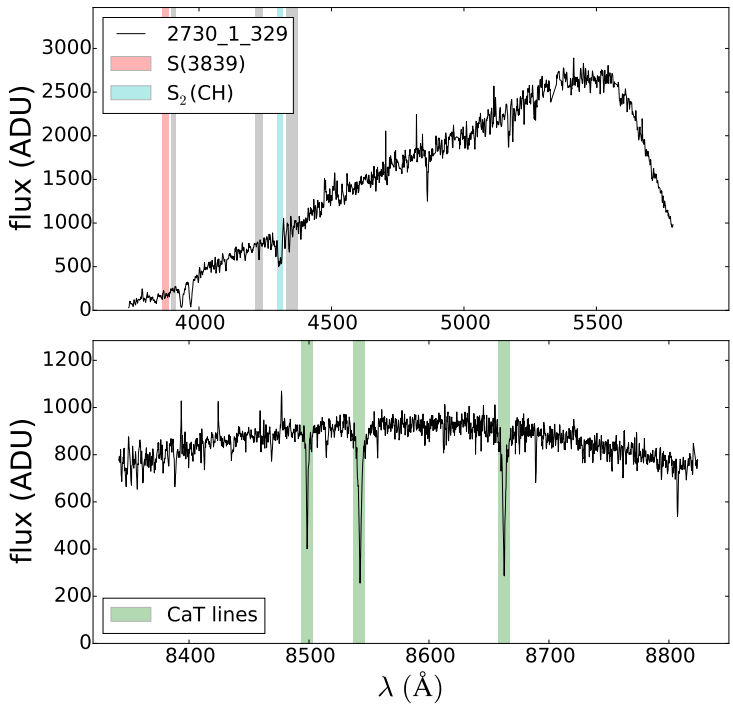

Figure C.20: AEGIS catalogue ID 2730_1_329, 2MASS ID 13472153-4502479

C.1.2 NGC 6541

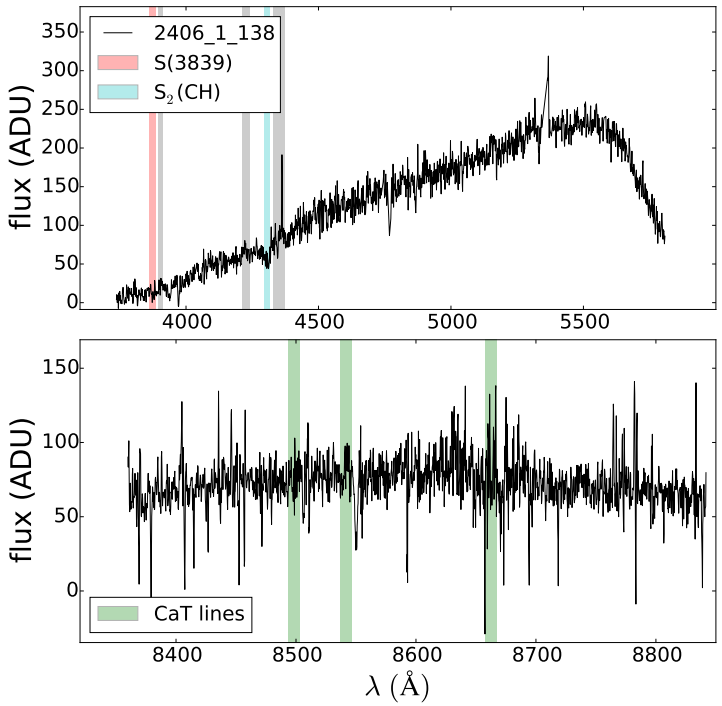

Figure C.21: AEGIS catalogue ID 2406_1_138, 2MASS ID 18154675-3931539

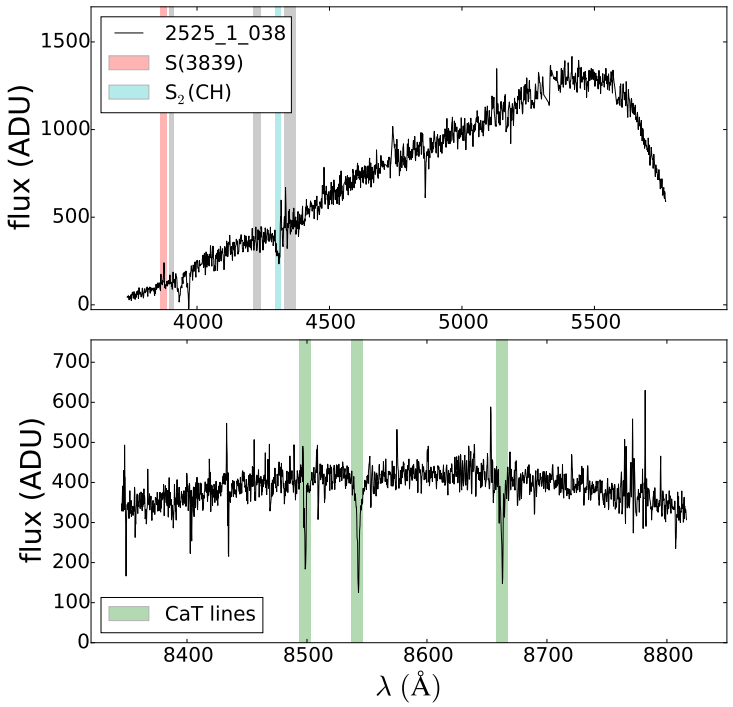

Figure C.22: AEGIS catalogue ID 2525_1_038, 2MASS ID 18221874-4152282

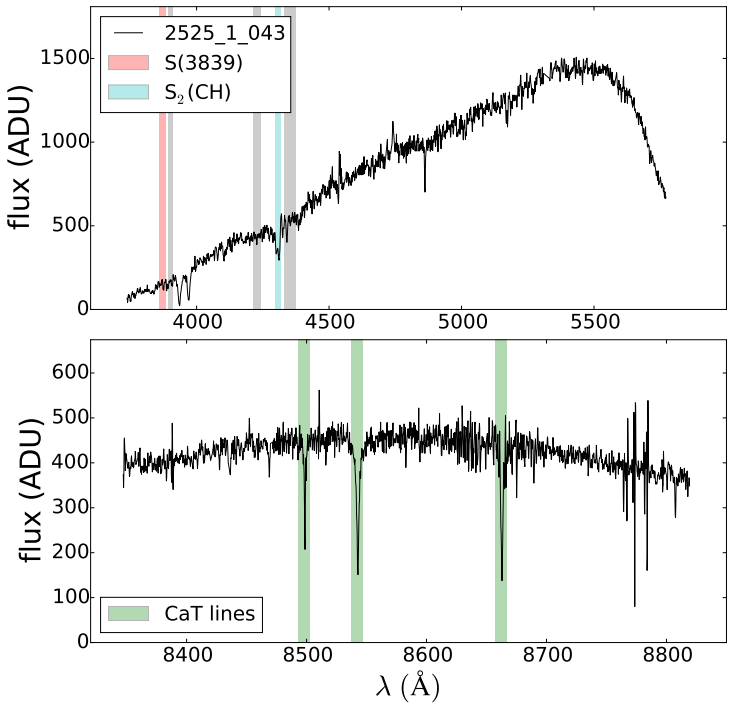

Figure C.23: AEGIS catalogue ID 2525_1_043, 2MASS ID 18195922-4134263

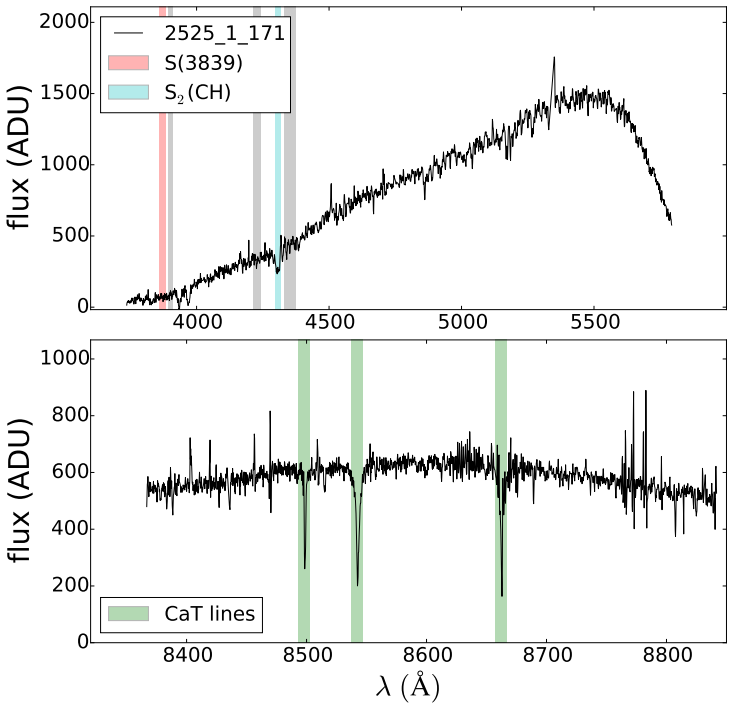

Figure C.24: AEGIS catalogue ID 2525_1_171, 2MASS ID 18140795-4140225

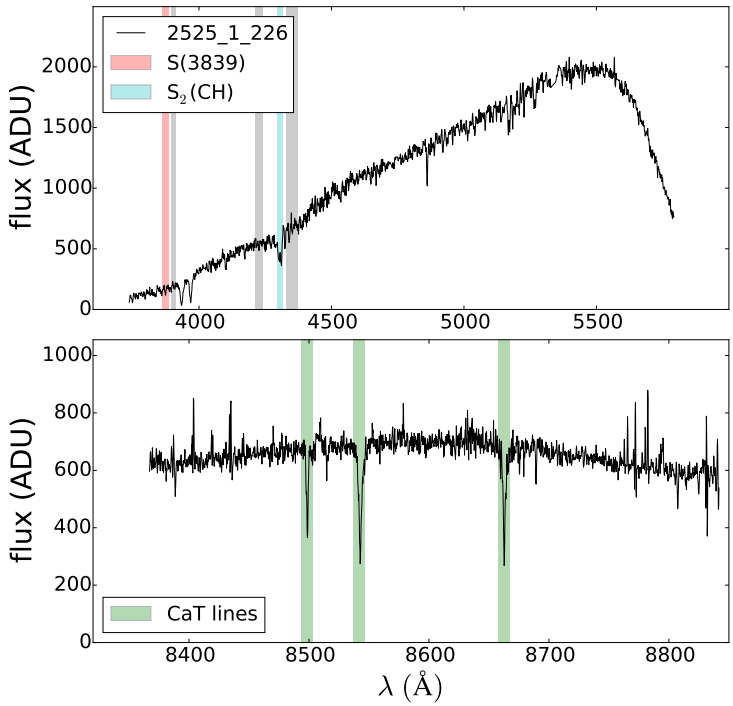

Figure C.25: AEGIS catalogue ID 2525_1_226, 2MASS ID 18141057-4059179

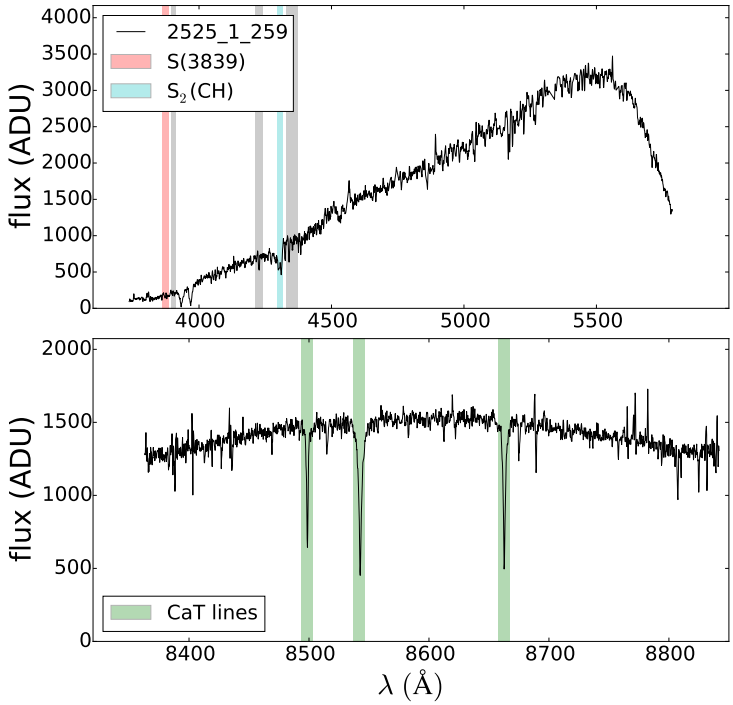

Figure C.26: AEGIS catalogue ID 2525_1_259, 2MASS ID 18152617-4036395

C.1.3 M70 (NGC 6681)

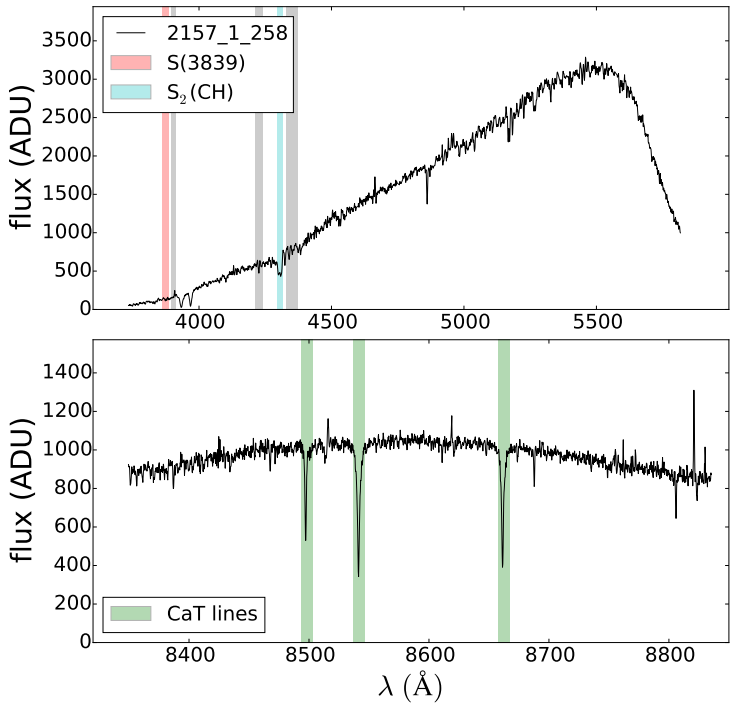

Figure C.27: AEGIS catalogue ID 2157_1_258, 2MASS ID 18280626-3356317

C.1.4 M55 (NGC 6809)

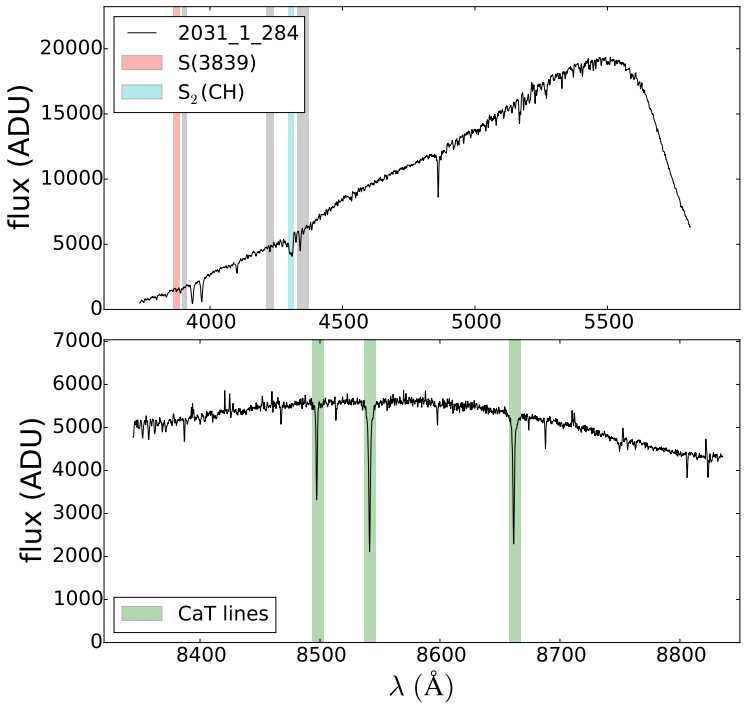

Figure C.28: AEGIS catalogue ID 2031_1_284, 2MASS ID 19173299-3101242

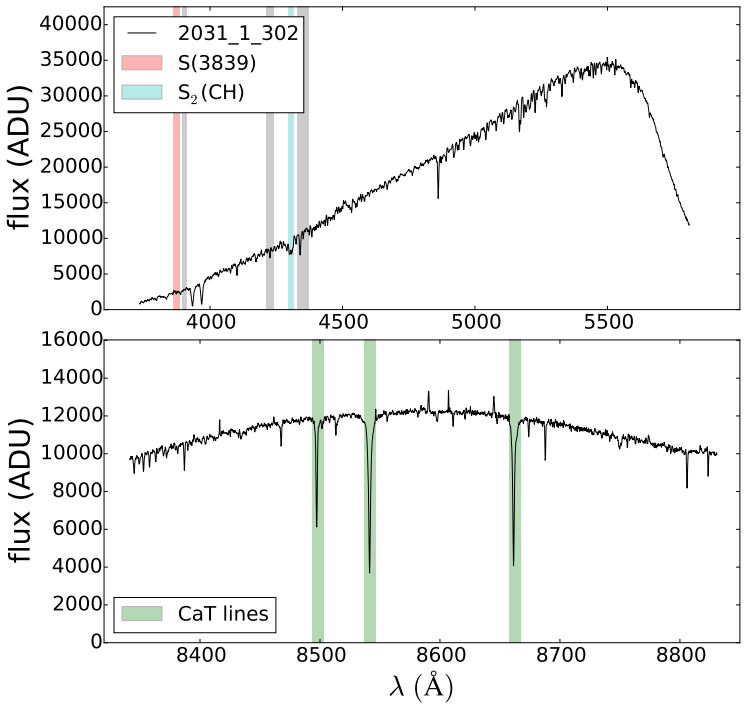

Figure C.29: AEGIS catalogue ID 2031_1_302, 2MASS ID 19182697-3056159

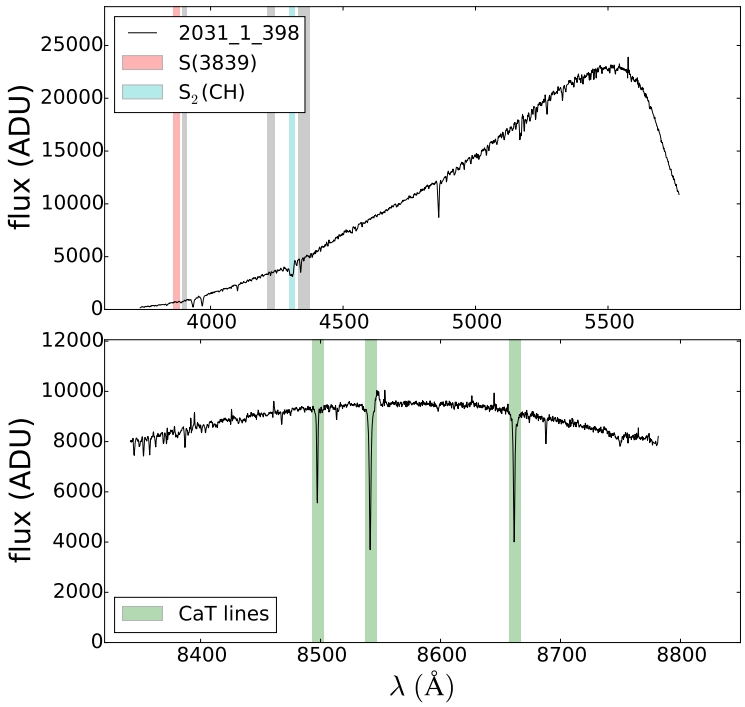

Figure C.30: AEGIS catalogue ID 2031_1_398, 2MASS ID 19205914-3145450

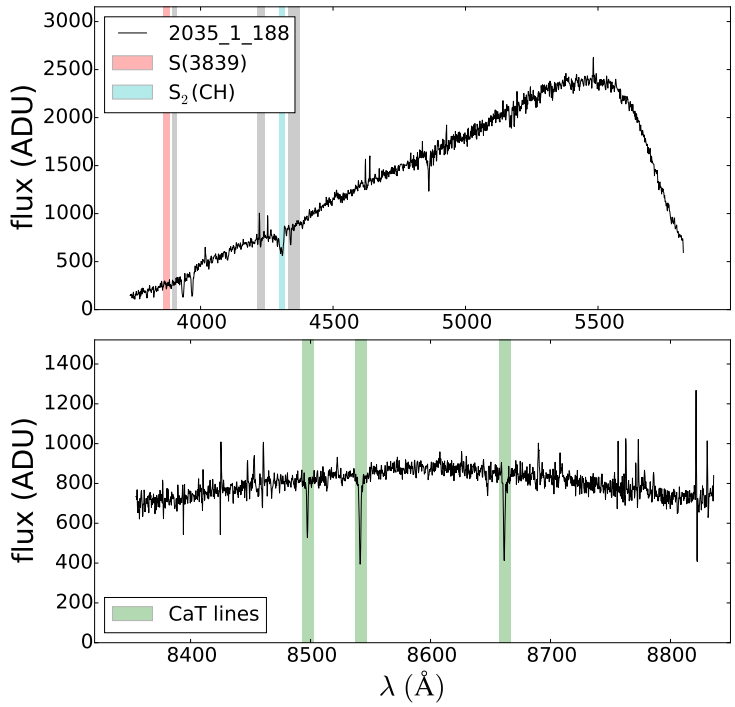

Figure C.31: AEGIS catalogue ID 2035_1_188, 2MASS ID 19593502-3157115

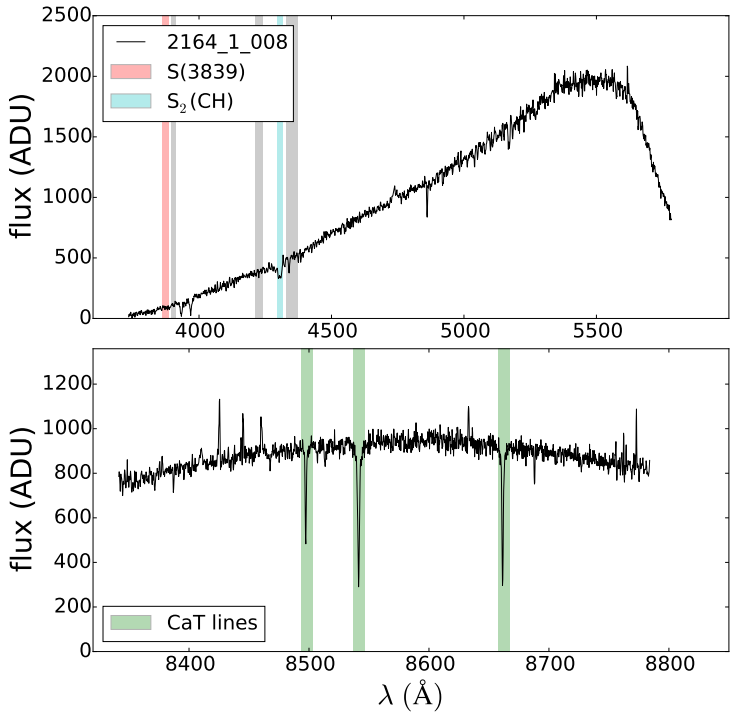

Figure C.32: AEGIS catalogue ID 2164_1_008, 2MASS ID 19454777-3403327

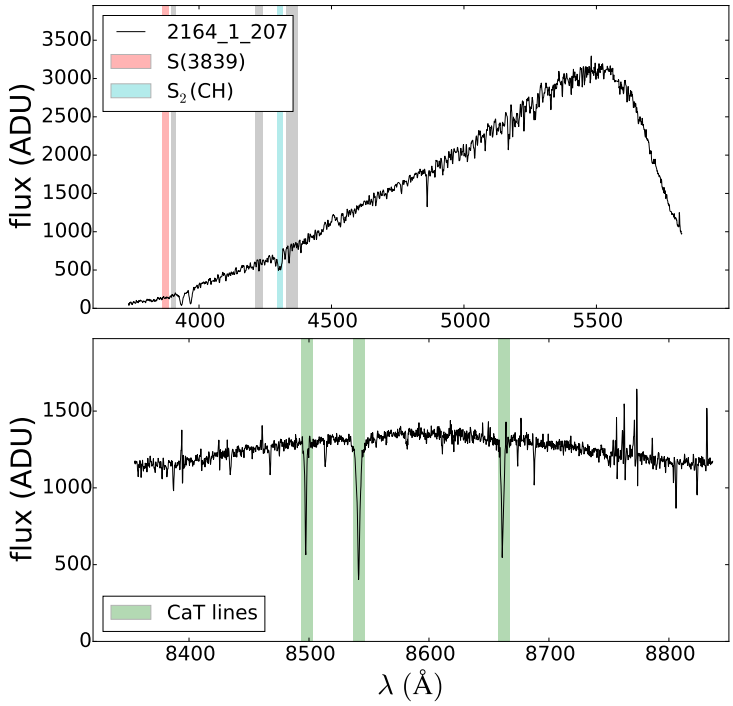

Figure C.33: AEGIS catalogue ID 2164_1_207, 2MASS ID 19412385-3402099

Symbols, abbreviations and acronyms

2dF . . . . . two degree Field fibre positioner on the AAT

2dfdr . . . . . 2df data reduction pipeline

2MASS . . . . . Two-Micron All Sky Survey (Skrutskie et al., 2006)

[α/Fe] . . . . . alpha capture element abundances

Å . . . . . Angstroms

AAOmega . . . Multi-object spectrograph on the AAT, fed by 2dF

AAT . . . . . Anglo-Australian Telescope

AAVSO . . . . . American Association of Variable Star Observers

ADU . . . . . Analog-to-Digital Units

AEGIS . . . . . Aaomega Evolution of GalactIc Structure survey

AGB . . . . . Asymptotic Giant Branch

APASS . . . . . AAVSO Photometric All Sky Survey (Henden et al., 2009)

b . . . . . Galactic latitude

CDM . . . . . Cold Dark Matter

CH(4300) . . . CH spectral index (Harbeck et al., 2003)

CMD . . . . . colour-magnitude diagram

Dec . . . . . declination

DES . . . . . Dark Energy Survey (The Dark Energy Survey Collaboration, 2005)

dIrr . . . . . Dwarf Irregular galaxy

DR1 . . . . . Data Release 1 of the LAMOST survey (Luo et al., 2015)

dSph . . . . . dwarf Spheroidal galaxy

E(B-V) . . . . . reddening

EW . . . . . Equivalent Width of spectra line

[Fe/H] . . . . . stellar metallicity

GALAH..... GALactic Archaeology with Hermes (De Silva et al., 2015, Martell, 2015)

GALAXIA .. code for synthetic modelling of the Milky Way (Sharma et al., 2011)

Gyr..... Gigayear

GMC ..... Giant Molecular Cloud

HERMES ... High Efficiency and Resolution Multi-Element Spectrograph on AAT, fed by 2df

HB ..... Horizontal Branch

HK′..... Calcium H and K lines spectral index (Lim et al., 2015)

IMF ..... Initial Mass Function

J, H, K_s ..... 2MASS photometric filters

kpc ..... kiloparsec

K-S test ..... Kolmogorov-Smirnov test

l..... Galactic longitude

$L_\odot$ ..... Solar luminosity

log g ..... log of stellar surface gravity

Λ CDM ..... Λ (cosmological constant) CDM paradigm

LAMOST ... Large sky Area Multi-Object fiber Spectroscopic Telescope (Zhao et al., 2006)

LMC..... Large Magellanic Cloud

$\mu_\alpha \cos(\delta)$ .... Absolute proper motion in RA

μ_δ ..... Absolute proper motion in Dec

$M_\odot$ ..... Solar mass

mas..... milliarcseconds

MACHO .... MAssive Compact Halo Objects

MS ..... Main Sequence

MSTO ..... Main Sequence Turn Off

MDF..... Metallicity Distribution Function

MWTD ..... Metal-Weak Thick-Disk

Myr..... Megayear

MWSC . . . . . Milky Way Star Clusters catalogue (Kharchenko et al., 2012)

Pan-STARRS Panoramic Survey Telescope and Rapid Response System (Chambers et al., 2016)

pc . . . . . parsec

R_{gc} . . . . . Galactocentric distance

r_h . . . . . cluster half-light radius

$R_\odot$ . . . . . Heliocentric distance

r_t . . . . . Cluster tidal radius

RA . . . . . right ascension

RAVE . . . . . RAdial Velocity Experiment (Steinmetz et al., 2006)

RGB . . . . . Red Giant Branch

S(3839) . . . . . CN spectral index (Harbeck et al., 2003)

S_2(CH) . . . . . CH spectral index (Martell et al., 2008)

SDSS . . . . . Sloan Digital Sky Survey (York et al., 2000)

SEGUE . . . . . SDSS Extension for Galactic Understanding and Exploration (Yanny et al., 2009)

SGB . . . . . Sub Giant Branch

SMC . . . . . Small Magellanic Cloud

T_{eff} . . . . . stellar effective temperature

UCAC 4 . . . . . USNO CCD Astrograph Catalog 4 (Zacharias et al., 2013)

V_t . . . . . cluster integrated V magnitude

V_{HB} . . . . . V magnitude of the HB of a globular cluster

V_r . . . . . radial velocity

VLT . . . . . Very Large Telescope

VST . . . . . VLT Survey Telescope

VST/ATLAS VST ATLAS survey (Shanks et al., 2015)

WIMPS . . . . . Weakly Interacting Massive Particles

yr . . . . . year

References

Aguilar L., Hut P., Ostriker J. P., 1988, ApJ, 335, 720

Alcock C., et al., 2000, ApJ, 542, 281

Allen C., Moreno E., Pichardo B., 2006, ApJ, 652, 1150

Allen C., Moreno E., Pichardo B., 2008, ApJ, 674, 237

Allende Prieto C., et al., 2008, AN, 329, 1018

Ashman K., Zepf S., 2008, Globular Cluster Systems. Cambridge University Press

Balbinot E., Gieles M., 2017, preprint, (arXiv:1702.02543)

Bastian N., Lamers H. J. G. L. M., de Mink S. E., Longmore S. N., Goodwin S. P., Gieles M., 2013, MNRAS, 436, 2398

Battaglia G., et al., 2005, MNRAS, 364, 433

Baumgardt H., Makino J., 2003, MNRAS, 340, 227

Bechtol K., et al., 2015, ApJ, 807, 50

Bedin L. R., Piotto G., Anderson J., Cassisi S., King I. R., Momany Y., Carraro G., 2004, ApJ, 605, L125

Beers T. C., et al., 2012, ApJ, 746, 34

Beers T. C., Norris J. E., Placco V. M., Lee Y. S., Rossi S., Carollo D., Masseron T., 2014, ApJ, 794, 58

Bekki K., Freeman K. C., 2003, MNRAS, 346, L11

Bell E. F., et al., 2008, ApJ, 680, 295

Belokurov V., Koposov S., 2015, preprint, (arXiv:1511.03667)

Belokurov V., Evans N. W., Irwin M. J., Hewett P. C., Wilkinson M. I., 2006a, ApJ, 637, L29

Belokurov V., et al., 2006b, ApJ, 642, L137

Belokurov V., et al., 2006c, ApJ, 647, L111

Belokurov V., et al., 2007a, ApJ, 654, 897

Belokurov V., et al., 2007b, ApJ, 657, L89

Belokurov V., et al., 2007c, ApJ, 658, 337

Belokurov V., Erkal D., Deason A. J., Koposov S. E., De Angeli F., Evans D. W., Fraternali F., Mackey D., 2016, preprint, (arXiv:1611.04614)

Bensby T., Feltzing S., Lundström I., 2003, A&A, 410, 527

Blumenthal G. R., Pagels H., Primack J. R., 1982, Nature, 299, 37

Blumenthal G. R., Faber S. M., Primack J. R., Rees M. J., 1984, Nature, 311, 517

Bonaca A., et al., 2012a, AJ, 143, 105

Bonaca A., Geha M., Kallivayalil N., 2012b, ApJ, 760, L6

Bond J. R., Szalay A. S., Turner M. S., 1982, PhRvL, 48, 1636

Bovy J., Rix H.-W., Schlafly E. F., Nidever D. L., Holtzman J. A., Shetrone M., Beers T. C., 2016, ApJ, 823, 30

Bromm V., Coppi P. S., Larson R. B., 1999, ApJ, 527, L5

Carballo-Bello J. A., Gieles M., Sollima A., Koposov S., Martínez-Delgado D., Peñarrubia J., 2012, MNRAS, 419, 14

Carlberg R. G., 2017, preprint, (arXiv:1706.01938)

Carlin J. L., Yam W., Casetti-Dinescu D. I., Willett B. A., Newberg H. J., Majewski S. R., Girard T. M., 2012, ApJ, 753, 145

Carollo D., et al., 2007, Nature, 450, 1020

Carollo D., et al., 2010, ApJ, 712, 692

Carretta E., et al., 2009, A&A, 505, 117

Carretta E., Bragaglia A., Gratton R. G., Recio-Blanco A., Lucatello S., D'Orazi V., Cassisi S., 2010a, A&A, 516, A55

Carretta E., et al., 2010b, ApJ, 714, L7

Carretta E., et al., 2010c, ApJ, 722, L1

Carretta E., Lucatello S., Gratton R. G., Bragaglia A., D'Orazi V., 2011, A&A, 533, A69

Carroll B. W., Ostlie D. A., 2006, An introduction to modern astrophysics, 2nd edn

Chambers K. C., et al., 2016, preprint, (arXiv:1612.05560)

Chen C. W., Chen W. P., 2010, ApJ, 721, 1790

Chun S.-H., et al., 2010, AJ, 139, 606

Chun S.-H., Kang M., Jung D., Sohn Y.-J., 2014, AJ, 149, 29

Coleman M. G., Da Costa G. S., Bland-Hawthorn J., Freeman K. C., 2005, AJ, 129, 1443

Coleman M. G., et al., 2007, preprint, (arXiv:0706.1669)

Conn B. C., et al., 2012, ApJ, 754, 101

Côté P., Djorgovski S. G., Meylan G., Castro S., McCarthy J. K., 2002, ApJ, 574, 783

Cottrell P. L., Da Costa G. S., 1981, ApJ, 245, L79

Dalton G., et al., 2014, in Ground-based and Airborne Instrumentation for Astronomy V. p. 91470L (arXiv:1412.0843), doi:10.1117/12.2055132

De Marchi G., Leibundgut B., Paresce F., Pulone L., 1999, A&A, 343, L9

De Silva G. M., et al., 2015, MNRAS, 449, 2604

Di Matteo P., Lehnert M. D., Qu Y., van Driel W., 2011, A&A, 525, L3

Dinescu D. I., 2002, in van Leeuwen F., Hughes J. D., Piotto G., eds, Astronomical Society of the Pacific Conference Series Vol. 265, Omega Centauri, A Unique Window into Astrophysics. p. 365 (arXiv:astro-ph/0112364)

Dinescu D., Girard T., van Altena W., 1999, AJ, 117, 1792

Dixon W. J., Massey F. J., 1951, Introduction to statistical analysis. McGraw-Hill, New York

Drlica-Wagner A., et al., 2015, ApJ, 813, 109

Eggen O., Lynden-Bell D., Sandage A., 1962, ApJ, 136, 748

Faber S. M., Gallagher J. S., 1979, ARA&A, 17, 135

Fellhauer M., et al., 2007, MNRAS, 375, 1171

Feng J. L., 2010, ARA&A, 48, 495

Fernández Trincado J. G., Vivas A. K., Mateu C. E., Zinn R., 2013, MmSAI, 84, 265

Freeman K., Bland-Hawthorn J., 2002, ARA&A, 40, 487

Frinchaboy P. M., Majewski S. R., 2008, AJ, 136, 118

Gaia Collaboration 2016, preprint, (arXiv:1609.04153)

Gilmore G., Reid N., 1983, MNRAS, 202, 1025

Gilmore G., Wyse R. F. G., Norris J. E., 2002, ApJ, 574, L39

Gilmore G., et al., 2012, Msngr, 147, 25

Gnedin O., Ostriker J., 1997, ApJ, 474, 223

Gonzalez O. A., Gadotti D., 2016, in Laurikainen E., Peletier R., Gadotti D., eds, Astrophysics and Space Science Library Vol. 418, Galactic Bulges. p. 199 (arXiv:1503.07252), doi:10.1007/978-3-319-19378-6_9

Gratton R. G., Bragaglia A., Carretta E., Clementini G., Desidera S., Grundahl F., Lucatello S., 2003, A&A, 408, 529

Gratton R. G., Carretta E., Bragaglia A., 2012, AARv, 20, 50

Grillmair C. J., 2009, ApJ, 693, 1118

Grillmair C. J., 2011, ApJ, 738, 98

Grillmair C. J., Dionatos O., 2006a, ApJ, 641, L37

Grillmair C. J., Dionatos O., 2006b, ApJ, 643, L17

Grillmair C. J., Johnson R., 2006, ApJ, 639, L17

Grillmair C. J., Freeman K. C., Irwin M., Quinn P. J., 1995, AJ, 109, 2553

Grillmair C. J., Ajhar E. A., Faber S. M., Baum W. A., Holtzman J. A., Lauer T. R., Lynds C. R., O'Neil Jr. E. J., 1996, AJ, 111, 2293

Harbeck D., Smith G. H., Grebel E. K., 2003, AJ, 125, 197

Harrington R. G., Wilson A. G., 1950, PASP, 62, 118

Harris W., 1996, AJ, 112, 1487

Helmi A., White S. D. M., de Zeeuw P. T., Zhao H., 1999, Nature, 402, 53

Henden A. A., Welch D. L., Terrell D., Levine S. E., 2009, BAAS, 41, 669

Homma D., et al., 2017, preprint, (arXiv:1704.05977)

Hut P., Djorgovski S., 1992, Nature, 359, 806

Ibata R., Gilmore G., Irwin M., 1994, Nature, 370, 194

Ibata R., Gilmore G., Irwin M., 1995, MNRAS, 277, 781

Ibata R., Lewis G. F., Irwin M., Totten E., Quinn T., 2001, ApJ, 551, 294

Ibata R., Irwin M., Lewis G., Ferguson A., Tanvir N., 2003, MNRAS, 340, L21

Irwin M., Bunclark P., Bridgeland M., McMahon R., 1990, MNRAS, 244, 16P

Johnson C. I., Pilachowski C. A., 2010, ApJ, 722, 1373

Johnston K. V., Hernquist L., Bolte M., 1996, ApJ, 465, 278

Jordi K., Grebel E., 2010, A&A, 522, A71

Jurić M., et al., 2008, ApJ, 673, 864

Kaiser N., et al., 2010, The Pan-STARRS wide-field optical/NIR imaging survey, doi:10.1117/12.859188, http://dx.doi.org/10.1117/12.859188

Keller S. C., da Costa G. S., Prior S. L., 2009, MNRAS, 394, 1045

Kharchenko N., Scholz R.-D., Lehmann I., 1997, A&A, 121

Kharchenko N. V., Piskunov A. E., Schilbach E., Röser S., Scholz R.-D., 2012, A&A, 543, A156

Kollmeier J. A., et al., 2009, ApJ, 705, L158

Koposov S. E., Belokurov V., Torrealba G., Wyn Evans N., 2015, ApJ, 805, 130

Krauss L. M., Chaboyer B., 2003, Science, 299, 65

Kruijssen J. M. D., Mieske S., 2009, A&A, 500, 785

Kruijssen J. M. D., Pelupessy F. I., Lamers H. J. G. L. M., Portegies Zwart S. F., Icke V., 2011, MNRAS, 414, 1339

Küpper A. H. W., Kroupa P., Baumgardt H., Heggie D. C., 2010, MNRAS, 401, 105

Laevens B. P. M., et al., 2015a, ApJ, 802, L18

Laevens B. P. M., et al., 2015b, ApJ, 813, 44

Lauchner A., Powell Jr. W. L., Wilhelm R., 2006, ApJ, 651, L33

Law D. R., Majewski S. R., 2010, ApJ, 718, 1128

Lee Y., Joo J., Sohn Y., Rey S., Lee H., Walker A., 1999, Nature, 402, 55

Lee Y., et al., 2013, ApJ, 778, L13

Lehmann I., Scholz R.-D., 1997, A&A, 320, 776

Leon S., Meylan G., Combes F., 2000, A&A, 359, 907

Lim D., Han S., Lee Y.-W., Roh D.-G., Sohn Y.-J., Chun S.-H., Lee J.-W., Johnson C. I., 2015, ApJ, 216, 19

Lind K., et al., 2015, A&A, 575, 12

Linden S. T., et al., 2017, ApJ, 843, 91

Loebman S. R., Roškar R., Debattista V. P., Ivezić Ž., Quinn T. R., Wadsley J., 2011, ApJ, 737, 8

Lopez-Corredoira M., Moitinho A., Zaggia S., Momany Y., Carraro G., Hammersley P. L., Cabrera-Lavers A., Vazquez R. A., 2012, preprint, (arXiv:1207.2749)

Luo A., et al., 2015, preprint, (arXiv:1505.01570)

Mackey A. D., Gilmore G. F., 2004, MNRAS, 355, 504

Mackey A. D., van den Bergh S., 2005, MNRAS, 360, 631

Mackey A. D., et al., 2010, ApJ, 717, L11

Majewski S., Skrutskie M., Weinberg M., Ostheimer J., 2003, ApJ, 599, 1082

Majewski S. R., Ostheimer J. C., Rocha-Pinto H. J., Patterson R. J., Guhathakurta P., Reitzel D., 2004, ApJ, 615, 738

Majewski S. R., Nidever D. L., Smith V. V., Damke G. J., Kunkel W. E., Patterson R. J., Bizyaev D., Pérez A. E. G., 2012, ApJ, 747, L37

Martell S. L., 2015, preprint, (arXiv:1507.00079)

Martell S. L., Grebel E. K., 2010, A&A, 519, A14

Martell S. L., Smith G. H., Briley M. M., 2008, PASP, 120, 839

Martell S. L., Smolinski J. P., Beers T. C., Grebel E. K., 2011, A&A, 534, A136

Martell S. L., et al., 2017, MNRAS, 465, 3203

Martin N., Ibata R., Bellazzini M., Irwin M., Lewis G., Dehnen W., 2004, MNRAS, 348, 12

Martin N. F., Ibata R. A., Irwin M., 2007, ApJ, 668, L123

Martin C., Carlin J. L., Newberg H. J., Grillmair C., 2013, ApJ, 765, L39

Martin N. F., et al., 2015, ApJ, 804, L5

Mathewson D., Cleary M., Murray J., 1974, ApJ, 190, 291

Mayer L., Moore B., Quinn T., Governato F., Stadel J., 2002, MNRAS, 336, 119

McConnachie A. W., 2012, AJ, 144, 4

Meza A., Navarro J. F., Abadi M. G., Steinmetz M., 2005, MNRAS, 359, 93

Milgrom M., 1983, ApJ, 270, 365

Mirabel I. F., Dottori H., Lutz D., 1992, A&A, 256, L19

Mizutani A., Chiba M., Sakamoto T., 2003, ApJ, 589, L89

Momany Y., Zaggia S. R., Bonifacio P., Piotto G., De Angeli F., Bedin L. R., Carraro G., 2004, A&A, 421, L29

Moore B., Ghigna S., Governato F., Lake G., Quinn T., Stadel J., Tozzi P., 1999, ApJ, 524, L19

Moreno E., Pichardo B., Velázquez H., 2014, ApJ, 793, 110

Morrison H. L., 1993, AJ, 106, 578

Morrison H. L., Flynn C., Freeman K. C., 1990, AJ, 100, 1191

Muñoz R. R., et al., 2006, ApJ, 649, 201

Myeong G. C., Evans N. W., Belokurov V., Koposov S., Sanders J. L., 2017, preprint, (arXiv:1704.01363)

Navin C., Martell S., Zucker D., 2015, MNRAS, 453, 531

Navin C. A., Martell S. L., Zucker D. B., 2016, ApJ, 829, 123

Newberg H., et al., 2002, ApJ, 569, 245

Newberg H. J., Yanny B., Willett B. A., 2009, ApJ, 700, L61

Niederste-Ostholt M., Belokurov V., Evans N. W., Koposov S., Gieles M., Irwin M. J., 2010, MNRAS, 408, L66

Norris J., Bessell M. S., Pickles A. J., 1985, ApJ, 58, 463

Odenkirchen M., Grebel E. K., 2004, in Prada F., Martinez Delgado D., Mahoney T. J., eds, Astronomical Society of the Pacific Conference Series Vol. 327, Satellites and Tidal Streams. p. 284 (arXiv:astro-ph/0307481)

Odenkirchen M., et al., 2001, ApJ, 548, L165

Odenkirchen M., et al., 2003, AJ, 126, 2385

Okamoto S., Arimoto N., Yamada Y., Onodera M., 2008, A&A, 487, 103

Olszewski E. W., Saha A., Knezek P., Subramaniam A., de Boer T., Seitzer P., 2009, AJ, 138, 1570

Palma C., Majewski S. R., Siegel M. H., Patterson R. J., Ostheimer J. C., Link R., 2003, AJ, 125, 1352

Pancino E., Rejkuba M., Zoccali M., Carrera R., 2010, A&A, 524, A44

Pancino E., Bellazzini M., Giuffrida G., Marinoni S., 2017, preprint, (arXiv:1701.03003)

Peebles P. J. E., 1982, ApJ, 263, L1

Phelps R. L., Janes K. A., Montgomery K. A., 1994, AJ, 107, 1079

Portegies Zwart S. F., McMillan S. L. W., Gieles M., 2010, ARA&A, 48, 431

Ramírez I., Meléndez J., Chanamé J., 2012, ApJ, 757, 164

Rix H.-W., Bovy J., 2013, AARv, 21, 61

Rocha-Pinto H. J., Scalo J., Maciel W. J., Flynn C., 2000, A&A, 358, 869

Rocha-Pinto H. J., Majewski S. R., Skrutskie M. F., Crane J. D., Patterson R. J., 2004, ApJ, 615, 732

Rockosi C. M., et al., 2002, AJ, 124, 349

Saha A., et al., 2010, AJ, 140, 1719

Schiavon R. P., et al., 2017, MNRAS, 465, 501

Schönrich R., Asplund M., Casagrande L., 2011, MNRAS, 415, 3807

Searle L., Zinn R., 1978, ApJ, 225, 357

Sesar B., et al., 2007, AJ, 134, 2236

Sesar B., et al., 2010, ApJ, 708, 717

Shanks T., et al., 2015, MNRAS, 451, 4238

Sharma S., Johnston K. V., Majewski S. R., Muñoz R. R., Carlberg J. K., Bullock J., 2010, ApJ, 722, 750

Sharma S., Bland-Hawthorn J., Johnston K. V., Binney J., 2011, ApJ, 730, 3

Sheffield A. A., Johnston K. V., Majewski S. R., Damke G., Richardson W., Beaton R., Rocha-Pinto H. J., 2014, ApJ, 793, 62

Simion I. T., Belokurov V., Irwin M., Koposov S. E., 2014, MNRAS, 440, 161

Simpson J. D., Martell S. L., Navin C. A., 2017a, MNRAS, 465, 1123

Simpson J. D., De Silva G., Martell S. L., Navin C. A., Zucker D. B., 2017b, MNRAS, 472, 2856

Skrutskie M., et al., 2006, ApJ, 131, 1163

Smith V. V., Suntzeff N. B., Cunha K., Gallino R., Busso M., Lambert D. L., Straniero O., 2000, AJ, 119, 1239

Sohn S. T., et al., 2007, ApJ, 663, 960

Steinmetz M., et al., 2006, AJ, 132, 1645

Testa V., Zaggia S. R., Andreon S., Longo G., Scaramella R., Djorgovski S. G., de Carvalho R., 2000, A&A, 356, 127

The Dark Energy Survey Collaboration 2005, preprint, (arXiv:astro-ph/0510346)

Tinsley B., Larson R., 1979, MNRAS, 186, 503

Toomre A., Toomre J., 1972, ApJ, 178, 623

Traven G., et al., 2017, ApJ, 228, 24

Twarog B. A., Anthony-Twarog B. J., 1994, AJ, 107, 1371

Urquhart J. S., Figura C. C., Moore T. J. T., Hoare M. G., Lumsden S. L., Mottram J. C., Thompson M. A., Oudmaijer R. D., 2014, MNRAS, 437, 1791

Vesperini E., Heggie D. C., 1997, MNRAS, 289, 898

Villanova S., Geisler D., Carraro G., Moni Bidin C., Muñoz C., 2013, ApJ, 778, 186

Vivas A. K., Zinn R., 2006, AJ, 132, 714

Vivas A. K., et al., 2001, ApJ, 554, L33

Wang L., et al., 2016, MNRAS, 458, 1450

Webb J. J., Leigh N. W. C., 2015, MNRAS, 453, 3278

White S. D. M., Rees M. J., 1978, MNRAS, 183, 341

Willman B., et al., 2005a, ApJ, 129, 2692

Willman B., et al., 2005b, ApJ, 626, L85

Willman B., et al., 2006, preprint, (arXiv:astro-ph/0603486)

Xu Y., Deng L. C., Hu J. Y., 2006, MNRAS, 368, 1811

Xu Y., Newberg H. J., Carlin J. L., Liu C., Deng L., Li J., Schönrich R., Yanny B., 2015, ApJ, 801, 105

Yanny B., et al., 2009, AJ, 137, 4377

Yong D., Grundahl F., 2008, ApJ, 672, L29

York D., et al., 2000, AJ, 120, 1579

Zacharias N., Finch C. T., Girard T. M., Henden A., Bartlett J. L., Monet D. G., Zacharias M. I., 2013, AJ, 145, 44

Zhang B., et al., 2015, RAA, 15, 1197

Zhao G., Chen Y.-Q., Shi J.-R., Liang Y.-C., Hou J.-L., Chen L., Zhang H.-W., Li A.-G., 2006, CJAA, 6, 265

Zinn R., 1985, ApJ, 293, 424

Zinn R., 1993, in Smith G. H., Brodie J. P., eds, Astronomical Society of the Pacific Conference Series Vol. 48, The Globular Cluster-Galaxy Connection. p. 38

Zucker D., et al., 2006, ApJ, 650, L41

Zwicky F., 1933, AcHPh, 6, 110

van den Bergh S., 1993, ApJ, 411, 178